universität wien

MASTERARBEIT / MASTER'S THESIS

Titel der Masterarbeit / Title of the Master's Thesis

„Biomimetic Synthesis of Multifunctional Silica Particles“

verfasst von / submitted by

Birgit Bräuer BSc

angestrebter akademischer Grad / in partial fulfilment of the requirements for the degree of

Master of Science (MSc)

Wien, 2017 / Vienna 2017

Studienkennzahl lt. Studienblatt / degree programme code as it appears on the student record sheet:	A 066 862
Studienrichtung lt. Studienblatt / degree programme as it appears on the student record sheet:	Masterstudium Chemie
Betreut von / Supervisor:	Univ.-Prof. Dr. Christian Friedrich Wilhelm Becker
Mitbetreut von / Co-Supervisor:	Meder Kamalov, BSc PhD

Table of Contents

Acknowledgements

First, I would like to thank Prof. Christian Becker for giving me the opportunity to perform my master's thesis in his working group.

I would also like to thank my co-supervisor, Meder Kamalov, BSc PhD, for his continuous supervision and support during my work in the laboratory and the writing process of my thesis.

Additionally, I would like to express my gratitude to the entire working group. Thank you all for providing advice whenever I needed it and the friendly and productive working atmosphere you created.

I am especially grateful to my parents, who have always encouraged me to pursue my goals and taught me that after every storm, if you look hard enough, a rainbow appears.

Special thanks also go to Patrick, my better half, for providing moral support and being so understanding, since he was in the same situation a few years ago.

I would also like to thank Prof. Christian Rentenberger and Dr. Stephan Puchegger for providing help with TEM and SEM imaging.

My gratitude also goes to Dr. Georgia Del Favero and Eva Attakpah for their support concerning fluorescence microscopy imaging and cell culture.

Abstract

Silica particles can be used in biotechnology and biomedicine for applications including immobilization of enzymes, imaging, biosensing, drug delivery and controlled drug-release. The biomimetic synthesis of such particles has become increasingly popular in recent years as it provides a variety of advantages compared to the traditional synthesis of silica particles including the sol-gel process and micro-emulsion synthesis. These advantages comprise mild synthesis conditions such as neutral pH, ambient temperature and synthesis in aqueous solutions as well as the possibility of producing hybrid materials of silica with biomolecules such as proteins and peptides. In this project, silica precipitations were carried out based on a previously established biomimetic synthesis approach involving a variant of the synthetic silaffin R5 peptide with an *N*-terminal cysteine residue. This R5 variant has been shown to exhibit silica precipitating activity in phosphate-buffered solutions containing silicic acid at neutral pH and ambient temperature. The investigation of the display and accessibility of the *N*- and *C*-terminus of the R5 peptide in silica particles derived from biomimetic silica precipitations using this peptide was attempted. The strategy employed for this investigation utilized the (strept)avidin-biotin interaction between *N*- or *C*-terminally biotinylated R5 variants with streptavidin-gold nanoparticle and avidin-sulforhodamine 101 conjugates. In addition, the effect of pH as well as R5 peptide and silica precursor concentrations on the morphology of the resultant precipitates was investigated in order to find optimal synthesis conditions for smooth spherical silica particles. Conditions for the synthesis of spherical silica particles modified with two different functionalities (cyanine-5 and fluorescein) based on the same biomimetic approach were then developed. For the generation of the doubly modified silica particles, a cyanine-5 functionality was introduced via covalent attachment to the *N*-terminus of the R5 peptide variant, which co-precipitates with the silica. In contrast, the fluorescein modification was incorporated directly into the silica material via the use of triethoxysilyl fluorescein as a silica precursor. The percentages of the cyanine-5 modified R5 variant and triethoxysilyl fluorescein incorporated into the particles were determined and cell studies were carried out in THP-1 cells to investigate the uptake of the doubly modified silica particles by these cells within 24 hours.

Zusammenfassung

Silica-Partikel können in der Biotechnologie und Biomedizin beispielsweise für die Immobilisierung von Enzymen, bildgebende Verfahren, als Biosensoren oder als Drug-Delivery-Systeme mit kontrollierter Freisetzung von Arzneistoffen Anwendung finden. Die biomimetische Synthese solcher Partikel hat in den letzten Jahren eine erhöhte Beliebtheit erfahren, da sie eine Reihe von Vorteilen gegenüber der traditionellen Synthese von Silica-Partikeln, wie der Sol-Gel-Synthese oder Mikroemulsions-Methode, aufweist. Zu diesen Vorteilen zählen milde Synthesebedingungen wie ein neutraler pH-Wert und Synthese bei Raumtemperatur in wässrigen Lösungen sowie die Möglichkeit Biomoleküle wie Proteine oder Peptide in Silica-Material zu inkorporieren. Im vorliegenden Projekt wurden Silica-Präzipitationen basierend auf einer bereits etablierten biomimetischen Synthesemethode unter Verwendung einer Variante des synthetischen Silaffin-Peptids R5, die ein *N*-terminales Cystein trug, durchgeführt. Über die Silica-Präzipitations-Fähigkeit dieser R5-Variante in Phosphat-gepufferten Lösungen mit Orthokieselsäure bei neutralem pH-Wert und Raumtemperatur ist bereits berichtet worden. Es wurde versucht, die Zugänglichkeit des *N*- und *C*-Terminus des R5-Peptids in Silica-Partikeln, die mithilfe dieses Peptids synthetisiert wurden, zu untersuchen. Der hierfür verwendete strategische Ansatz basierte auf der (Strept)avidin-Biotin Interaktion zwischen *N*- und *C*-terminal biotinylierten Varianten des R5-Peptids mit Streptavidin-Goldnanopartikel- oder Avidin-Sulforhodamin 101-Konjugaten. Außerdem wurde der Einfluss des pH-Werts und der Konzentrationen des R5 Peptids und des Silica-Precursors auf die Morphologien der resultierenden Präzipitate untersucht, um die optimalen Synthesebedingungen für sphärische Silica-Partikel mit glatten Oberflächen zu finden. In weiterer Folge wurden Bedingungen für die Synthese von sphärischen Silica-Partikeln, die mit zwei Modifikationen (Cyanin-5 und Fluoreszein) versehen waren, basierend auf dem gleichen biomimetischen Synthesekonzept entwickelt. Für die Produktion der dual modifizierten Silica-Partikel wurde die Cyanin-5-Funktionalität über die kovalente Bindung an den *N*-Terminus der R5-Peptid-Variante, die mit dem Siliziumdioxid co-präzipitiert, eingeführt. Im Gegensatz dazu wurde die Fluoreszein-Modifikation über die Verwendung von Triethoxysilyl-Fluoreszein als-Silica-Precursor direkt in das Silica-Material integriert. Die Anteile der Cyanin-5-modifizierten R5-Variante und des Triethoxysilyl-Fluoreszeins, die in die Partikel inkorporiert worden waren, wurden bestimmt. Zusätzlich wurden Zellstudien in THP-1-Zellen durchgeführt, um die Aufnahme der doppelt modifizierten Silica-Partikel in diese Zellen innerhalb von 24 Stunden zu untersuchen.

Abbreviations

ACN	acetonitrile
APTES	3-aminopropyltriethoxysilane
APTS	3-aminopropyltrimethoxysilane
Biotin-OSu	biotin-oxysuccinimide
CTAB	cetyl trimethylammonium bromide
Cy-5	cyanine-5
DCM	dichloromethane
DETA	trimethoxysilylpropyldiethylenetriamine
DIEA	*N*,*N*-diisopropylethylamine
DMF	*N*,*N*-dimethylformamide
DMS	dimethyl sulfide
DMSO	dimethylsulfoxide
EPL	expressed protein ligation
EPTES	*N*-(β-ethylenamine)-γ-propylamine
EtOH	ethanol
FCS	fetal calf serum
Fmoc	fluorenylmethoxycarbonyl
HATU	1-[Bis(dimethylamino)methylene]-1H-1,2,3-triazolo[4,5-b]pyridinium 3-oxid hexafluorophosphate
HOBt	hydroxybenzotriazole
HPLC	high-performance liquid chromatography
HPLC-MS	high-performance liquid chromatography-mass spectrometry
LCPA	long-chain polyamine
M-cells	microfold cells
MeOH	methanol
MCM-41	Mobil Composition of Matter No. 41
MPTS	3-mercaptopropyltrimethoxysilane
natSil-1A	native Silaffin-1A
natSil-1B	native Silaffin-1B
natSil-2	native Silaffin-2
NHS	*N*-hydroxysuccinide
NMP	*N*-methyl-2-pyrrolidone
PBS	phosphate-buffered saline
PEG	polyethyleneglycol
PTM	posttranslational modification
RP-HPLC	reversed-phase high-performance liquid chromatography
rpm	revolutions per minute
RPMI-1640	Roswell Park Memorial Institute-1640
RT	room temperature
SBA-15	Santa Barbara Amorphous 15
SDV	silica deposition vesicle

SEM	scanning electron microscopy
TEM	transmission electron microscopy
TEOS	tetraethoxysilane
TFA	trifluoroacetic acid
THPMP	(3-trihydroxy)silylpropyl methylphosphonate
TIPS	triisopropylsilane
TMOS	tetramethoxysilane
UV-Vis	ultraviolet-visible

1. Introduction

Silica as a material can be utilized for various applications owing to its unique physical and chemical properties such as good physicochemical stability and, especially in the case of colloidal silica, large surface areas, relatively low toxicity and high biocompatibility. Another significant advantage of colloidal silica is the relative ease of modification of the free silanol groups. As a result, colloidal silica is involved in numerous applications including catalysis, metallurgy, personal care products and chromatography. Mesoporous silica can be used in biomedical applications such as drug delivery vehicles. Silica particles can be synthesized using traditional techniques including the sol-gel process, but also via a biomimetic approach inspired by biomineralization processes in living organisms such as diatoms. In the biomimetic approach, silica particles are produced using biomolecules involved in the formation of biogenic silica such as silaffin peptides. The biomimetic synthesis method provides a variety of advantages over traditional synthesis techniques such as mild synthesis conditions (neutral pH, ambient temperature), which allow for the production of hybrid materials of silica with biomolecules. [1-6]

1.1 Traditional synthesis of silica particles

Different methods have been established to produce silica (nano)particles, such as chemical vapour deposition, the sol-gel process, flame spray pyrolysis and micro-emulsion techniques. Among these methods, the sol-gel process is the most popular as it allows for the synthesis of silica nanoparticles with controlled sizes, shapes and surface structures via the adjustment of reaction parameters. [6-8].

The two basic categories of the production of silica nanoparticles are top-down and bottom-up methods. In the bottom-up approach, the particles are generated through the formation of clusters from the atoms or molecular constituents to an intermediate state between the micro and macro levels. In contrast, in the top-down technique, the particles are produced via size reduction techniques such as etching or grinding from the corresponding bulk materials (Figure 1). [7, 9]

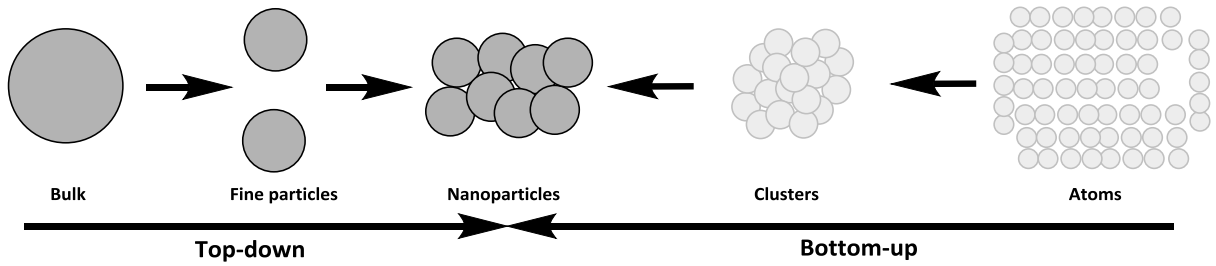

Figure 1: Schematic representation of the top-down (left) and bottom-up (right) approaches towards nanoparticles (adapted from [7])

Within the top-down/bottom-up techniques of silica (nano)particle production, the three basic categories of preparation methods are the gaseous state preparation, the solid state preparation and the liquid state preparation. [7]

The gaseous state preparation allows for the production of nanomaterials based on metals, metal oxides and ceramics and comprises the gas condensation technique, the vacuum deposition and vaporization method as well as the chemical vapor deposition technique, which are based on vaporization of the precursor materials followed by collision-induced atom condensation and particle nucleation, deposition in a vacuum or deposition on a heated surface via a chemical reaction. Solid state preparation of nanoparticles can be achieved through mechanical milling. [7, 10]

1.1.1 Micro-emulsions and sol-gel synthesis

Two examples of liquid state preparations of nanoparticles utilizing a bottom-up approach are commonly used: the micro-emulsion method and the sol-gel process. In the micro-emulsion method, water-in-oil and oil-in-water emulsions, which are composed of colloidal nanosized droplets exhibiting thermodynamic stability that is attributed to a layer of surfactant, are used as reaction vessels mediating the generation of nanomaterials. In the reverse micro-emulsion technique, following dissolution of the surfactants in organic solvents, the individual molecules organize themselves in spherical micellar assemblies. If the mixture contains water, the polar head groups of the surfactants arrange themselves forming microscopic "reverse micelles" that encapsulate water and provide the environment for the synthesis of silica nanoparticles if silicon alkoxides and a catalyst are added to the mixture. [7, 9] A different method, the sol-gel process, is the most commonly used liquid state preparation technique for nanoparticles owing to the possibility to control particle sizes, size distribution and microstructure via appropriate adjustment of the reaction parameters. The most commonly used precursors in sol-gel processes for the formation of silica particles are tetramethoxysilane (TMOS) and tetraethoxysilane (TEOS). The method generally consists of four steps: hydrolysis, condensation, growth and aggregation. In the first step, the alkoxide precursor is hydrolyzed by mixing with water and an acid or base catalyst (Scheme 1). [7, 9, 11]

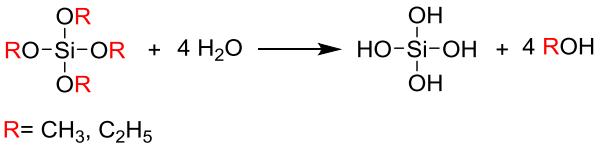

Scheme 1: The first step in the sol-gel synthesis of silica nanoparticles: hydrolysis of the alkoxide precursor (adapted from [11])

The silicic acid monomers formed in the hydrolysis reaction then interact in a condensation reaction, initially generating dimers connected via siloxane bonds (Si-O-Si, Scheme 2). [11]

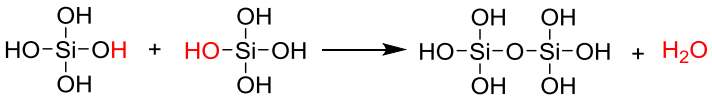

Scheme 2: The second step in the sol-gel synthesis of silica nanoparticles: condensation of two silicic acid monomers to form a dimer accompanied by the release of water (adapted from [11])

In a polycondensation (or growth) process, more interconnecting siloxane bonds are formed (Scheme 3) and eventually colloidal particles are produced, resulting in a sol, which describes a dispersion of colloidal particles with diameters between 1 and 100 nm in a liquid. Over time, the colloidal particles can aggregate and form a three-dimensional network. Depending on the specific reaction conditions (pH), the sol-gel process can result in the formation of a sol of uniformly-sized spherical particles via growth of the initially formed particles (pH >7) or in gel networks through aggregation of initial particles (pH < 7) [7, 9, 11, 12]

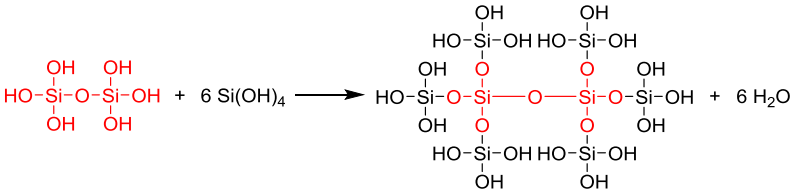

Scheme 3: The third step in the sol-gel synthesis of silica nanoparticles: polycondensation reaction between the initially formed dimeric silicic acid and additional monomers (adapted from [11])

1.1.2 Stöber synthesis of non-porous particles

An important method for the sol-gel type synthesis of monodispersed nonporous silica particles controlled via reaction kinetics, which many modern synthesis strategies are based on, was established in 1968 by Stöber *et al* [13]. This group of researchers synthesized silica particles with diameters ranging from 50 nm to 2 µm using TEOS or other tetraalkoxysilanes (such as TMOS) as a silica precursor in a hydrolysis-condensation reaction sequence using water and short-chain alcohols as solvents and ammonia as a catalyst (Figure 2). [7, 14]

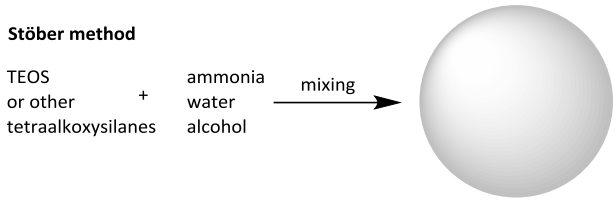

Figure 2: General procedure for the synthesis of silica particles via the Stöber method (adapted from [15])

The reaction was performed at room temperature and a pH of around 10 and resulted in the formation of silica particles with homogeneous size distributions depending on the specific pH of the mixture, the concentrations of the reactants as well as the temperature. It was discovered that the particle size is also significantly influenced by the silica precursor and the type of alcohol used. [7, 14, 15]

1.1.3 Stöber synthesis of mesoporous silica particles

Mesoporous silica materials, including MCM-41 and SBA-15, are solids and possess a porous structure with a large number of honeycomb-shaped pores, which are empty channels that can effectively accommodate biomolecules via absorbing or entrapment. [3] Nanoparticles consisting of mesoporous silica materials are characterized by high surface areas and large pore sizes, controllable and uniform pore-sizes and particle sizes, two surfaces that are available for functionalization (the internal surface, which comprises the cylinder-shaped pores, and the external surface, which corresponds to the exterior of the mesoporous silica sphere) as well as a chemically and thermally stable and robust framework, which is a feature of silica materials in general. [3, 15] In addition to the possibility of controlling particle and pore size, the morphology and pore structure of the particles can also be adjusted. [16]

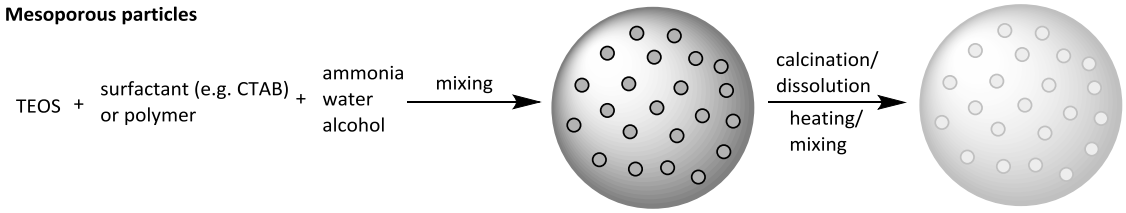

Figure 3: General procedure for the synthesis of mesoporous silica particles (adapted from [15])

Mesoporous silica nanoparticles or microparticles are produced employing an adapted version of the Stöber method under addition of various surfactants including cetyl trimethylammonium bromide (CTAB), compounds that form micelles, polymers and other types of additives (Figure 3). [15, 17-19] This synthesis method for mesoporous silica materials utilizing surfactant-micelles as templates was developed in 1992 by Kresge *et al*. [20] and Gruen *et al*. [21] were among the first researchers to synthesize mesoporous silica microparticles possessing uniform sizes. [3] The surfactant-micelles formed in the surfactant-templated synthesis method function as templates for silica growth with TEOS as a silica precursor and are responsible for the presence of pores in the mesoporous silica nanoparticles after removal of the micelles. Depending on the materials as well as concentrations employed for preparation of the pores in mesoporous silica nanoparticles, the size and structure of

the pores and the particle crystallinity can be precisely adjusted. Particles with pore sizes ranging from 10 to 300 Å, which are influenced by the type of surfactant or other morphology directing materials, have been synthesized. [15, 22] Several different techniques have been developed to control the particle shape of mesoporous silica nanoparticles (including spherical, ellipsoid, tube- and rod-shapes [3, 23]), which has already been demonstrated to influence agglomeration and circulation behavior of nonporous silica nanoparticles *in vitro* as well as biodistribution, bioavailability and endocytosis potential of silica particles *in vivo*. [3, 15, 24-27]

1.1.4 Surface functionalization of silica particles for bioconjugation

Principles of the covalent modification of silica surfaces with functional groups

The surface of silica nanoparticles can be chemically modified in order to enhance or control the surface properties of the particles by functionalization for specific applications. [28] Surface modification can be performed using various different approaches (Figure 4), the easiest of which is the reaction of the silica surface with alkoxysilanes or halosilanes that are available for purchase. The modification of silica nanoparticles with alkoxysilanes is based on a condensation reaction between those molecules and silanol groups present on the silica surface, which results in the generation of 1-3 Si-O-Si bonds. In the case of reaction with halosilanes, in the presence of water, the surface modification is facilitated by hydrolysis of the halosilane, which results in exchange of the halide for an alcohol group. The alcohol group can then bind to the silica surface via a condensation reaction involving the surface silanol groups. If the reaction is carried out in the absence of water, the halosilanes directly interact with silanol groups present on the silica surface in a condensation reaction. [15] The most commonly used alkoxysilanes for silica surface functionalization include 3-aminopropyltriethoxysilane (APTES), 3-mercaptopropyltrimethoxysilane (MPTS) as well as PEG-silanes. PEG-modification of silica particles can be employed to enhance important properties such as stability of silica particles in physiological environments [29], biocompatibility and the duration of circulation of silica particles in *vivo* [30]. Modification of the silica surface using APTES and MPTS attaches commonly used linker molecules, which include N-hydroxysuccinide (NHS), isothiocyanate or maleimide modified molecules among others. [15, 31] Incorporation of functional groups required for further modification of the silica particles can be achieved via post coating in the case of silica particles that are generated via the Stöber process. In the post-coating approach, an additional layer of silica is deposited. This extra layer contains the functional group (anchor group) required for further modification of the silica particle with, for example, biomolecules or fluorescent dyes. Another method for the incorporation of these anchor functionalities is the co-condensation of TEOS with appropriately modified alkoxysilanes. Advantages of the introduction of anchor groups via co-condensation compared to post-coating include a low number of production steps, a homogeneous distribution of the functionalities and complete integration of the anchor groups into the silica network. [32] The silanol groups located on the surface of silica particles can be derivatized post-synthesis by cyanogen bromide (CNBr) [33] in dry solvents such as anhydrous DMF, acetonitrile or DMSO (to avoid hydrolytic cleavage of the activated species), which results in the generation of a highly reactive cyanate ester. Molecules possessing amine groups can then form covalent bonds with these functionalities in coupling buffers under alkaline conditions, which leads to the production of isourea derivatives. [32] Another method, which allows for the attachment of biomolecules with amine functional groups (such as proteins) to silica surfaces, involves a combination of silica particles functionalized with carboxyl groups and carbodiimides with sufficient solubility in water. Modification of silica nanoparticle surfaces with carboxyl groups has been achieved via silanization with APTES [34] or trimethoxysilylpropyl-diethylenetriamine (DETA) [35] followed by addition of succinic anhydride. Subsequent treatment of

such particles with carbodiimide hydrochloride and an enzyme such as lactate dehydrogenase or glutamate dehydrogenase in PBS buffer resulted in the successful immobilization of these enzymes on the particles. [35] Immobilization of glutamate dehydrogenase on silica particles was achieved by Blasi and co-workers [36], who performed silanization of the particles using APTES before glutaraldehyde was added and the thereby activated silica particles reacted with the primary amine groups of the enzyme resulting in the generation of Schiff's bases [36]. A different technique has been developed for the functionalization of mesoporous silica particles with carboxyl groups, which involves the hydrolysis and co-condensation of TEOS with carboxyethylsilanetriol sodium salt as a structure-determining additive. [32, 37] Silica particle surfaces can also be functionalized with amine groups via co-hydrolysis or post coating with different appropriately modified silica precursors such as N-(β-ethylenamine)-γ-propylamine (EPTES) [38], 3-aminopropyltrimethoxysilane (APTS) [39] and APTES [32, 40]. Amine-modified silica nanoparticles can then be functionalized with biomolecules containing amines via suitable homobifunctional crosslinkers including glutaraldehyde, followed by a reduction of the generated Schiff base employing reducing agents such as sodium cyanoborohydride. [32] Modification of silica particles with amine-functionalized organosilanes can result in a reduction of colloidal stability and cause the formation of particle-aggregates in water (due to a decrease in the particle surface charge at neutral pH). To counteract this disadvantage, silanes carrying negative charges (which, for example, possess phosphonate groups (3-trihydroxy)silylpropyl methylphosphonate (THPMP)) or hydrophilic PEG-modified silanes, can be added. [32]

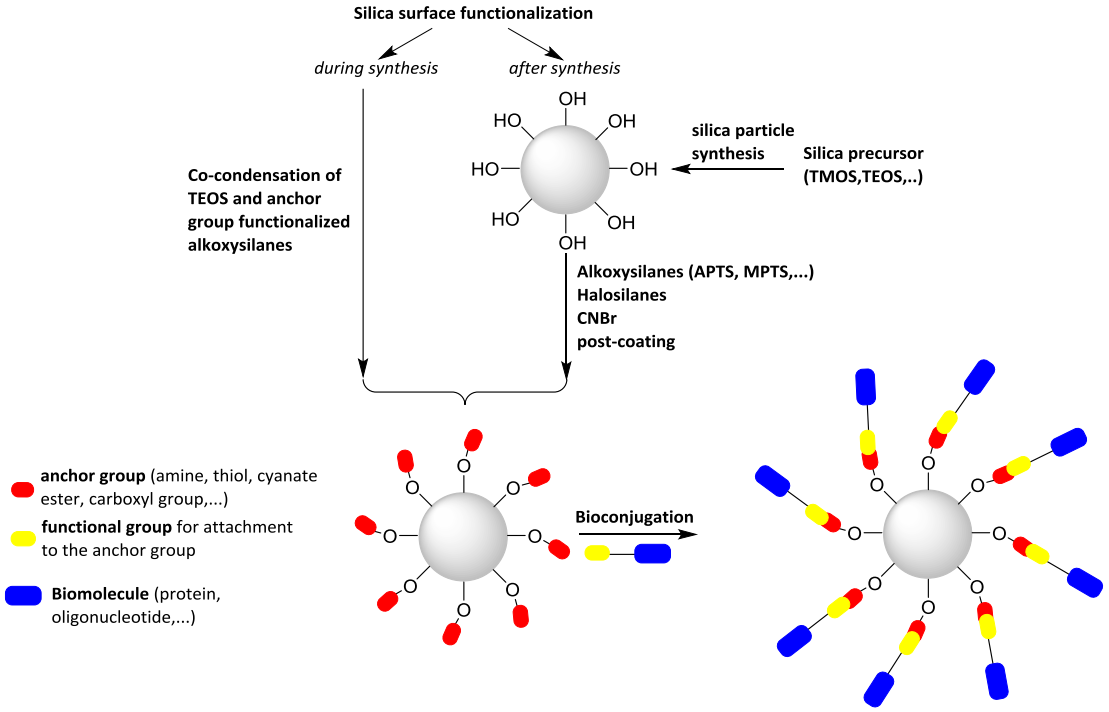

Figure 4: General overview of the strategies employed for the surface functionalization (and subsequent bioconjugation) of silica particles during and after synthesis

Silica particle surfaces can also be functionalized with thiol groups, which allow for the conjugation of biomolecules utilizing the formation of disulfide-bonds. Thiol groups can be incorporated into silica particles via mixing of MPTS with TEOS followed by co-hydrolysis or through silanization of newly synthesized silica nanoparticles with MPTS [41]. Following surface modification of silica particles with thiol groups, biomolecules containing disulfides, such as oligonucleotides, can then undergo conjugation to silica particles employing thiol-disulfide exchange reactions. [32]

In addition, silica particles and other inorganic materials can be surface-functionalized with polymers to produce non-aggregating organic-inorganic hybrid materials using different techniques. Methods that are frequently employed are chemisorption, covalent modification of an activated surface with polymers containing functionalized ends in a condensation reaction (grafting-to method) as well as polymerization from previously introduced initiating surface groups under the addition of monomers and co-initiators (grafting-from method). [42, 43] In the grafting-from technique, one or two initiating surface functionalities including azo-, peroxide- or photoinitiators are incorporated and after initiation, the polymer chains are elongated away from the surface with each step. Polymerization types that are utilized in the grafting-from approach include cationic [44] and anionic [45] polymerization, ring-opening polymerization [46], free radical polymerization [47], reversible addition fragmentation chain transfer polymerization [48], nitroxide-mediated radical polymerization and atom transfer radical polymerization [42, 43, 49].

Encapsulation of biomolecules in silica particles during and post synthesis

Functionalization of silica materials with biomolecules can not only be achieved by appropriate surface modification and covalent attachment of complementarily functionalized biomolecules, or by physical adsorption via electrostatic interactions, but also via physical encapsulation of these molecules in the silica material in the course of the sol-gel process. The use of silica for the encapsulation of biomolecules provides advantages over the utilization of polymers, which include controllable surface area and pore size, chemical stability of the material, optical transparency, absence of susceptibility to attacking by microbes and protection of biomolecules against external stressors such as changes in temperature or pH, thereby increasing their stability. In addition, encapsulation of biomolecules in silica results in a decrease in their susceptibility to leaching. [32] The entrapment of biomolecules including enzymes and antibodies in silica nanoparticles has been carried out using different methods such as the Stöber approach [50], the reverse micro-emulsion technique [51] or a tailored process consisting of only one step [52] involving conditions suitable for proteins. An example for enzyme encapsulation into silica nanoparticles was demonstrated in 1998 by Jain *et al*. [51], who performed entrapment of horseradish peroxidase into silica nanoparticles utilizing TMOS as a silica precursor, Triton-X-100 as a surfactant and employing the reverse micellar method which led to the formation of uniformly sized enzyme-modified silica nanoparticles with diameters below 100 nm. [32]

Mesoporous silica nanoparticles have been studied extensively as potential delivery vehicles for numerous biomolecules and can also be loaded with a variety of small molecules such as drugs. Loading is typically facilitated by physical adsorption as well as solvent evaporation. The physical adsorption technique was employed by Wang *et al* [53] who incubated mesoporous silica nanoparticles in a drug solution for a sufficient amount of time to establish an equilibrium and enable a deep diffusion of the drug molecules into the pores of the silica particles. The physical adsorption loading method can be combined with solvent evaporation [54], which later results in a faster drug release, as the molecules adsorbed on the exterior of the particle are immediately detached from the particle surface in the release medium, while significantly more time is required for the diffusion-mediated release of molecules that are located deep inside the pores of the mesoporous silica nanoparticles. In general, loading and release of the cargo molecules is affected by pore morphology and size as certain pore structures and sizes can increase or reduce diffusion hindrance. [55]

Functionalization of silica particles with fluorescent dyes

Silica particles can also be modified with fluorescent dyes for bioanalytical applications during or after particle synthesis and can encapsulate hundreds or thousands of inorganic or organic fluorescent dye

molecules to overcome disadvantages of commonly used fluorescent probes (including fluorescein isothiocyanate, rhodamine or cyanine dyes) such as low photostability and signal intensity. Therefore, silica nanoparticles that are modified with fluorescent dyes provide the advantage of intense fluorescence signals, improved photostability and their surfaces can additionally be functionalized with numerous biomolecules. The absorption and emission wavelengths of the fluorophores stay approximately the same as in the native fluorescent probes. Silica nanoparticles can be modified with fluorescent dyes via the encapsulation of these molecules in the production process of the nanoparticles or surface functionalization with fluorophores after the nanoparticle synthesis has been completed. The most common method for the generation of nanoparticles modified with hydrophobic fluorescent dyes is the Stöber technique, while hydrophilic fluorophores are mostly incorporated into the silica nanoparticles using the micro-emulsion approach. These fluorescent-modified particles have been shown to be applicable to various methods for fluorescence labelling such as DNA and protein microarrays, immunocyto- and –histochemistry as well as fluorescent linked immunosorbent assays. [32]

Attachment of small molecules and biomolecules to silica particles based on affinity binding

Biomolecules and small molecules such as fluorescent dyes can also be conjugated to silica particles utilizing the interaction between avidin or streptavidin and biotin. While avidin is a glycoprotein naturally occurring in egg white, streptavidin is a non-glycosylated protein that is found in *Streptomyces avidinii.* Both of these proteins possess a high binding affinity towards biotin, which is a small molecule that does not change the biological activity (e.g. binding of antibodies or catalytic activity in enzymes) of biomolecules it is attached to. The stability of the (strept)avidin-biotin complex is exceptional for a non-covalent interaction, with an affinity constant of 10^{15} $L \cdot mol^{-1}$ and the complex is therefore resistant against variations in pH or temperature, chaotropes or washing procedures of the immobilized complex. [56] Both avidin and streptavidin consist of four subunits, each of which contains one binding pocket for biotin. Avidin and streptavidin can be attached to silica particles via electrostatic interactions (at a pH below the pI of the protein) between avidin or streptavidin carrying a positive charge and the silica surface possessing a negative charge. The attachment of (strept)avidin to the silica surface is subsequently stabilized by the addition of a bifunctional glutaraldehyde functioning as a crosslinker. Silica particles can subsequently be modified with various biomolecules and fluorescent agents via biotin-(strept)avidin complex formation since biotinylated conjugates of many biomolecules including proteins, carbohydrates and nucleic acids are available for purchase. [32, 56]

1.2 Biomimetic synthesis of silica particles

1.2.1 Silica in living organisms

In addition to the chemical and physical synthesis methods, silica particles can also be produced by synthesis techniques inspired by natural biomineralization processes providing a variety of advantages explained in section 1.2.3. A wide variety of minerals is produced in such biomineralization processes by living organisms in nature such as amorphous and (organic or inorganic) crystalline minerals that fulfill numerous functions. [57-59] Approximately one half of all known minerals that are produced through biomineralization contain calcium, which is in agreement with the high abundance of calcium in the ocean. In addition to the biological function of calcium itself as a cellular messenger, calcium minerals such as calcium carbonate (calcite and aragonite) and calcium phosphate (dahllite) exhibit skeleton-stabilizing properties [58, 59]. Apart from crystalline calcium carbonate and phosphate, amorphous silica has also been shown to be involved in the generation of skeletons produced by

various different organisms including diatoms, unicellular protozoans native to the sea, sponges, radiolarians as well as higher plants. [59, 60] Biosilica formed by these organisms possesses diverse structural properties, densities and compositions. It can be encountered in different forms of appearance such as helical, tube-shaped, spherical, fibrillar and sheet-like structures depending on the corresponding organism. Biogenic siliceous structures found in nature also exhibit a great amount of diversity concerning their extent of structural organization, which ranges from siliceous nanometer-sized granules, which can be found in bacteria, to three-dimensional skeletal structures encountered in glass sponges native to the sea that exhibit a height of up to 2 m and width of up to 70 cm [61].

Many of the diverse organisms that possess the ability to produce biogenic silica are native to the sea. As the concentration of silicic acid in sea water is relatively low (10-180 µM [62]), marine organisms that produce silica must employ a strategy which allows for the uptake and accumulation of this compound to such an extent that the previously described polycondensation process (section 1.1.1) can occur. [63] While transport and polymerization of silicon is dependent on facilitation by enzymes in sponges [64], other organisms including radiolarians and diatoms generate siliceous frustules through the accumulation of aqueous monosilicic acid ($Si(OH)_4$), which can subsequently undergo polymerization, within the cell. [4, 65]

The frustule-forming diatoms are unicellular algae that exhibit lengths between 1 and 500 µm and can be encountered in various habitats [66, 67]. The exoskeleton of a diatom completely envelopes the organism and consists of silica in its amorphous state (exhibiting elaborate nanoscale patterning) that is associated with various proteins, long-chain polyamines (LCPAs) and polysaccharides. [60] Two different parts, termed the epitheca and the hypotheca, (Figure 5) constitute the diatom frustulum. Both parts comprise a valve, which represents the larger exterior surface of each half, which often possesses a plate-, dome or bowl-like shape, and several strips made of silica exhibiting circular shapes, which are referred to as girdle bands and represent the region where the two halves of the frustulum overlap (Figure 5 A and B). [67-69]

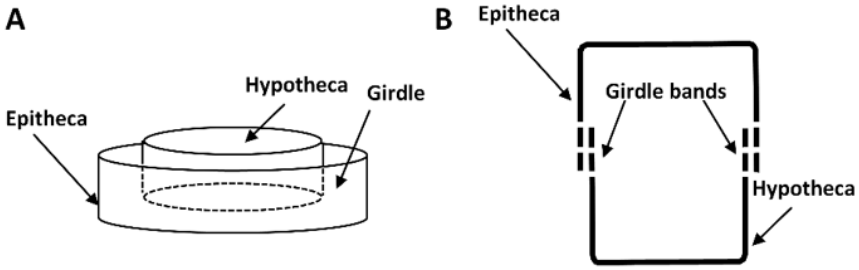

Figure 5: Schematic three-dimensional (A) and two-dimensional (B) representation of the two parts of a diatom frustulum (A adapted from [67], B adapted from [68])

In the course of the reproduction process of a diatom, the epitheca and the hypotheca separate and the organism produces new valves and girdle bands in subcellular compartments termed silica deposition vesicles (SDVs) that are positioned inside the cells and release the biomineral building blocks, which are then incorporated into the cell wall, via exocytosis [57, 69]. When silica is produced, the SDVs are located in the cytosol at the plasma membrane across from the part of the frustulum where the new biosilica building block will be inserted. [69] Although several factors have been identified as playing a role in the production of biogenic silica in diatoms, the mechanisms of biogenesis as well as exocytosis are still not elucidated for SDVs. [69, 70] In general, very little is known about membrane proteins in subcellular compartments responsible for biomineralization in eukaryotes. [69]

1.2.2 Silaffin proteins and peptides

In contrast to the lack of knowledge about membrane proteins of SDVs, three major types of proteins have been discovered as organic constituents in the frustulum of the diatom *Cylindrotheca fusiformis* [71]: frustulins [72], pleuralins [73, 74] and silaffins [75-79]. In addition to these protein families, long chain polyamines (LCPAs) have also been discovered in diatom frustules [77]. They are constituted by repeating *N*-methylpropylamine entities bound to putrescine or one of its derivatives (Scheme 4) [80].

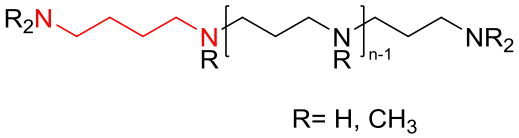

Scheme 4: General structure of LCPAs found in diatoms, putrescine shown in red (adapted from [80])

It has been shown that LCPAs located in and extracted from diatom cell walls mediate the generation of precipitated silica *in vitro* in an environment designed to simulate the native circumstances in the SDV via self-assembly facilitated by cross-linking through multivalent anions. [80-82]

Among the cell-wall associated proteins in diatoms, frustulins and pleuralins do not directly play a role in the precipitation of biogenic silica [72, 74, 82], which is in contrast to silaffins that have been shown to be strongly involved in silica biomineralization processes. Extraction of silaffins from diatom cell walls with anhydrous HF yielded a low molecular weight fraction of polypeptides with masses between 4 and 17 kDa [75]. The 17 kD polypeptide was named silaffin-2, another one with a mass of 8 kDa was termed silaffin-1B and a third one possessing a molecular weight of 4 kDa was named silaffin-1A [75, 82]. *N*-terminal sequence information from silaffin-1B facilitated cloning of the sil1 gene, which encodes the precursor for silaffin polypeptides, sil1p. The *N*-terminal part of sil1p is constituted by a domain possessing a high amount of negative charges from acidic amino acid residues (amino acids 20-107, Figure 6) following a characteristic signal peptide sequence (amino acids 1-19, shown in red in Figure 6).[75, 82]

```
          MKLTAIFPLLFT    12
      AVGYCAAQSIADLAAANLS    31
      TEDSKSAQLISADSSDDAS    50
      DSSVESVDAASSDVSGSSV    69
      ESVDVSGSSLESVDVSGSS    88
      LESVDDSSEDSEEEELRIL    107
R1    SSKKSGSYYSYGTKK        122
         SGSYSGYSTKKSASRRIL  140
R2    SSKKSGSYSGYSTKKSGSRRIL 162
R3    SSKKSGSYSGSKGSKRRIL    181
R4    SSKKSGSYSGSKGSKRRNL    200
R5    SSKKSGSYSGSKGSKRRIL    219
R6    SSKKSGSYSGSKGSKRRNL    238
R7    SSKKSGSYSGSKGSKRRIL    257
      SGGLRGSM               265
```

Figure 6: Amino acid sequence of the silaffin-precursor polypeptide sil1p. The signal peptide on the N*-terminal part of sil1p is highlighted in red and the* C*-terminal part with the repeat units R1-R7 is depicted in bold. The clustered lysine residues in the* C*-terminal part of the protein are highlighted in grey. (adapted from [82])*

The *C*-terminal part of the sil1p protein (amino acids 108-265) is constituted by two long repeat units, R1 (33 amino acids, residues 108-140) and R2 (22 amino acids, residues 141-162), as well as five shorter repeat entities (R3-R7), consisting of 19 amino acids each. All repeat units are composed of small groups of basic lysines and arginines linked via amino acids containing hydroxyl groups (serine and tyrosine) and glycine residues. The *C*-terminal repetitive section of the protein undergoes proteolysis *in vivo,* which results in the liberation of each repeat section (R1-R7) as a peptide with the corresponding sequence. While silaffin-1B originates from the R1 repeat section, silaffin-1A is

composed of a mixture of peptides resulting from repeat units R2-R7. [75, 82] The four amino acids located on the *C*-terminus of each repeat section are removed during proteolysis which results in the generation of identical peptides derived from repeat units R3-R7, consisting of 15 amino acids each. As a result, silaffin-1A is a combination of only two different peptides, silaffin-$1A_1$ and silaffin-$1A_2$. Silaffin-2 is not derived from the sil1 gene. [75, 82]

The native forms of silaffins, termed natSil-1A, natSil-1B and natSil-2, include posttranslational modifications on serine and lysine residues, which were cleaved off in the extraction with anhydrous HF, but can be retained via extraction with slightly acidic ammonium fluoride. [78, 82] The native structure of natSil-1A is depicted in Scheme 5. [78, 82]

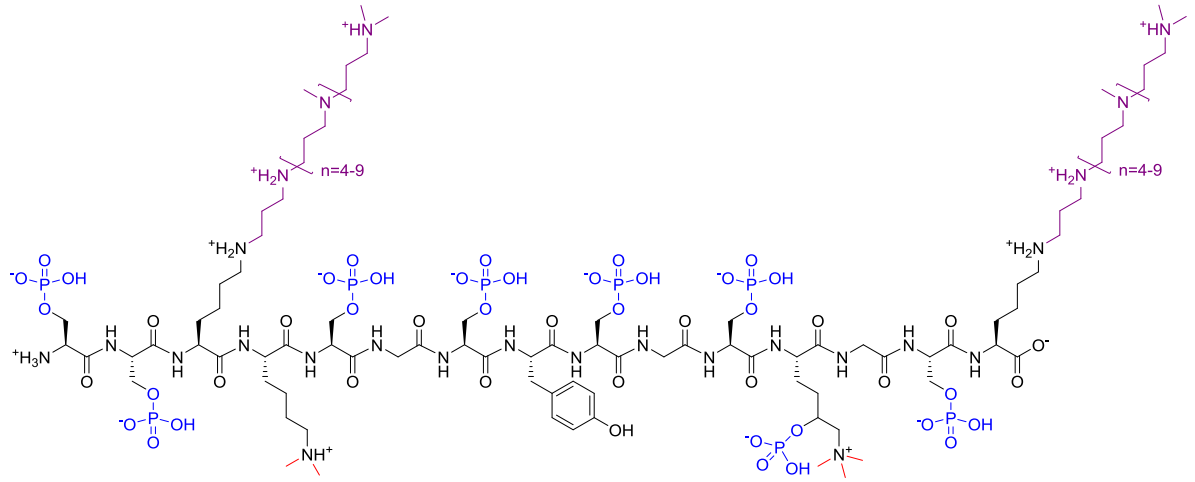

Scheme 5: Complete structure of natSil-1A extracted from the Cylindrotheca fusiformis *cell wall (annotation of charges for a solution at pH 5). The native posttranslational modifications are highlighted in different colors: blue for phosphorylation, red for methylation and purple for the polyamine modification (adapted from [78])*

The structure of natSil-1A is characterized by positive charges on the differently modified lysine residues and negative charges introduced via phosphate groups, which both contribute to the zwitterionic nature of natSil-1A, which affects its biological and chemical properties. [82] Previous experiments have indicated that all types of posttranslational modifications found in native silaffins contribute to their silica precipitating activity. [78] It has been suggested that the tendency of natSil-1A to self-assemble (facilitated via its PTMs) is the basis of the silica-precipitating activity of silaffins as these aggregates presumably act as templates for polycondensation of silicic acid species and that the silaffins co-precipitate with the produced silica. [76, 78] An inhibition of silaffin-mediated silica formation in the absence of phosphate groups probably occurs as a result of natSil-1A without phosphorylation being a highly positively charged peptide and losing its tendency to form aggregates due to electrostatic repulsion. However, if phosphate anions are added to the solution, they possibly function as ionic crosslinkers that facilitate assembly of highly positively charged silaffin-1A molecules and reestablish the silica-precipitating function of silaffin-1A. [78, 82]

The synthetic R5 peptide is constituted by the same amino acids in the same order as in repeat section R5 of the silaffin precursor sil1p (Figure 6) and possesses no posttranslational modifications. [75, 83] R5 peptide-facilitated silica-formation hypothetically takes place via the same mechanism that was proposed for silica precipitation mediated by silaffins, which occurs via self-aggregation of the peptide and the formed aggregates then act as templates for polycondensation of silicic acid species. The generation of the siloxane (Si-O-Si) bonds is facilitated by amino groups that are present in the lysine residues themselves or, in the case of native silaffins, in their polyamine modifications (Figure 7). In contrast to native silaffins that possess phosphorylations as posttranslational modifications on their

serine residues, the addition of polyvalent anions such as phosphate is a prerequisite for the silica precipitation activity of silaffin peptides lacking those modifications, such as the R5 peptide, as the self-assembly of natively modified silaffins requires electrostatic interactions between the negatively charged phosphate groups and the protonated and positively charged amine moieties. [75, 78, 84, 85]

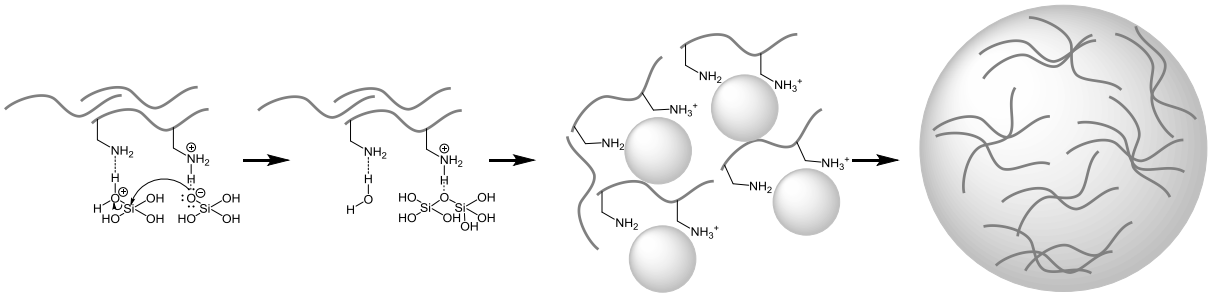

Figure 7: Proposed mechanism for silica polycondensation mediated by the R5 peptide (adapted from [84])

The amine groups within the assemblies likely function as acid-base catalysts (Figure 7), with deprotonated amine groups receiving a proton from silicic acid, thereby functioning as bases and generating negatively charged silanolate groups, while protonated amines might act as acids and provide the driving force for the liberation of water through the protonation of silicic acid species. [86] Furthermore, the areas on the surface of the peptide structure carrying positive charges might exhibit electrostatic interactions with growing silica seeds possessing negative charges causing the entrapment of the peptide within the silica. [86] The structure and morphology of silica produced by different silica precipitating agents is dependent on the nature of the silicifying biomolecule and the specific reaction conditions and ranges from spherical particles to sheet-like precipitates. [75, 87, 88]

1.2.3 Advantages of the biomimetic synthesis and applications of silica particles

As described above, the discovery of proteins and other molecules originating from biominerals, possessing diverse structures and properties as well as being associated with the production of biominerals, has inspired researchers to design biomimetic syntheses of minerals utilizing these compounds and the different roles they play in biomineralization *in vivo*. Various biomolecules with biomineralization activity have successfully been expressed from *Escherichia coli* including silaffins [89]. In addition to the expression of proteins obtained from full-length genes, the sil1 gene has been produced in differently truncated versions for the expression of shorter peptides with biomineralization activity including the R5 peptide. [75, 80, 86, 90]

Production of silica via biomimetic synthesis rather than chemical synthesis provides a variety of advantages such as control over the rate of silica condensation and growth, different structures and morphologies (including spherical particles, fibrillar structures, films and sheet-like structures, hollow tubes and particles as well as porous gels), particle sizes and porosities. In contrast to traditional synthesis of silica materials, which often has to be carried out under extreme temperatures, pH values and pressure [91], biomimetic synthesis allows for fine-tuned silica production under mild synthesis conditions such as ambient temperature, in aqueous solutions and at around pH 7, which can lead to a decrease in process expenses and is less damaging to the environment [6]. In addition, the processing conditions of biomimetic silica production facilitate the generation of organic-inorganic hybrid materials of silica with, for example, peptides [5], proteins and enzymes [92-96], low molecular-weight

compounds (such as fluorescent dyes [97] or drugs [98]), (bio)polymers [99] and quantum dots [100]. [101]

In principle, hybrid materials of silica with some of the organic compounds listed above can be produced in a non-biomimetic approach via the sol-gel method [102], which can be carried out with organic additives, or by utilizing silica precursors with appropriate organic functionalities for the sol-gel process. However, incompatibility of this technique with biomolecules including proteins and enzymes and viable materials such as cells is caused by the required acidic pH values, silica precursors possessing a high reactivity as well as denaturation of biomolecules in the course of size-reduction of materials as a result of drying. [101]

Silica (nano)materials are utilized in a wide variety of application fields due to their surface properties, possibility to modify and functionalize the surfaces with biomolecules or small molecules as well as encapsulation of these compounds in silica particles and easy, inexpensive and quick synthesis. Other advantageous features of silica (nano)particles include their high specific surface area and low density. [103] Biomimetic synthesis of silica materials in particular has facilitated the incorporation of silica materials with high physicochemical stability into biotechnology as well as biomedicine (including applications such as entrapment of enzymes for biocatalysis [104], imaging [105], biosensing [106] or delivery and tunable release of drugs [105, 106]) [84] Applications of silica particles in general include, among many others, the immobilization and purification of proteins, detection and separation of DNA and RNA, delivery vehicles for genes and cargo molecules such as drugs, targeting of cells, immunoassays, biosensors, imaging as well as pharmaceutical applications. [32, 103] The most commonly used types of silica nanoparticles for the delivery of drugs are mesoporous silica nanoparticles. Drugs can be loaded into their pores and kept inside by the utilization of gold or CdS [107] nanoparticles as gatekeepers (caps). Through this technique, release of the drugs can be controlled precisely as the CdS nanoparticles can be removed from the pores of the mesoporous silica nanoparticles through the reduction of previously formed disulfide bonds via the addition of reducing agents such as dithiothreitol or mercaptoethanol [103]. Although among silica-based materials, mesoporous silica nanoparticles are the most commonly used agents for drug delivery and release, biomimetic synthesis conditions provide advantages including a pH of around 7, ambient temperature as well as incorporation of cargo molecules in the course of silica precipitation and could therefore be employed in the synthesis of delivery vehicles for various cargo molecules. [5] In the case of biomimetic silica particles produced employing the R5 peptide as a template for silicic acid polycondensation, it has been shown that attachment of a fluorescent dye to the *N*-terminus of the R5 peptide resulted in the formation of silica particles with a homogeneous distribution of this cargo molecule [108]. The attachment of other types of cargo molecules to the R5 peptide and encapsulation of these molecules in silica particles during silica precipitation can be achieved via covalent bonds such as disulfide linkages which provide the option of controlled release of the attached molecules by cleavage of the disulfide bond employing reducing conditions. Additionally, it has been shown that the R5 peptide, which undergoes co-precipitation during silica precipitation, can be released from the silica particles when they are resuspended in buffers such as sodium acetate buffer (pH 5) or PBS (pH 7.4) and higher release rates are observed at pH 5, which indicates that the release of the R5 peptide is pH-dependent. [5]

Further applications of silica nanoparticles include functioning as antigen carriers and vaccine adjuvants, which are designed to promote the activation of antigen-presenting cells, which results in the generation of a strong immune response. [109] Properties such as the structure of the particles and proteins, the extent to which the particles can bind proteins, conformation and concentration of

proteins, charges on the exterior surfaces of particles and proteins, release of the proteins from the particles as well as uptake of protein-particle-conjugates by M-cells and antigen-presenting cells seem to determine whether or not these functionalized mesoporous silica nanoparticles are suitable as vaccine adjuvants and potentiate immune responses [110-113]. The incorporation of protein-based antigens into a mesoporous silica particle acting as a delivery vehicle and depot for these protein-antigens is mediated by adsorption or physical entrapment of the biomolecules. [109]

1.3 Aims of this project

In this project, we aim to evaluate the display and binding accessibility of the *N*- and *C*-terminus of the R5 peptide in silica particles generated according to a biomimetic approach using the R5 peptide as a silica precipitating agent (as described in section 1.2.2, Figure 7). An accessible and appropriately modified *N*- or *C*-terminus of the peptide on the particle surface could provide a site for (surface) modification of the silica particles and attachment of complementarily modified cargo molecules. This would potentially provide a new method for the use of such particles as delivery agents. In our project, the high-affinity interaction between biotin and (strept)avidin will be employed for the investigation of the accessibility of the *N*- and *C*-terminus of the R5 peptide, as an exposed and accessible *N*- or *C*-terminal biotinylation of the R5 peptide on the particle surface should result in the binding of (strept)avidin conjugates. The corresponding conjugates that will be used are avidin-sulforhodamine 101 (binding detectable via UV-Vis absorbance measurements) and a streptavidin-gold nanoparticle conjugate (binding detectable via TEM imaging).

Furthermore, this project aims at the development of a suitable biomimetic synthesis method for bifunctional silica particles. Depending on the types of modifications, such doubly modified silica particles could be utilized for different types of applications. Potential applications include use of the particles as vehicles for simultaneous delivery of two different cargo molecules such as proteins and fluorescent probes or vehicles for targeted delivery of cargo molecules (if a targeting agent is introduced in addition to the cargo). Additionally, bifunctional silica particles could possibly be used as vaccine adjuvants if the modifications introduced comprise an antigen and a pathogen-associated signal molecule designed to stimulate an innate immune response.

In the achievement of this dual modification of silica particles, the use of a biomimetic synthesis approach of silica particles employing the R5 peptide as a precipitation promoting agent is favourable as it provides a variety of advantages over other types of silica materials such as mesoporous silica particles. These advantages include the possibility to generate silica particles under conditions suitable for sensitive biomolecules (pH around 7, ambient temperature), as well as simultaneous entrapment of these cargo molecules in the silica particles during the precipitation. [5] First, the effect of the pH as well as peptide concentrations, TMOS or TEOS concentrations on the precipitates obtained from the biomimetic synthesis approach using the R5 peptide will have to be investigated to determine if the morphology of the precipitates can be influenced by variations in these parameters. This knowledge will help to establish optimal synthesis conditions for smooth spherical particles. Using this biomimetic synthesis method, one of the two desired modifications will be attached to the *N*-terminus of the R5 peptide, which becomes entrapped in the silica particles in the course of the precipitation. The second modification will be introduced via the use of an appropriately modified silica precursor. In contrast to an introduction of a second modification into the R5 peptide (on the *C*-terminus or the *N*-terminal cysteine of the R5 variant containing this residue), this will provide the advantage that this functionality is independent from release of the R5 peptide from the particles as it is incorporated into the silica material itself. To investigate the applicability of this approach towards the generation of doubly

modified silica particles, the described biomimetic approach will be employed using an R5 peptide variant with an *N*-terminal cyanine-5 modification and a fluorescein-modified silica precursor (triethoxysilyl fluorescein).

2. Materials and Methods

2.1. General

2.1.1 Preparation of SEM samples

For imaging via scanning electron microscopy (SEM), the silica precipitates were applied onto Thermanox™ coverslips and dried on air. A layer of gold was subsequently applied to all samples by sputter coating in high vacuum (Bal-Tec SCD 005) and SEM imaging was performed with a Zeiss SEM supra 55 VP at 20 kV.

2.1.2 Preparation of TEM samples

For imaging via transmission electron microscopy (TEM), the silica precipitates were applied onto a copper grid equipped with a carbon layer and looked at via a Philips CM200 at 200 kV. Images of the precipitates were taken using an Orius™ SC600 Gatan CCD camera.

2.1.3 UV-Vis measurements

UV-Vis measurements were performed on a Nanodrop 2000C spectrophotometer with 100 µl of sample solution in micro-cuvettes suitable for UV-Vis measurements. For all measurements, UV-Vis spectra were recorded between 190 and 840 nm using a path length of 10 mm. Solutions with the same composition as the samples to be measured but without the particular analyte were used as blanks in all cases.

2.1.4 Cell imaging and Fluorescence Microscopy

Silica particles with and without cells were imaged (bright field images and images visualizing the fluorescent dyes fluorescein, cyanine-5, Hoechst 33258 (DNA stain), Alexa Fluor 594 (lysosome stain) and sulforhodamine 101) using the BioTek™Cytation™3 Cell Imaging Multi-Mode Reader at magnifications of 4 times or 20 times. Excitation and emission wavelengths for the fluorescent dyes are given in Table 1.

Table 1: Excitation and emission wavelengths for the fluorescent dyes used in cell studies or avidin-biotin binding experiments

Fluorescent dye	Excitation wavelength [nm]	Emission wavelength [nm]
Fluorescein	495	525
Cyanine-5	620	670
Hoechst 33258	352	461
Alexa Fluor 594	550	590
Sulforhodamine 101	561	615

Cells were stained using a staining solution consisting of 0.1 % (v/v) Hoechst 33258 and 0.1 % (v/v) Alexa Fluor 594 in live cell imaging solution from Thermo Fisher Scientific (140 mM NaCl, 2.5 mM KCl, 1.8 mM $CaCl_2$, 1.0 mM $MgCl_2$, 20 mM HEPES, pH 7.4). Prior to staining, the medium was aspirated from the cells, before 500 µl of staining solution were added to each well containing cells to be stained and the cells were subsequently incubated at 37°C and 5% CO_2 for 30 minutes. The staining solution was then removed and the cells were washed with 500 µl live cell imaging solution per well once before 500 µl of the same solution were added to each well for live cell imaging.

2.2 Investigation of silica particle binding to (strept)avidin conjugates 8 and 9

2.2.1 Synthesis and purification of 3

2.2.1.1 *Synthesis*

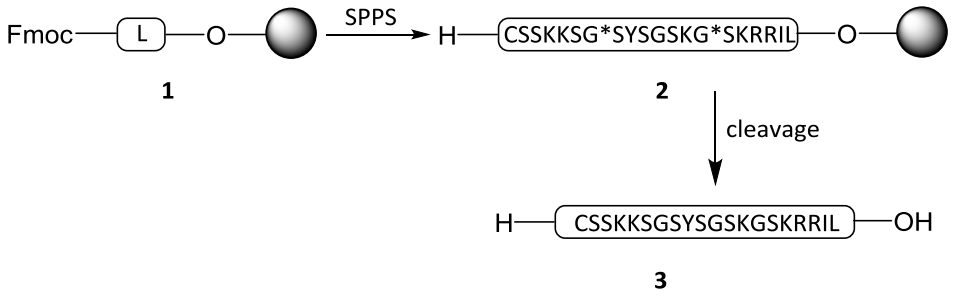

Scheme 6: Schematic representation of the synthesis procedure of the Cys-R5L peptide (compound 3)

The synthesis of peptide **3** (sequence given in Scheme 6) was carried out manually in a 10 ml syringe using fluorenylmethoxycarbonyl (Fmoc) chemistry on a 0.05 mmol scale. 156.3 mg (0.05 mmol) of Wang-resin (substitution level: 0.32 mmol/g, Fmoc-Leu-Wang LL resin), preloaded with leucine, were swollen in DMF for 30 minutes prior to the start of peptide synthesis. Fmoc-deprotection was achieved by the addition of 4 ml 20 % piperidine in DMF for 3 minutes (with occasional stirring), followed by washing of the resin 3 times with 8 ml DMF and addition of another 4 ml 20 % piperidine in DMF for 10 minutes (occasional stirring). After Fmoc deprotection, the resin was thoroughly washed 3 times with 8 ml DMF. 3 eq of Fmoc-protected amino acid (amounts given in Table 2) were dissolved in 2.5 eq HATU (250 µl of a 0.5 M solution of HATU in DMF), 10 eq (85 µl) of DIEA were added and the mixture was incubated at RT for 3 minutes before it was diluted to 1 ml with DMF and the activated amino acid was added to the resin for 20 minutes (with occasional stirring). After completion of the coupling step, the resin was washed 3 times with 8 ml DMF before the next deprotection cycle. Deprotection and coupling cycles were performed in this manner alternatingly until the last amino acid was coupled. The type of amino acids (type of side-chain protecting groups) used, their molecular weights and the required amounts are denoted in Table 2.

*Table 2: Specific amino acids used for the synthesis of **3**, their abbreviations, molecular weights and required amounts for 3 eq.*

Amino acid	Abbreviation[a]	Molecular weight [g/mol]	Amount required for 3 eq (0.15 mmol) [mg]
Fmoc-Cys(Trt)-OH	C	585.70	87.9
Fmoc-Ser(tBu)-OH	S	383.44	57.5
Fmoc-Lys(Boc)-OH	K	468.54	70.3
Fmoc-Tmb-Gly-OH[b]	G*	477.51	71.6
Fmoc-Tyr(tBu)-OH	Y	459.53	69.0
Fmoc-Arg(Pbf)-OH	R	648.77	97.3
Fmoc-Ile-OH	I	353.41	53.0
Fmoc-Gly-OH	G	297.31	44.6

[a] abbreviation of the amino acid after incorporation into the peptide (Scheme 6)

[b] Two Fmoc-Tmb-Gly-OH building blocks were used in the synthesis, because electron-rich benzyl groups such as Tmb are suitable for backbone amide protection, which prevents backbone N-H from participating in aggregation and β-sheet formation of resin-bound peptides. Such electron-rich benzyl groups are cleaved during final TFA cleavage of the peptide from the resin. Disruption of on-resin

peptide aggregation is important as it interferes with Fmoc-deprotection and amino acid coupling cycles in the course of the peptide synthesis. [114]

When the coupling of the last amino acid was complete, the last Fmoc group was removed and the resin was washed several times with DMF and subsequently with DCM and MeOH. A fifth (0.01 mmol) of resin was transferred into a new syringe and the side chain protecting groups as well as the Tmb groups were removed when the peptide was cleaved from the resin via the addition of 1 ml cleavage solution (95 % TFA, 2.5 % TIPS, 2.5 % H_2O) and rotation for 2 hours. The peptide was then precipitated by the addition of 8 ml ice-cold diethyl ether to the peptide solution and centrifuged (4 °C, 5 min, 5400 rpm), before the pellet was washed with ice-cold diethyl ether, dried under argon, dissolved in 5 ml buffer A (H_2O with 0.1 % TFA) and lyophilized.

2.2.1.2 Purification

Per purification run, 9.2 mg of crude **3** were dissolved in 10 ml 5 % buffer B (ACN with 0.1 % TFA) in buffer A (H_2O with 0.1 % TFA). An analytical run of the crude was performed on an analytical Kromasil C18 RP-HPLC column using a gradient of 5 % buffer B in buffer A to 65 % buffer B in buffer A over 10 minutes at a flow rate of 1 ml/min. The peptide was then injected for purification on the Waters HPLC-MS auto purification system on a Kromasil C18 semi preparative RP-HPLC column using a gradient of 5 % buffer B in buffer A to 45% buffer B in buffer A over 30 minutes at a flow rate of 10 ml/min. The fractions of the peptide were collected by monitoring the two most abundant m/z peaks from the analysis. Based on the observed purity, the fractions were combined and lyophilized.

For final analysis, purified **3** was dissolved in buffer A (H_2O with 0.1 % TFA) at a concentration of 2 mg/ml and 0.03 mg of peptide were injected for RP-HPLC analysis on a Dionex Ultimate 3000 HPLC system with an analytical Kromasil C18 RP-HPLC column using a gradient of 5 % buffer B (ACN with 0.08 % TFA) in A to 65 % buffer B in A over 40 minutes at a flow rate of 1 ml/min and UV-Vis measurement at a wavelength of 214 nm to monitor elution of the peptide. In addition, the purified peptide was dissolved in buffer A at a concentration of 2 mg/ml and 0.03 mg **3** were directly injected into the Thermo Fisher HPLC-MS system. (RP-HPLC chromatogram and mass spectrum shown in Figure 9 in section 3.1.1)

2.2.2 Synthesis and purification of 4

2.2.2.1 Synthesis (Biotin coupling)

The synthesis of peptide **4** was carried out via the coupling of Biotin-oxysuccinimide (Biotin-OSu) to the *N*-terminus of resin-bound peptide **3** (compound **2**) under the addition of HOBt (Scheme 7).

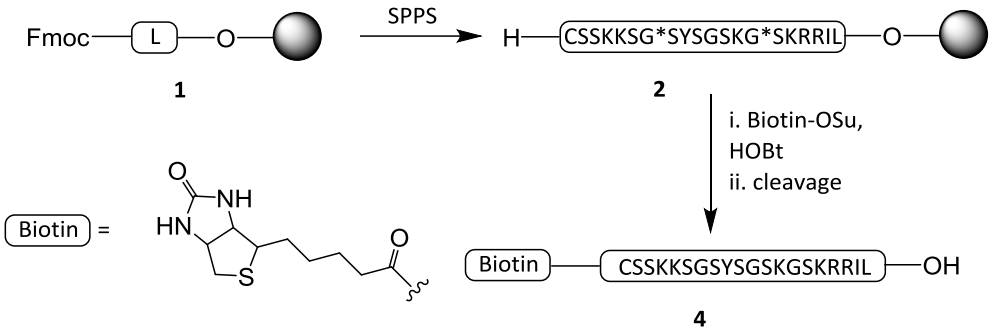

*Scheme 7: Scheme for the synthesis of **4** via the addition of Biotin-OSu and HOBt to compound **2***

The synthesis of compound **2** was carried out as described in section 2.2.1.1. A tenth (0.005 mmol) of the resulting amount of dried compound **2** was transferred into a new syringe and swollen in NMP for one hour prior to the coupling of Biotin-OSu. 8 eq Biotin-OSu (0.04 mmol, 13.6 mg) were dissolved in

416 µl of NMP (0.096 mM solution) and added to 4 eq HOBt (0.02 mmol, 2.7 mg). The mixture was then added to the resin and rotated overnight. Afterwards, the resin was washed with DMF and DCM prior to treatment with 1 ml cleavage solution (95 % TFA, 2.5 % H_2O, 2.5 % TIPS) for 2 hours. The peptide was precipitated by addition of 9 ml ice-cold diethyl ether, centrifuged (5 min, 4°C, 5400 rpm) and washed with ice-cold diethyl ether before it was dried under argon, dissolved in 2.5 ml 10 % buffer B (ACN with 0.1 % TFA) in buffer A (H_2O with 0.1 % TFA) and lyophilized.

2.2.2.2 Purification

For purification, 9.2 mg of crude **4** were dissolved in 10 ml 5 % buffer B (ACN with 0.1 % TFA) in buffer A (H_2O with 0.1 % TFA). An analytical run of the crude peptide was carried out on an analytical Kromasil C18 RP-HPLC column using a gradient of 5 % buffer B in A to 65 % buffer B in A over 10 minutes at a flow rate of 1 ml/min. The peptide was subsequently injected for purification on the Waters HPLC-MS auto purification system on a semi-preparative Kromasil C18 RP-HPLC column using a gradient of 5 % buffer B in A to 45 % buffer B in A over 30 minutes at a flow rate of 10 ml/min. The peptide fractions were collected based on the two most abundant m/z peaks from the analytical run and combined based on their purity.

For a final analysis of **4**, the purified peptide was dissolved in buffer A (H_2O with 0.1 % TFA) at a concentration of 2 mg/ml and 0.02 mg were injected for HPLC-MS analysis, which was carried out on the Thermo Fisher HPLC-MS system using an analytical Kromasil C4 RP-HPLC column and a gradient of 5 % buffer B (ACN with 0.05 % TFA) in buffer A (H_2O with 0.05 % TFA) to 65 % buffer B in A over 20 minutes at a flow rate of 1 ml/min (chromatogram in Figure 11 A, section 3.1.2) with monitoring of the UV-Vis absorbance at 214 nm starting at 6 minutes after injection of the sample. Additionally, the purified peptide was dissolved in buffer A (H_2O with 0.1 % TFA) at a concentration of 2 mg/ml and 0.02 mg were directly injected into the Thermo Fisher HPLC-MS system (mass spectrum shown in Figure 11 B, section 3.1.2).

2.2.3 Synthesis and purification of **7**

2.2.3.1 Synthesis

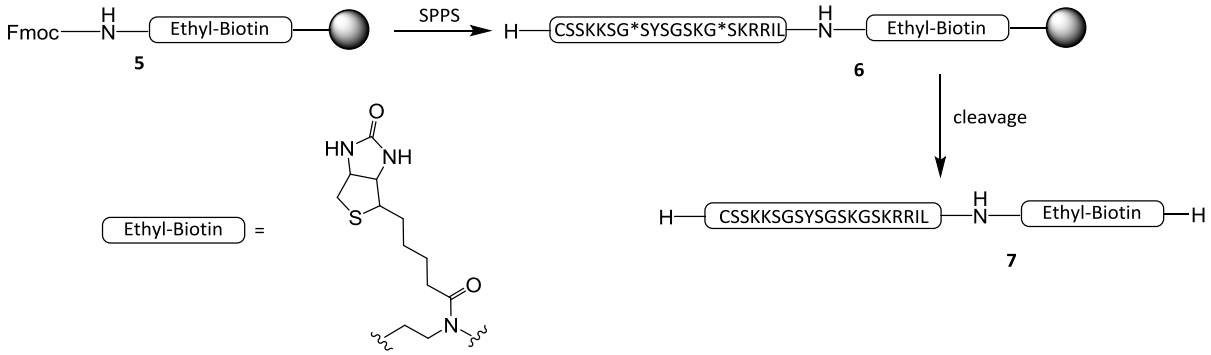

*Scheme 8: Scheme for the synthesis of **7** using SPPS and starting from Fmoc-Biotin-NovaTag resin*

The synthesis of **7** (sequence given in Scheme 8) was performed manually in a 5 ml syringe employing Fmoc chemistry on a 0.02 mmol scale. 32.8 mg of Fmoc-Biotin-NovaTag resin (substitution level 0.61 mmol/g) were swollen in DMF overnight prior to synthesis. The Fmoc group was cleaved from the resin using the conditions described in section 2.2.1.1. As the Biotin-NovaTag resin was not preloaded, the first amino acid coupled was leucine. The same amino acid coupling and Fmoc deprotection conditions were used as described for the synthesis of **3** in section 2.2.1.1 and the same Fmoc amino acids were used as shown in Table 2. After removal of the last Fmoc group, the resin was washed with DMF, DCM and MeOH and a fourth (0.005 mmol) was treated with 1 ml cleavage solution (90 % TFA, 2.5 % TIPS,

2.5 % H_2O and 5 % DMS) for 2 hours. The peptide was then precipitated by addition of 8 ml ice-cold diethyl ether to the peptide solution and centrifuged (5 min, 4°C, 5400 rpm). The pellet was washed with 8 ml ice-cold diethyl ether and subsequently dried under argon before it was dissolved in 2 ml 10 % buffer B (ACN with 0.1 % TFA) in A (H_2O with 0.1 % TFA) and lyophilized.

2.2.3.2 Purification

Crude peptide **7** was purified in 1 mg portions on a Dionex Ultimate 3000 HPLC system. For each purification run, 1 mg of peptide was dissolved in 100 µl 5 % buffer B (ACN with 0.08 % TFA) in buffer A (H_2O with 0.1 % TFA). Prior to the first purification run, an analytical run was carried out using an analytical Kromasil C4 RP-HPLC column with a gradient of 5 % buffer B in A to 65 % buffer B in A over 40 minutes at a flow rate of 1 ml/min. The purification runs were carried out on the same column using the same gradient and flow rate. Collection of the fractions was performed manually and they were combined based on purity assessed by HPLC-MS analysis on the Thermo-Fisher HPLC-MS system with an analytical Kromasil C4 RP-HPLC column using a gradient of 5 % buffer B (ACN with 0.05 % TFA) in buffer A (H_2O with 0.05 % TFA) to 65 % buffer B in A over 20 minutes at a flow rate of 1 ml/min. The combined pure fractions were lyophilized.

For final analysis of purified **7**, the purified peptide was dissolved in buffer A (H_2O with 0.1 % TFA) at a concentration of 2 mg/ml and 0.03 mg of peptide were injected for RP-HPLC analysis on a Dionex Ultimate 3000 HPLC system using an analytical Kromasil C4 RP-HPLC column and a gradient of 5 % buffer B (ACN with 0.08 % TFA) in buffer A (H_2O with 0.1 % TFA) to 65 % buffer B in A over 30 minutes at a flow rate of 1 ml/min. The UV-Vis absorbance was monitored at 214 nm (chromatogram depicted in Figure 13 A in section 3.1.3). Furthermore, the purified peptide was dissolved in buffer A at a concentration of 2 mg/ml and 0.03 mg were directly injected into the Thermo Fisher HPLC-MS system (mass spectrum shown in Figure 13 B in section 3.1.3).

2.2.4 Biomimetic silica precipitations with 3, 4 or 7 and TMOS

0.1 mg of **3, 4** or **7** were incubated at 1 mg/ml in 50 mM potassium phosphate buffer (pH 7) at RT for 24 hours. Afterwards, silicic acid was freshly prepared by hydrolysis of 270 mM TMOS in 1 mM HCl at RT for 4 minutes and subsequently added to the solutions of **3, 4** or **7** at a final concentration of 25 mM. The precipitations were allowed to proceed for 30 minutes at RT before the suspensions were centrifuged (RT, 3 min, 14 000 rpm) and the precipitates were washed twice with 200 µl H_2O each. Finally, the precipitates were resuspended in H_2O at a concentration of 1 mg/ml for the preparation of TEM and SEM samples as described in section 2.1.2 and 2.1.1.

2.2.5 Investigation of silica particle binding to streptavidin-gold nanoparticle conjugate 8

2.2.5.1 General experimental conditions for the binding of compound 8 to biomimetically generated silica particles containing 3, 4 or 7

The biomimetic silica precipitations with **3**, **4** or **7** and TMOS were carried out as described in section 2.2.4. After washing, the precipitates were resuspended in 50 mM potassium phosphate buffer (pH 7) at a concentration of 2 mg/ml. Compound **8** (10 or 20 µl, streptavidin-gold nanoparticle conjugate with streptavidin from *Streptomyces avidinii* with 20 nm gold particle size, suspended in 50 mM potassium phosphate buffer (pH 7.4) with 75 mM NaCl and 20 % glycerol, absorption (520 nm) ≤ 3.0) was added directly to the resuspended silica particles (0.02 mg). Alternatively, compound **8** (10 or 20 µl) was washed 1 to 5 times with 50 mM potassium phosphate buffer (pH 7), resuspended in 10 µl 50 mM potassium phosphate buffer (pH 7) and sonicated for 5 minutes prior to addition of **8** to different amounts of silica precipitates (2 mg/ml, 0.02-0.08 mg precipitate). The silica precipitates were

incubated with compound **8** at RT for 10 minutes or 1 hour before they were directly applied to the SEM coverslips or TEM copper grids (as described in section 2.1.1 and 2.1.2) or centrifuged (RT, 3 min, 14 000 rpm), washed with 100 µl H_2O and finally resuspended in 100 µl H_2O for SEM and TEM sample preparation as described in section 2.1.1 and 2.1.2. The specific combinations of conditions used for each experiment are outlined in the results section.

2.2.6 Investigation of silica particle binding to avidin-sulforhodamine 101 conjugate 9

2.2.6.1 General experimental conditions for the binding of compound 9 to the biomimetically generated silica particles containing 3, 4 or 7

Biomimetic precipitations for the preparation of silica particles containing **3**, **4** or **7** with TMOS were carried out as described in section 2.2.4. After washing, the precipitates were incubated in 50 mM potassium phosphate buffer (pH 4 or 7) at particle concentrations of 2 mg/ml for 24 hours at RT, subsequently centrifuged (RT, 3 min, 14 000 rpm), washed twice with 100 µl 50 mM potassium phosphate buffer (pH 7) and then resuspended in solutions of compound **9** in 50 mM potassium phosphate buffer (pH 7) at concentrations of conjugate **9** of 0.083 mg/ml or 0.088 mg/ml (silica particle concentrations of 1 mg/ml) and incubated at RT for 1.5 hours.

Alternatively, the precipitates containing **3**, **4** or **7** were prepared as described in section 2.2.4 and directly incubated in an aqueous solution of compound **9** (0.025-0.1 mg/ml compound **9**, 1 mg/ml particle concentration) for 1.5 hours at RT. In all experiments, after incubation with **9**, the suspensions were centrifuged (RT, 3 min, 14 000 rpm) and these initial supernatants were collected for UV-Vis absorbance measurements (section 2.1.3). The precipitates were washed 5 times with H_2O or 50 mM potassium phosphate buffer (pH 7, particle concentrations 2 mg/ml) and all supernatants were again collected for measurements of the UV-Vis absorbance. The UV-Vis absorbance of the initial solutions of compound **9** used for incubation of the silica particles was measured as well in order to determine the exact concentration of **9**. The exact combinations of conditions used for each experiment are outlined in the results section. Silica particles were resuspended in H_2O at 1 mg/ml for SEM and TEM sample preparation. Time points at which SEM and TEM samples were prepared are mentioned in the results section.

Additionally, the silica particles that had been incubated in aqueous solutions of compound **9** and subsequently washed with H_2O as described above, were suspended in 50 mM potassium phosphate buffer (pH 7) at particle concentrations of 2 mg/ml for one hour at RT to monitor release of compound **9**. The suspensions were then centrifuged (3 min, RT, 14 000 rpm) and the concentration of compound **9** in the supernatants was determined via measurements of the UV-Vis absorbance (section 2.1.3).

Calibrations for compound **9** were established in H_2O and 50 mM potassium phosphate buffer (pH 7) by preparing solutions of **9** with concentrations of 0.1 mg/ml, 0.066 mg/ml, 0.05 mg/ml, 0.025 mg/ml, 0.022 mg/ml as well as 0.01 mg/ml and measuring their UV-Vis absorbance at 592 nm as described in section 2.1.3. Using these calibrations, the concentrations of compound **9** in all investigated solutions (initial conjugate **9** solutions prior to incubation with silica particles, initial supernatants after incubation and supernatants obtained from the washes) were determined from the corresponding absorbance at 592 nm (equation 1 for solutions of **9** in H_2O, equation 2 for solutions of **9** in 50 mM potassium phosphate buffer (pH 7)):

$$x = \frac{y + 0.0935}{14.034} \quad (1)$$

x…concentration (compound **9**) [mg/ml]
y…absorbance at 592 nm

$$x = \frac{y + 0.0893}{9.6174} \quad (2)$$

The amount of compound **9** in the investigated solutions was determined from the corresponding concentrations of **9** and volumes (0.2 ml for the initial conjugate **9** solution prior to incubation with the silica particles and the initial supernatants after incubation of silica particles with compound **9**, 0.1 ml for washes) according to equation 3:

$$m = c \times V \quad (3)$$

m…amount of compound **9** [mg]
c…concentration (compound **9**) [mg/ml]
V…Volume of the particular solution [ml]

From the amount of compound **9** in the initial conjugate solutions and in the initial supernatants, the amount and percentage of conjugate **9** attached to the particles was determined according to equations 4 and 5:

m (b)…amount of compound **9** bound to the particles [mg]
m (i)…amount of compound **9** in the initial conjugate solution [mg]
m (s)…amount of compound **9** in the initial supernatant [mg]
p (b)…percentage of compound **9** bound to the particles [%]

$$m\,(b) = m(i) - m\,(s) \quad (4)$$

$$p\,(b) = \frac{m(b)}{m(i)} \quad (5)$$

The percentage of compound **9** washed off after the first wash was determined from the amount of **9** in the first wash and the amount of **9** initially bound to the particles after incubation with **9** according to equation 6:

p (w)…percentage of compound **9** washed off after the first wash [%]
m (w)…amount of compound **9** washed off after the first wash [mg]
m (b)…see eq. 4/5

$$p\,(w) = \frac{m(w)}{m(b)} \quad (6)$$

2.2.6.2 Fluorescence microscopy

For fluorescence microscopy imaging of the particles containing **3**, **4** or **7** that were prepared as described in section 2.2.4, subsequently incubated with 0.073 mg/ml compound **9** in H_2O (1 mg/ml particle concentration) for 1.5 hours at RT, washed with 100 µl H_2O 5 times and incubated in 50 mM potassium phosphate buffer (pH 7) for one hour at RT (particle concentration 2 mg/ml), the particles were resuspended in H_2O at a concentration of 0.4 mg/ml before 500 µl of the particle suspensions were transferred into one well of a 24-well plate each and imaged using the BioTek™Cytation™3 Cell Imaging Multi-Mode Reader (see section 2.1.4, channels used: bright field and sulforhodamine 101).

2.3 Investigation of the effect of different precipitation parameters on the morphologies of silica particles derived from 3 with TMOS and TEOS

2.3.1 Biomimetic silica precipitations with 3 and TMOS at different pH values

6 precipitations were carried out at pH values ranging from 4 to 9. For each precipitation, 0.1 mg of **3** was incubated at 1 mg/ml in 50 mM potassium phosphate buffer with a pH between 4 and 9 at RT for 24 hours. Afterwards, silicic acid was freshly prepared by hydrolysis of 270 mM TMOS in 1 mM HCl at RT for 4 minutes and subsequently added to the solutions of **3** at a final concentration of 25 mM. The precipitations were allowed to proceed for 30 minutes at RT before the suspensions were centrifuged

(RT, 3 min, 14 000 rpm) and the precipitates were washed twice with 200 µl H_2O each. Finally, the precipitates were resuspended in H_2O at a concentration of 1 mg/ml for the preparation of TEM and SEM samples (section 2.1.2 and 2.1.1).

2.3.2 Biomimetic silica precipitations with **3** and TEOS at different pH values

6 precipitations were performed with a variation of the pH from 4 to 9. 0.1 mg of **3** per precipitation was dissolved at 1 mg/ml in 50 mM potassium phosphate buffer at a pH between 4 and 9 before TEOS was added yielding a TEOS concentration of 45 mM. The precipitations were allowed to proceed for 24 hours at RT before the suspensions were centrifuged (RT, 3 min, 14 000 rpm) and the precipitates were washed twice with 200 µl H_2O each. For the preparation of TEM and SEM samples (section 2.1.2 and 2.1.1), the precipitates were resuspended in H_2O at a concentration of 1 mg/ml.

2.3.3 Biomimetic silica precipitations with different concentrations of **3** and TEOS at pH 6 and 7

Precipitations were carried out as described in section 2.3.2. The concentrations of **3** used were 0.5 mg/ml, 1 mg/ml or 2 mg/ml, final TEOS concentrations in the peptide solutions were 45 mM or 22.5 mM and precipitations were carried out in 50 mM potassium phosphate buffer at pH 6 or 7. The particular combinations of conditions for each precipitation are given in the results section.

2.4 Synthesis of doubly fluorescent modified silica particles

2.4.1 Biomimetic silica precipitations with **3** and TMOS using silane **10**

2.4.1.1 Precipitations

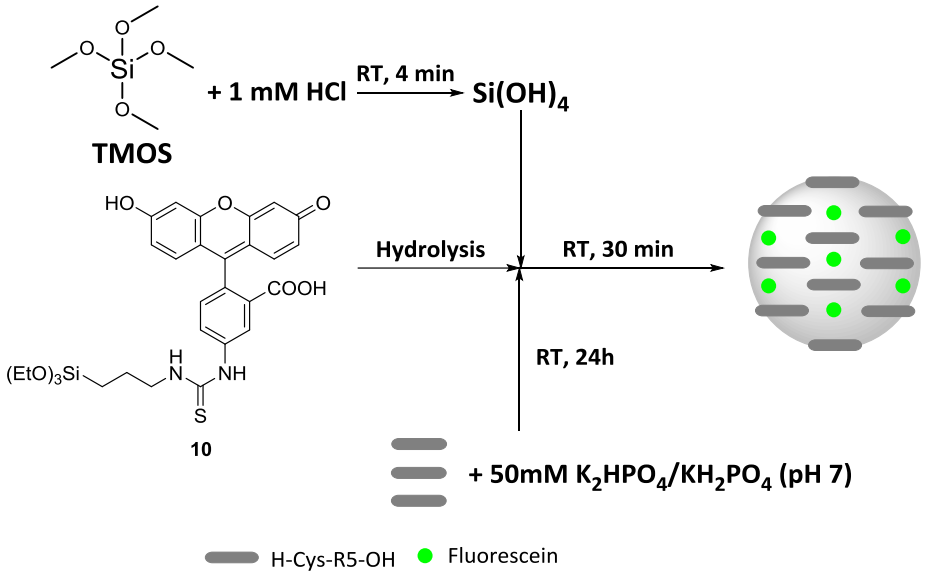

*Scheme 9: Overview for the general experimental procedure for the preparation of fluorescein-modified silica particles with **3** using TMOS and compound **10** as silica precursors*

Biomimetic silica precipitations were carried out with **3** using TMOS and compound **10** as silica precursors. Scheme 9 gives an overview of the general experimental procedure, which required the hydrolysis of compound **10** and addition of hydrolyzed **10** as well as silicic acid to 0.1 mg of **3**, which had previously been incubated in 50 mM potassium phosphate buffer at pH 7 for 24 hours at RT at a concentration of 1 mg/ml or 1.25 mg/ml. Silicic acid was freshly generated via hydrolysis of 270 mM TMOS in 1mM HCl at RT for 4 minutes and added to the mixtures of **3** and **10** at a final concentration of 25 mM or 27 mM. The precipitations were allowed to proceed for 30 minutes before the silica suspensions were centrifuged (RT, 3 min, 14 000 rpm) and the precipitates were washed twice with

100 µl H_2O each. The precipitates were resuspended in H_2O at 1 mg/ml for the preparation of TEM and SEM samples (section 2.1.2 and 2.1.1). Various different conditions were tested for the hydrolysis of compound **10** and the preparation of spherical fluorescein-modified silica particles, which are described in detail in the results section.

*2.4.1.2 Percentage of compound **10** incorporated into and released from the particles*

Silica precipitations with TMOS and compound **10** as silica precursors were carried out using peptide **3**. 0.1 mg peptide **3** was dissolved in 50 mM potassium phosphate buffer (pH 7) at a concentration of 1.25 mg/ml and incubated at RT for 24 hours. Compound **10** was dissolved in 100 mM K_2HPO_4 (pH 9) at a concentration of 0.65 mM (0.4 mg/ml) and incubated at RT for hydrolysis for 3 hours. Afterwards, silicic acid was freshly prepared via hydrolysis of 270 mM TMOS in 1 mM HCl for 4 minutes at RT and added to the peptide solution at a final concentration of 27 mM silicic acid. Hydrolyzed compound **10** was added to the peptide solution at a final concentration of 0.065 mM (0.04 mg/ml). The precipitation was allowed to proceed for 30 minutes at RT before the resultant silica suspension was centrifuged (RT, 3 min, 14 000 rpm). The UV-Vis absorbance of the supernatant was measured (section 2.1.3) for the determination of the percentage of compound **10** incorporated into the particles and the precipitate was washed twice with 100 µl H_2O.

The particles were then divided into 2 aliquots and resuspended in 50 mM potassium phosphate buffer (pH 4 or 7) at a concentration of 1 mg/ml and incubated at RT for one week. For the determination of the percentage of compound **10** released from the particles, the suspensions were centrifuged afterwards (RT, 3 min, 14 000 rpm) and the UV-Vis absorbance of the supernatants was measured (section 2.1.3). For the particles after release of compound **10**, TEM samples were prepared according to section 2.1.2 (1 mg/ml particle concentration).

The concentration of compound **10** in the supernatants obtained after the precipitation and after the incubation of the particles in 50 mM potassium phosphate buffer at pH 4 and 7 was determined via a calibration (linking the absorbance at 495 nm to the corresponding concentration of compound **10**) that was established using standard solutions with 5 different concentrations of **10** (Table 3)). Prior to the preparation of the standard solutions, compound **10** was incubated in 100 mM K_2HPO_4 (pH 9) at a concentration of 0.4 mg/ml for 3 hours. The standard solutions were then prepared by further dilution of this stock solution with 100 mM K_2HPO_4 (pH 9) and addition of 1 mM HCl and 50 mM potassium phosphate buffer (pH 7) according to Table 3. The UV-Vis absorbance of the standard solutions was measured at 495 nm as described in section 2.1.3

*Table 3: Concentrations of compound **10** and compositions of the standard solutions used for the calibration linking the absorbance at 495 nm to the corresponding concentration of compound **10***

Final concentration of 10 [mg/ml]	Composition
0.08	10 µl 0.8 mg/ml **10** (in 100 mM K_2HPO_4 pH 9)+ 10 µl 1 mM HCl + 80 µl 50 mM potassium phosphate buffer (pH 7)
0.04	10 µl 0.4 mg/ml **10** (in 100 mM K_2HPO_4 pH 9)+ 10 µl 1 mM HCl + 80 µl 50 mM potassium phosphate buffer (pH 7)
0.02	10 µl 0.2 mg/ml **10** (in 100 mM K_2HPO_4 pH 9)+ 10 µl 1 mM HCl + 80 µl 50 mM potassium phosphate buffer (pH 7)
0.01	10 µl 0.1 mg/ml **10** (in 100 mM K_2HPO_4 pH 9)+ 10 µl 1 mM HCl + 80 µl 50 mM potassium phosphate buffer (pH 7)
0.005	10 µl 0.05 mg/ml **10** (in 100 mM K_2HPO_4 pH 9)+ 10 µl 1 mM HCl + 80 µl 50 mM potassium phosphate buffer (pH 7)

For the determination of the percentage of compound **10** incorporated into the particles, the concentration of silane **10** in the supernatant obtained after 30 minutes of precipitation and subsequent centrifugation was compared to the concentration of compound **10** in the initial precipitation mixture (mixture for the measurement of the initial concentration of silane **10**: 10 µl of 0.65 mM (0.4 mg/ml) compound **10** in 100 mM K_2HPO_4 (pH 9), 10 µl 1 mM HCl and 80 µl 50 mM potassium phosphate buffer (pH 7)).

The concentration of silane **10** in all investigated solutions was determined from the absorbance at 495 nm via the calibration following equation 7:

$$x = \frac{y - 0.0161}{21.751} \tag{7}$$

x…concentration (compound **10**) [mg/ml]
y…absorbance at 495 nm

The amount of compound **10** in the solutions of interest was determined from the corresponding concentrations and volumes (0.1 ml for all investigated solutions) of the solutions according to equation 3 (also see section 2.2.6):

$$m = c \times V \tag{3}$$

m…amount of compound **10** [mg]
c…concentration (compound **10**) [mg/ml]
V…Volume of the particular solution [ml]

The amount and percentage of compound **10** incorporated into the particles was determined from the amount of compound **10** in the initial precipitation mixture and the amount of compound **10** in the supernatant after 30 minutes of precipitation and centrifugation of the precipitate according to equations 4 and 5:

$$m\,(b) = m(i) - m\,(s) \tag{4}$$

$$p\,(b) = \frac{m(b)}{m(i)} \tag{5}$$

m (b)…amount of compound **10** incorporated into the particles [mg]
m (i)…amount of compound **10** in the initial solution [mg]
m (s)…amount of compound **10** in the supernatant after centrifugation [mg]
p (b)…percentage of compound **10** incorporated into the particles [%]

Finally, the amount of compound **10** released was determined from the amount of compound **10** in the supernatants after incubation of the particles for one week in 50 mM potassium phosphate buffer (pH 4 or 7) and the amount initially incorporated into the particles according to equation 6:

$$p\,(r) = \frac{m(r)}{m(b)} \tag{6}$$

p (r)…percentage of compound **10** released after 1 week incubation in 50 mM potassium phosphate buffer (pH 4 or 7) [%]
m (r)…amount of compound **10** released after 1 week incubation in 50 mM potassium phosphate buffer (pH 4 or 7) [mg]
m (b)…see eq. 4/5

2.4.1.3 Cell studies and Fluorescence Microscopy

Fluorescence Microscopy

For imaging of the fluorescein modified particles (derived from silane **10**) without cells, the particles were suspended in RPMI 1640 medium with 10% FCS and 1% Penicillin-Streptomycin at a concentration of 0.00625 mg/ml and 400 µl of this suspension were transferred into a well of a 24-well plate. The particles were immediately imaged using the BioTek™Cytation™3 Cell Imaging Multi-Mode Reader as described in section 2.1.4 with 2 channels (fluorescein and bright field).

Cell study A

The cell studies were performed with THP-1 cells that were cultured in RPMI 1640 medium with 10 % FCS and 1% Penicillin-Streptomycin at 37°C and 5% CO_2 and had previously been differentiated to macrophages according to a protocol established by Genin *et al*. [115]

For cell study A, 0.4 mg of silica particles modified with compound **10** (prepared according to section 2.4.1.2) were suspended at a concentration of 1 mg/ml in medium (stock solution) with the same composition as the medium the cells were cultured in. Particle concentrations of 0.1 mg/ml, 0.05 mg/ml, 0.025 mg/ml and 0.0125 mg/ml were prepared by appropriate dilution of the stock solution with medium. The medium was aspirated from the cells and they were subsequently treated with 500 µl of particle suspensions. Treatments were performed in duplicates for each concentration. All wells were imaged (bright field and fluorescein channel) 1.5 hours after treatment of the cells with particles using the BioTek™Cytation™3 Cell Imaging Multi-Mode Reader (section 2.1.4). The particle-treated cells were then incubated at 37 °C and 5% CO_2 for 24 hours. Afterwards, the medium was removed from the cells and they were stained as described in section 2.1.4. Images were then acquired with 4 different channels (bright field, Hoechst 33258, fluorescein and Alexa Fluor 594).

Cell study B

For cell study B, 0.2 mg of particles modified with compound **10** synthesized as described in section 2.4.1.2 were suspended in Dulbecco's PBS 1x (200 mg/l KCl, 200 mg/l KH_2PO_4, 8000 mg/l NaCl, 2160 mg/l $Na_2HPO_4 \cdot 7H_2O$) at a concentration of 0.01 mg/ml. Before treatment of the cells with particles, they were stained (section 2.1.4, without Alexa Fluor 594). The staining solution was then removed and the cells were washed with 500 µl Dulbecco's PBS 1x per well before the cells were treated with 500 µl particle suspension (0.01 mg/ml) in triplicates and the wells were viewed and imaged with the BioTek™Cytation™3 Cell Imaging Multi-Mode Reader (section 2.1.4) using 4 channels (bright field, fluorescein, cyanine-5 and Hoechst 33258). Viewing and imaging of the cells was carried out immediately after, 2 hours after and 24 hours after (cells were incubated at 37 °C and 5% CO_2) treatment of the cells with silica particles containing compound **10**. Cell study B was carried out in the same 24-well plate as the cell studies for particles containing **17** (section 2.4.2.6) as well as particles with **10** and **17** (section 2.4.3.4). Therefore, imaging with the cyanine-5 channel was necessary to rule out cross-contaminations of the particles derived from **10** with other types of particles.

2.4.2 Biomimetic silica precipitations with 3, 17 and TMOS

*2.4.2.1 Synthesis of Cyanine-5 (compound **16**)*

Synthesis of 1-(4-carboxybutyl)-2,3,3-trimethyl-3H-indol-1-ium bromide (compound 13)

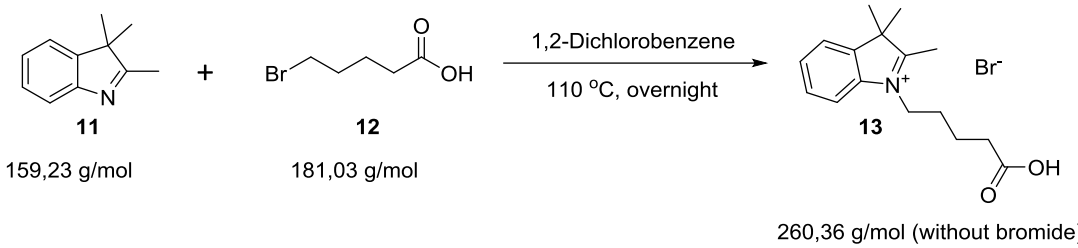

*Scheme 10: The reaction leading to the formation of the intermediate, 1-(4-carboxybutyl)-2,3,3-trimethyl-3H-indol-1-ium bromide (compound **13**)*

For the synthesis of compound **13** (Scheme 10), 5 g (31.4 mmol) of 2,3,3-trimethylindolenine (compound **11**) were weighed into a 250 ml flask, before 50 ml of 1,2-dichlorobenzene and 8,1 g (44.7 mmol) of bromovaleric acid (compound **12**) were added. The reaction mixture was stirred in an oil bath at 110 °C overnight. Afterwards, the mixture was cooled to RT and incubated in an ice bath for one hour to complete precipitation of the product. Compound **13** was isolated as a slightly pink solid using a glass filter, washed with 20 ml of an ice-cold 60:40 mixture of diethyl ether and ACN and dried under vacuum.

Synthesis of 16

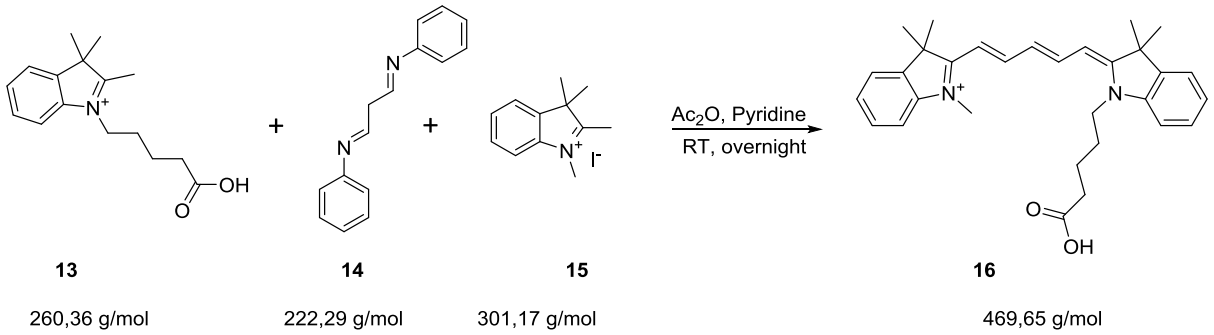

*Scheme 11: Second reaction in the synthesis of compound **16***

For the synthesis of compound **16** from compound **13** (Scheme 11), 0.7 g (2.7 mmol) of compound **13** and 0.8 g (3.6 mmol) of malonaldehydebis(phenylimine)monohydrochloride (compound **14**) were weighed into a 500 ml flask, 50 ml Ac_2O were added and the suspension was stirred at room temperature for 10 minutes and afterwards at 120 °C for 30 min (solution turned dark red). The reaction mixture was subsequently cooled to room temperature before 1.44 g (4.8 mmol) 1,2,3,3-tetramethyl-3H-indolium iodide (compound **15**) were added in 65 ml pyridine (solution turned green, then blue after 30 minutes) and the mixture was stirred at RT overnight. Afterwards, 150 ml of toluene were added to the mixture for co-evaporation and removal of pyridine and Ac_2O on the rotary evaporator. The addition of toluene and subsequent evaporation was repeated 7 times until Ac_2O and pyridine were completely removed from the product. The residue was dissolved in 40 ml $CHCl_3$ and 200 ml of hexane were added to precipitate the crude product as a blue solid, before it was filtered over a glass filter and dissolved in 150 ml $CHCl_3$. The solution was washed twice with 150 ml H_2O and once with 150 ml 0.1 M HCl, dried over $MgSO_4$ and concentrated on the rotary evaporator. The concentrated crude product was dry-loaded onto silica and purified via silica column chromatography. For elution of the product from the column, the mobile phase initially consisted of pure DCM, followed by 5% MeOH in DCM, 10 % MeOH in DCM and finally 10 % MeOH in DCM with 1% AcOH. The collected

fractions were analyzed via TLC (mobile phase 10 % MeOH in DCM with 1% AcOH) and direct injections on a Thermo Fisher HPLC-MS system (for direct injections 1 µl of each fraction was diluted 1:100 in ACN). Depending on purity, the fractions were combined and concentrated on the rotary evaporator. Toluene was added for co-evaporation with AcOH. The blue residue was finally dried in high vacuum, dissolved in a mixture of 50 % ACN and 50 % H_2O and lyophilized.

For ^{1}H-NMR analysis, 2 mg of compound **16** were dissolved in $CDCl_3$ at a concentration of 2.9 mg/ml. The following shifts and coupling constants were obtained:

^{1}H NMR (600 MHz, $CDCl_3$) δ 7.85 (dd, *J* = 26.3, 13.2 Hz, 2H), 7.40 – 7.33 (m, 4H), 7.24 – 7.20 (m, 2H), 7.11 – 7.02 (m, 3H), 6.49 (dd, *J* = 23.0, 13.5 Hz, 2H), 4.13 – 4.08 (m, 2H), 3.67 (s, 3H), 2.72 – 2.64 (m, *J* = 5.1 Hz, 3H), 1.91 – 1.85 (m, 4H), 1.70 (d, *J* = 6.3 Hz, 10H)

*2.4.2.2 Synthesis and purification of **17***

Synthesis

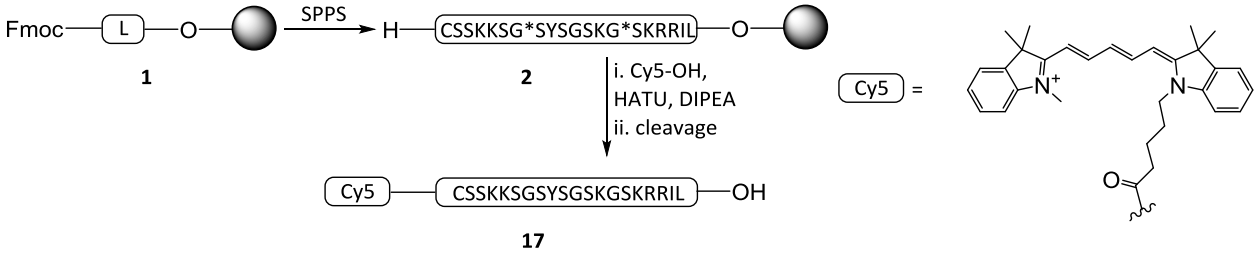

*Scheme 12: Scheme for the synthesis of **17** via SPPS starting from Fmoc-Leu-Wang resin with post synthetic coupling of **16** to resin-bound **3** (compound **2**)*

The synthesis of compound **2** was carried out as described in section 2.2.1.1. A fifth of the dried resin (0.01 mmol) was transferred into a new syringe and swollen in DMF for 30 minutes. 4 eq **16** (0.04 mmol, 18.8 mg) were dissolved in a solution of 3.5 eq HATU in DMF (0.035 mmol HATU, 70 µl of a 0.5 M solution of HATU in DMF) and 10 eq DIEA (0.1 mmol, 17 µl) were added to the mixture before it was diluted to 1 ml with DMF and added to the resin overnight. Afterwards the resin was washed with DMF, DCM and MeOH and treated with 1 ml cleavage solution (95 % TFA, 2.5 % TIPS, 2.5 % H_2O) for 2 hours. The peptide was precipitated by the addition of 8 ml ice-cold diethyl ether to the peptide solution and centrifuged (5 min, 4°C, 5400 rpm). The pellet was then washed with 8 ml ice-cold diethyl ether and dried under argon before it was dissolved in 5 ml 20 % buffer B (ACN with 0.1 % TFA) in buffer A (H_2O with 0.1 % TFA) and lyophilized.

Purification

Per purification run, 12 mg of crude **17** were dissolved in 10 ml 100 % buffer A (H_2O with 0.1 % TFA). An analytical run was carried out prior to purification on the Waters HPLC-MS auto purification system on an analytical Kromasil C18 RP-HPLC column using a gradient from 5 % buffer B (ACN with 0.1 % TFA) in buffer A to 65 % buffer B in buffer A over 10 minutes at a 1 ml/min flow rate. The peptide was then injected for purification on the Waters HPLC-MS auto purification system on a semi-preparative Kromasil C18 RP-HPLC column using a gradient of 5% buffer B in A to 45% buffer B in A over 30 minutes at a flow rate of 10 ml/min. The peptide fractions were collected by monitoring the 3 most abundant m/z peaks from the analytical run, combined depending on purity and lyophilized. As the purity of the peptide was still not satisfying, 1 mg of **17** per run was dissolved in 100 µl 100 % buffer A (H_2O with 0.1 % TFA) and repurified on a Dionex Ultimate 3000 HPLC system using an analytical Kromasil C4 RP-HPLC column and a gradient of 5 % buffer B (ACN with 0.08 % TFA) in A (H_2O with 0.1 % TFA) to 65 % buffer B in A over 40 minutes at a flow rate of 1 ml/min. The fractions were collected manually and combined

based on their purity which was assessed by HPLC-MS analysis on a Thermo-Fisher HPLC-MS system with an analytical Kromasil C4 RP-HPLC column using a gradient of 5 % buffer B (ACN with 0.05 % TFA) in buffer A (H_2O with 0.05 % TFA) to 65 % buffer B in A over 20 minutes at a flow rate of 1 ml/min. The pure fractions were combined and lyophilized.

For final analysis of peptide **17**, it was dissolved in buffer A (H_2O with 0.1 % TFA) at a concentration of 1 mg/ml and 0.02 mg of peptide were injected for HPLC-MS analysis, which was performed on the Thermo Fisher HPLC-MS system on an analytical Kromasil C4 RP-HPLC column with a gradient of 5 % buffer B (ACN with 0.05 % TFA) in buffer A (H_2O with 0.05 % TFA) to 65 % buffer B in A over 20 minutes at a flow rate of 1 ml/min (chromatogram in Figure 56 A, section 3.3.2.2) while the UV-Vis absorbance at 214 nm was monitored starting at 6 minutes after injection of the sample. Additionally, 0.02 mg of peptide (1 mg/ml in buffer A (H_2O with 0.1 % TFA)) were directly injected into the Thermo Fisher HPLC-MS system. The corresponding mass spectrum is depicted in Figure 56 B (section 3.3.2.2).

2.4.2.3 Precipitations

Biomimetic precipitations were carried out with a mixture of **17** and **3**. 0.1 mg **3** were dissolved in 50 mM potassium phosphate buffer (pH 7) at 1 mg/ml and 1 µl (1 % **17** (w/w)) or 5 µl (4.8 % **17** (w/w)) of a 1 mg/ml solution of **17** in H_2O were added to the solution of **3** before the mixture was incubated at RT for 24 hours. Silicic acid was then freshly prepared via hydrolysis of 270 mM TMOS in 1 mM HCl for 4 minutes at RT and added to the peptide solution at an exact final concentration of 24 mM (for 1 % **17** (w/w)) or 23.5 mM (for 4.8 % **17** (w/w)). The precipitation was allowed to proceed for 30 minutes at RT before the precipitates were isolated by centrifugation (RT, 3 min, 14 000 rpm), washed with 100 µl H_2O twice and resuspended in H_2O at 1 mg/ml for the preparation of SEM and TEM samples (section 2.1.1 and 2.1.2).

*2.4.2.4 Determination of the percentage of **17** incorporated into the particles*

The percentage of **17** incorporated into the particles was determined for the particles prepared with 4.8 % (w/w) **17** in **3** and the precipitation was carried out as described in section 2.4.2.3 (with 0.35 mg **3** and 17.5 µl of a 1 mg/ml aqueous solution of **17**). The UV-Vis absorbance of the initial precipitation mixture and the supernatant obtained after the isolation of the precipitate obtained after 30 minutes of precipitation by centrifugation was determined at 641 nm as described in section 2.1.3.

For the determination of the concentration of **17** in all investigated solutions, a calibration (connecting the absorbance at 641 nm and the corresponding concentration of **17**) was established using standard solutions with concentrations of **17** in 50 mM potassium phosphate buffer (pH 7) of 0.1 mg/ml, 0.075 mg/ml, 0.05 mg/ml, 0.02 mg/ml and 0.01 mg/ml. The UV-Vis absorbance of all standard solutions was measured as described in section 2.1.3. The percentage of **17** incorporated into the particles in the course of the precipitation was determined via comparison of the concentration of **17** in the supernatant obtained from centrifugation after 30 minutes of precipitation with the concentration of **17** in the initial precipitation mixture (mixture for the measurement of the initial concentration of **17**: 10 µl 1 mM HCl, 100 µl 50 mM potassium phosphate buffer (pH 7) and 5 µl of an aqueous 1 mg/ml solution of **17**).

The concentration of peptide **17** in the investigated solutions was determined from their absorbance at 641 nm from the calibration via equation 8:

$$x = \frac{y + 0.0786}{9.5018} \quad (8)$$

x…concentration (peptide **17**) [mg/ml]
y…absorbance at 641 nm

The amount of peptide **17** in the initial solution prior to the precipitation (volume: 402 µl) and in the supernatant obtained after precipitation and centrifugation (volume: 402 µl) as well as the percentage of peptide **17** incorporated into the particles was determined using the same equations as for compound **10** in section 2.4.1.2 (equations 3, 4 and 5).

*2.4.2.5 Release of **17** from the particles*

Silica particles derived from a solution of 4.8 % (w/w) **17** in **3** were prepared according to the procedure described in section 2.4.2.4 and subsequently incubated in 50 mM potassium phosphate buffer at pH 4 or 7 at a particle concentration of 1 mg/ml for one week at RT. Afterwards, the suspensions were centrifuged (3 min, RT, 14 000 rpm) and washed with 300 µl H_2O twice before they were resuspended in H_2O at a particle concentration of 1 mg/ml for the preparation of TEM samples (section 2.1).

2.4.2.6 Cell study and fluorescence microscopy

Fluorescence microscopy

For fluorescence microscopy imaging, 0.2 mg of the particles (derived from 1 % (w/w) **17** and 4.8 % (w/w) **17** in **3**) prepared as described in section 2.4.2.3 were resuspended in RPMI 1640 medium with 10 % FCS and 1 % Penicillin-Streptomycin at a concentration of 0.01 mg/ml and 400 µl of particle suspension were each transferred into a well of a 24-well plate. The wells were then viewed and imaged using the BioTek™Cytation™3 Cell Imaging Multi-Mode Reader as described in section 2.1.4 (cyanine-5 channel).

Cell study

The cell study was carried out using THP-1 cells that were cultured in RPMI 1640 medium with 10 % FCS and 1 % Penicillin-Streptomycin at 37°C and 5 % CO_2 and had previously been differentiated to macrophages according to an already established protocol [115]. Cell studies were performed with particles derived from 4.8 % (w/w) **17** in **3**. 0.2 mg of particles were resuspended in 1 ml Dulbecco's PBS 1x (200 mg/l KCl, 200 mg/l KH_2PO_4, 8000 mg/l NaCl, 2160 mg/l $Na_2HPO_4 \cdot 7H_2O$) at a concentration of 0.01 mg/ml. Prior to the addition of the particles, the cells were stained (section 2.1.4, without Alexa Fluor 594). After removal of the staining solution and washing of the cells with 500 µl Dulbecco's PBS 1x per well, the cells were treated with 500 µl of previously prepared silica particle suspension (0.01 mg/ml) in triplicates. The wells were viewed and imaged immediately after addition of the particles as well as 2 hours and 24 hours (incubation of cells at 37 °C and 5 % CO_2) after treatment of the cells with the particles using the BioTek™Cytation™3 Cell Imaging Multi-Mode Reader as described in section 2.1.4. The images were acquired using 4 different channels (bright field, cyanine-5, Hoechst 33258 and fluorescein)

2.4.3 Biomimetic silica precipitations with 3, 17, TMOS and 10

2.4.3.1 Precipitations

The precipitations for the cyanine-5 and fluorescein modified silica particles were carried out as described in section 2.4.1.2 for fluorescein-modified particles derived from silane **10** with the only difference being the addition of 1 µl (1 % (w/w) **17** in **3**) or 5 µl (4.8 % (w/w) **17** in **3**) of a 1 mg/ml solution of **17** in H_2O to the 1,25 mg/ml solution of **3** (0.1 mg of peptide) in 50 mM potassium phosphate buffer (pH 7) before the peptide mixture was incubated at RT for 24 hours. After

precipitation, the particles were suspended in H_2O at 1 mg/ml for the preparation of SEM and TEM samples (section 2.1.1 and 2.1.2).

*2.4.3.2 Determination of the percentage of compound **10** and **17** incorporated into the particles during the precipitation*

For the particles derived from 4.8 % (w/w) **17** in **3** (prepared according to section 2.4.3.1, but with 0.35 mg **3** and 17.5 µl of the 1 mg/ml solution of **17** in H_2O), the percentages of compound **10** and **17** incorporated into the particles were determined via UV-Vis measurements of the supernatant at 495 nm and 641 nm obtained after 30 minutes of precipitation (section 2.1.3). The concentrations of **10** and **17** in the supernatant were determined using the calibration for **17** established in section 2.4.2.4 and the calibration for **10** from section 2.4.1.2. Determination of the percentages of **17** and **10** incorporated into the particles was then achieved via the comparison of the concentrations and amounts of **17** and **10** in the supernatant obtained after 30 minutes of precipitation with the concentrations and amounts of **10** and **17** in the initial precipitation mixture (mixture for the measurement of the initial concentration: 10 µl 1 mM HCl, 10 µl of 0.65 mM compound **10** in 100 mM K_2HPO_4 (pH 9), 80 µl 50 mM potassium phosphate buffer (pH 7) and 5 µl of a 1 mg/ml aqueous solution of **17**). The concentrations and amounts of **10** and **17** in the investigated solutions as well as the percentages of the compounds incorporated into the silica particles were determined from the equations in section 2.4.1.2 for compound **10** and the equations in section 2.4.2.4 for peptide **17**. The volumes for the initial solution of compound **10** and peptide **17** in which the precipitation was carried out and for the supernatant obtained after 30 minutes of precipitation were 367 µl each.

*2.4.3.3 Release of **10** and **17** from the particles*

The fluorescein and cyanine-5 modified particles derived from 4.8 % **17** in **3** were produced as described in section 2.4.3.1. After washing, they were incubated in 50 mM potassium phosphate buffer (pH 4 or 7) at particle concentrations of 1 mg/ml at RT for one week. The suspensions were then centrifuged (RT, 3 min, 14 000 rpm), washed with 100 µl H_2O twice and resuspended in H_2O at a particle concentration of 1 mg/ml for the preparation of SEM and TEM samples (section 2.1.1 and 2.1.2).

2.4.3.4 Cell studies and Fluorescence Microscopy

Fluorescence microscopy

Fluorescence microscopy imaging without cells was carried out for the particles derived from the solution containing 1 % (w/w) of **17** or 4.8% (w/w) **17** in **3** in addition to **10**. The silica particles (prepared as described in section 2.4.3.1) were suspended in RPMI 1640 medium containing 10 % FCS and 1 % Penicillin-Streptomycin at 0.01 mg/ml. 400 µl of the particle suspensions were transferred into one well of a 24-well plate each. The wells were subsequently viewed and imaged using the BioTek™Cytation™3 Cell Imaging Multi-Mode Reader (section 2.1.4, fluorescein and cyanine-5 channel).

Cell study

The cell study was carried out with the particles derived from a solution containing 4.8 % **17** in **3** in addition to compound **10** in THP-1 cells (differentiated to macrophages according to a previously established protocol [115]). The cells were cultured in RPMI 1640 medium containing 10 % FCS and 1 % Penicillin-Streptomycin at 37°C and 5 % CO_2. 0.2 mg of the particles were suspended in Dulbecco's PBS 1x (200 mg/l KCl, 200 mg/l KH_2PO_4, 8000 mg/l NaCl, 2160 mg/l $Na_2HPO_4 \cdot 7H_2O$) at 0.01 mg/ml. The cells were stained (section 2.1.4, without Alexa Fluor 594), washed once with 500 µl Dulbecco's PBS 1x per well and treated with 500 µl of silica particle suspension (0.01 mg/ml) per well in triplicates. The

treated cells were imaged using the BioTek™Cytation™3 Cell Imaging Multi-Mode Reader as described in section 2.1.4 immediately after, 2 hours and 24 hours (cells were incubated at 37 °C and 5 % CO_2) after treatment with the silica particles. (channels: fluorescein, Hoechst 33258, cyanine-5 and bright field)

3 Results and Discussion

3.1 Investigation of silica particle binding to (strept)avidin conjugates 8 and 9

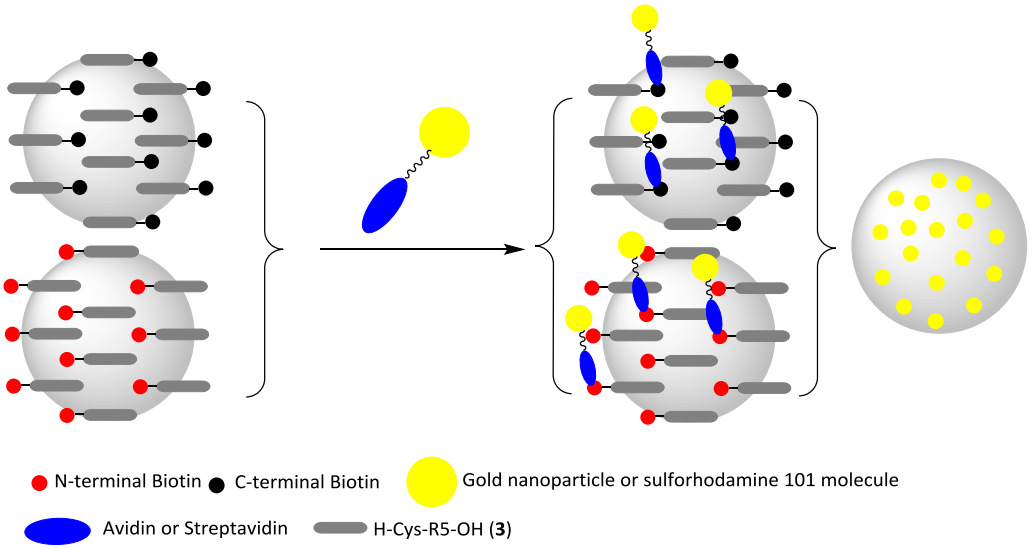

Figure 8: General overview of the strategy employed for the investigation of the display and accessibility of the N- *and* C-*terminus of peptide* ***3*** *involving streptavidin-conjugated gold nanoparticles or avidin-conjugated sulforhodamine 101*

Accessible and appropriately modified *N*- or *C*-termini of the R5 peptide variant **3** (containing an *N*-terminal cysteine) could be used for the attachment of complementarily modified cargo molecules to silica particles derived from TMOS with peptide **3** as a silica precipitating agent. This would potentially result in a new method for the use of such particles as delivery agents. Our aim was therefore to investigate the accessibility of the *N*-and *C*-terminus of peptide **3** in these particles. The strategy employed (Figure 8) was based on the assumption that accessibility of either the *N*- or *C*-terminus of peptide **3** could be visualized in silica particles by use of appropriately biotinylated peptides **4** or **7.** Streptavidin-conjugated gold nanoparticles or avidin-conjugated sulforhodamine 101 would then be used for visualization, as they would bind to the biotin modified variants of **3** via biotin-(strept)avidin interaction. The streptavidin-gold nanoparticle conjugates attached to the silica particles would be visible on the transmission electron microscope. Attached avidin-sulforhodamine 101 conjugates would be detectable through the determination of the avidin-sulforhodamine 101 concentration (via measurement of UV-Vis absorbances and calibration) in the solution of the conjugate before and after incubation with the silica particles containing the biotinylated peptides. Particles containing **3** without biotin served as a negative control for the binding experiments as the streptavidin-gold nanoparticle conjugate **8** or avidin-sulforhodamine 101 conjugate **9** cannot bind to these particles via (strept)avidin-biotin interaction. Thus, if the *N*- and/or *C*-terminus of peptide **3** were exposed, the streptavidin-gold nanoparticle conjugates should bind to the particles containing **4** and/or **7** but not to the particles containing the non-biotinylated peptide **3**.

3.1.1 Synthesis and purification of 3

Peptide **3** was synthesized and purified according to section 2.2.1. While the crude yield after cleavage of a fifth (0.01 mmol) of the peptide was 18.4 mg, the yield after HPLC-MS purification decreased to 8.2 mg (39 % of the theoretical yield of 21.2 mg for 0.01 mmol peptide).

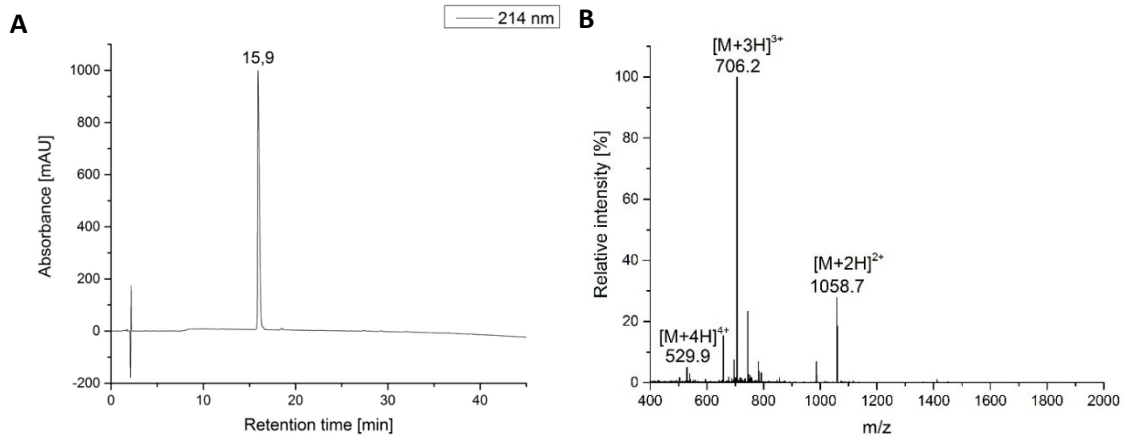

*Figure 9: A: HPLC chromatogram of purified peptide **3** B: Mass spectrum obtained from a direct injection of purified peptide **3** on the Thermo Fisher HPLC-MS system*

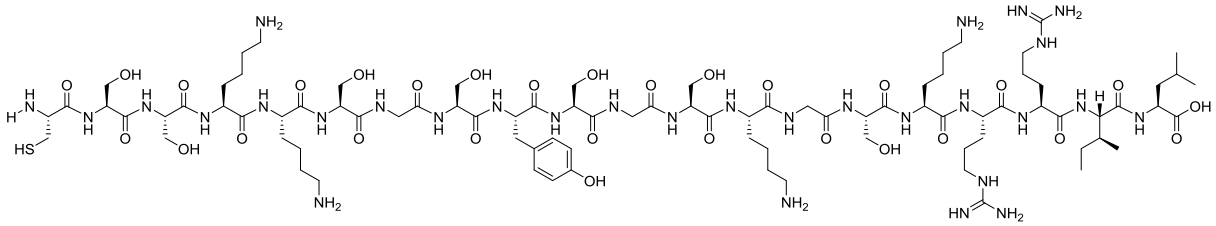

*Figure 10: Structure of peptide **3***

Figure 9 A depicts the chromatogram (at 214 nm, absorbance wavelength of the peptide bond) from the RP-HPLC analysis of purified peptide **3** (structure shown in Figure 10, retention time 15.9 minutes) and the corresponding mass spectrum is visualized in Figure 9 B, which shows peaks corresponding to an observed mass of 2115.6 Da, which is in good agreement with the expected mass for peptide **3** (2115.1 Da). An additional peak observed at 744.5 m/z can be attributed to a three times protonated species of a TFA adduct of the peptide with a mass of 2115.6+114 Da, while the peak at 658 Da could not be identified and might arise from an impurity.

3.1.2 Synthesis and purification of **4**

Peptide **4** was synthesized and purified as described in section 2.2.2. Prior to purification the crude yield of the peptide (0.005 mmol) was 9.2 mg, which decreased to a yield of 1.3 mg of pure peptide after HPLC-MS purification (11 % of the theoretical yield of 11.7 mg for 0.005 mmol peptide).

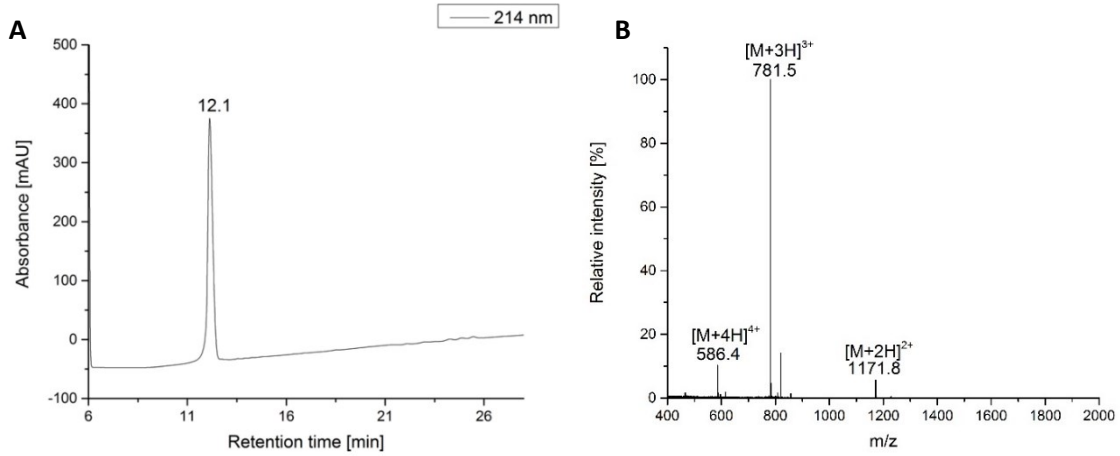

*Figure 11: A: HPLC chromatogram of purified peptide **4**, B: Mass spectrum obtained from a direct injection of purified peptide **4** on the Thermo Fisher HPLC-MS system*

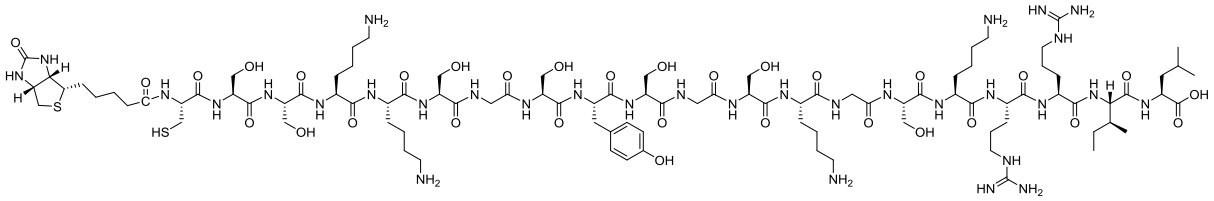

*Figure 12: Structure of peptide **4***

The RP-HPLC-chromatogram obtained from the final analysis of purified peptide **4** (Figure 11 A) shows the elution of the peptide at a retention time of 12.1 minutes and the corresponding mass spectrum (Figure 11 B) exhibits a charge pattern that corresponds to an observed mass of 2341.6 Da which is in good agreement with the expected mass for peptide **4** (2341.2 Da). The additional peak at 819.5 m/z can be attributed to the three times protonated species of a TFA adduct of the peptide with the mass of 2341.6+114 Da. In combination with the HPLC chromatogram in Figure 11 A, the mass spectrum indicates good purity of peptide **4**.

3.1.3 Synthesis and purification of 7

Synthesis and purification of peptide **7** was carried out as described in section 2.2.3. Following cleavage of a fourth (0.005 mmol) of the peptide, 7.8 mg of crude peptide **7** were obtained. After purification of the crude peptide via RP-HPLC, the yield decreased to 1.9 mg (16 % of the theoretical yield of 11.9 mg for 0.005 mmol peptide)

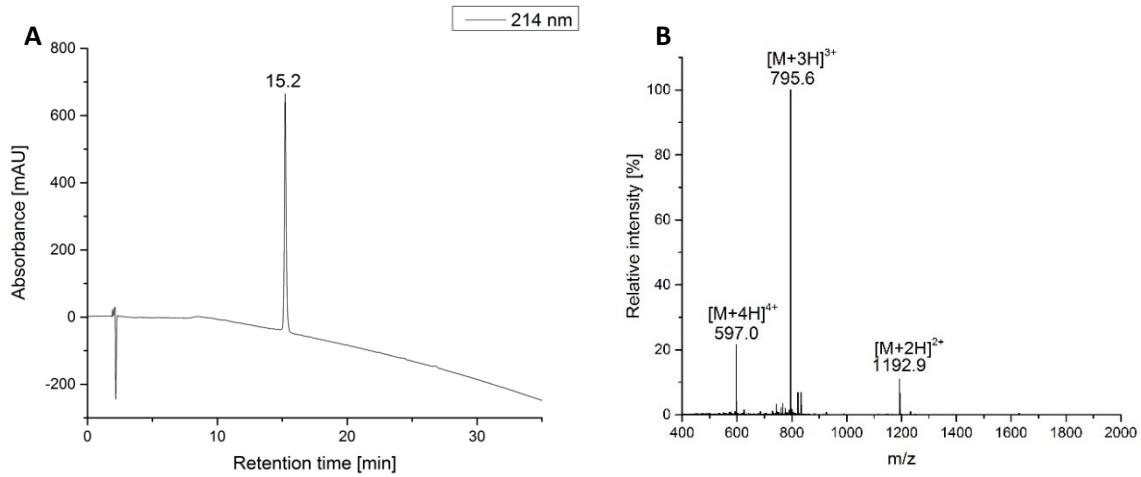

*Figure 13: A: HPLC chromatogram of purified peptide **7**, B: Mass spectrum obtained from a direct injection of purified peptide **7** on the Thermo Fisher HPLC-MS system*

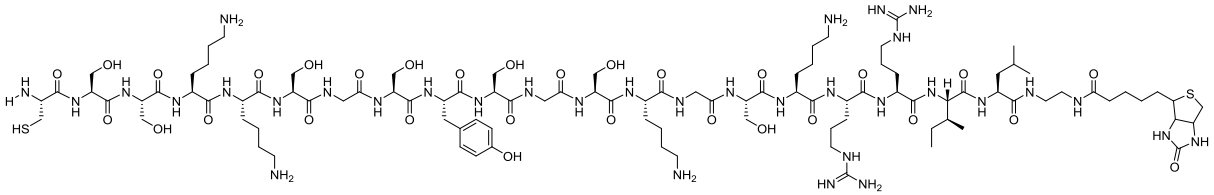

*Figure 14: Structure of peptide **7***

The HPLC chromatogram of purified peptide **7** is depicted in Figure 13 A and demonstrates the elution of the peptide at 15.2 minutes while the corresponding mass spectrum (Figure 13 B) shows a charge pattern corresponding to an observed mass of 2383.8 Da which is in good agreement with the expected mass for peptide **7** (2383.3 Da). An additional peak can be observed at 833.5 m/z which probably originates from the three times protonated species of the TFA adduct of the desired peptide with a mass of 2383.8+114 Da. The mass spectrum confirms the good purity of purified **7** suggested by the chromatogram.

3.1.4 Biomimetic silica precipitations with 3, 4 or 7 and TMOS

Biomimetic precipitations with **3** (scanning electron microscopy image shown in section 3.2.1 in Figure 34 A), **4** or **7** (1 mg/ml) with TMOS (25 mM final silicic acid concentration in the precipitation mixtures) as a silica precursor were performed in 50 mM potassium phosphate buffer (pH 7) as described in section 2.2.4 and the morphologies of the resultant precipitates were investigated via SEM and TEM (Figures 15 and 16).

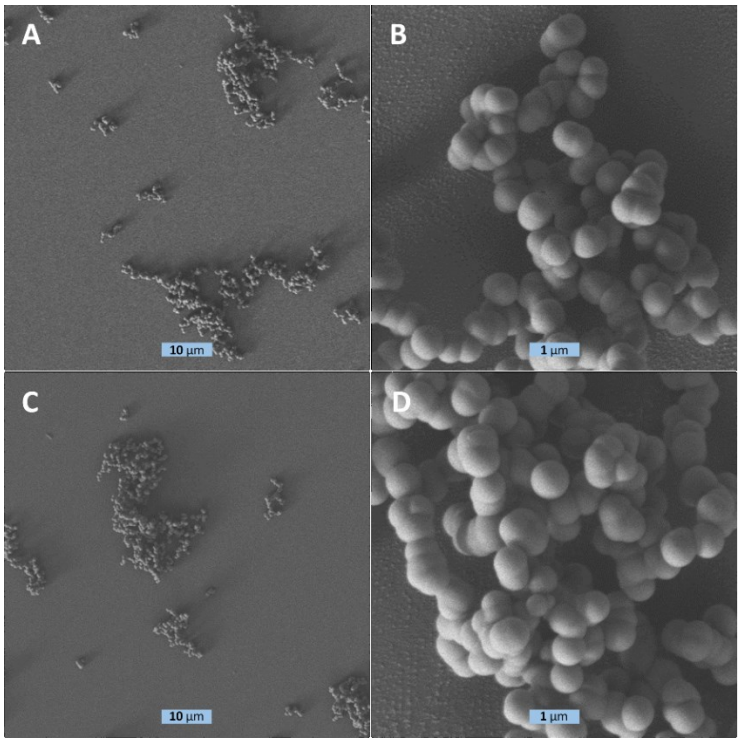

*Figure 15: SEM images of the precipitates obtained from the biomimetic precipitations with 1 mg/ml **4** (A and B) or **7** (C and D) and 25 mM silicic acid at pH 7*

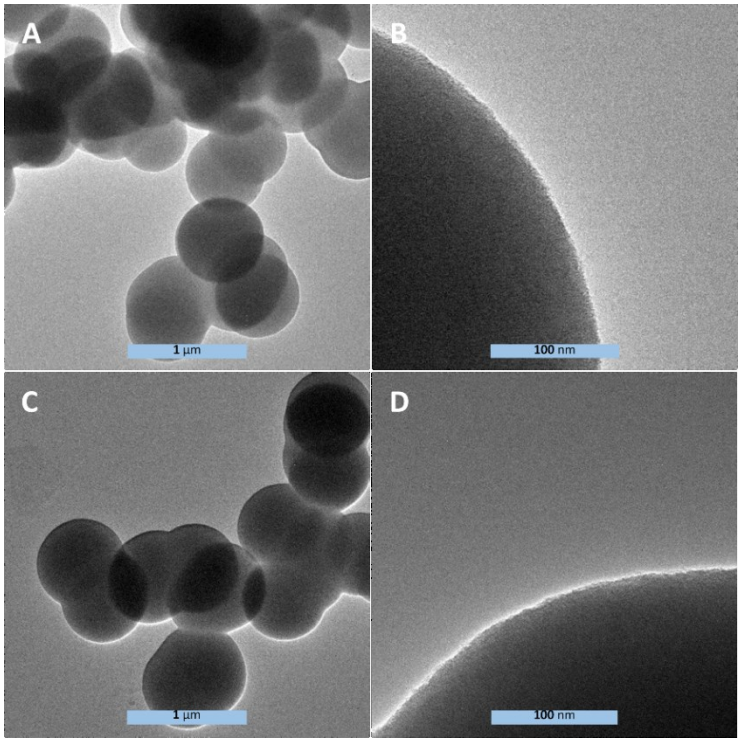

*Figure 16: TEM images of the precipitates obtained from the biomimetic precipitations with 1 mg/ml **4** (A and B) or **7** (C and D) and 25 mM silicic acid at pH 7*

The precipitates in Figures 15 and 16 are composed of aggregates of spherical silica particles possessing a smooth morphology and diameters of less than 1 µm. They resemble the structure and morphology of the precipitates obtained from peptide **3** under the same conditions (Figure 34 A).

3.1.5 Investigation of silica particle binding to streptavidin-gold-nanoparticle conjugate 8

In order to investigate the display and accessibility of the *N*- and/or *C*-terminus of peptide **3** on the surface of biomimetically generated silica particles, the first strategy, as described at the beginning of section 3.1, employed the attachment of streptavidin-gold nanoparticle conjugate **8** to silica particles containing *N*-or *C*-terminally biotinylated peptides **4** and **7**, respectively, with particles containing peptide **3** as negative controls. The investigation of the silica precipitates after the addition of streptavidin-gold nanoparticle conjugate **8** to the silica particles via TEM and SEM could reveal whether or not the conjugates had been attached to the silica particles.

Biomimetic precipitations were first carried out with **4** and **7** as described in section 2.2.4. Incubation of silica particles (0.02 mg) containing **4** or **7** with 10 µl unwashed (Figure 17) or once washed (Figure 18) and resuspended streptavidin-gold nanoparticle conjugate **8** for one hour at RT and washing after incubation before TEM and SEM sample preparation was carried out as described in section 2.2.5.

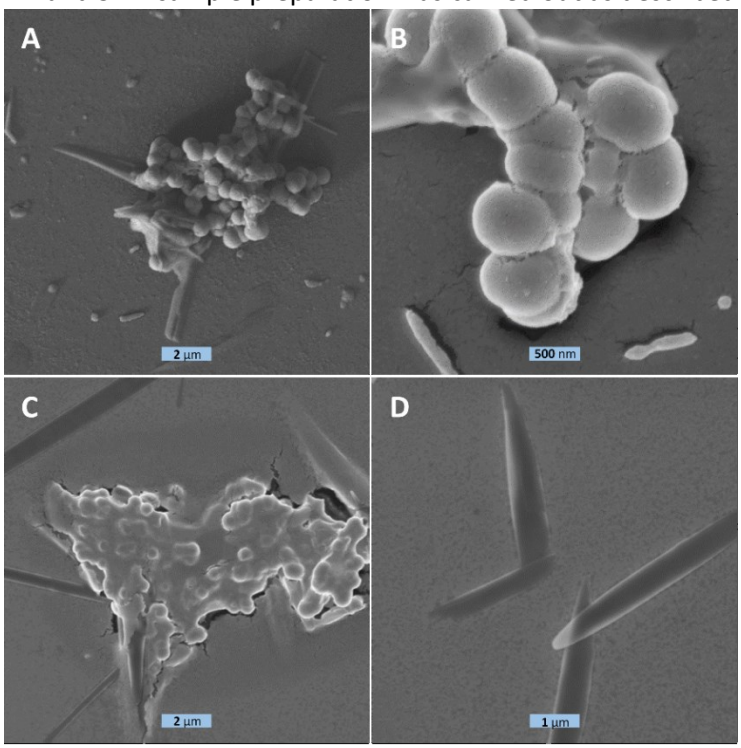

*Figure 17: SEM images obtained from the biomimetic precipitates with **4** (C and D) and **7** (A and B) after incubation with 10 µl unwashed compound **8** for one hour at RT*

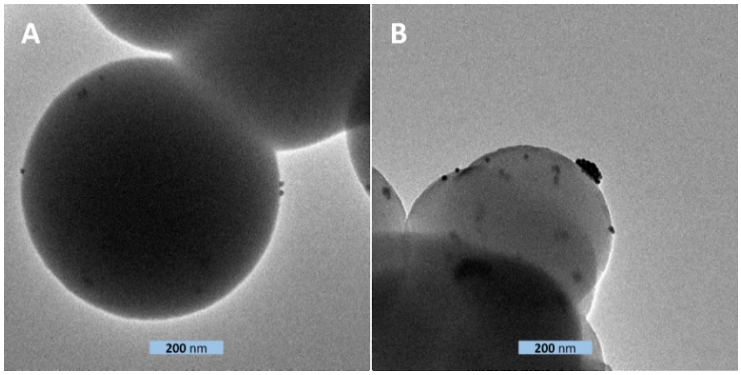

*Figure 18: TEM images obtained from the precipitates with **4** (A) or **7** (B) after incubation with 10 µl once washed compound **8** for one hour at RT*

The SEM images of the precipitates with **4** (Figure 17 C and D) and **7** (Figure 17 A and B) acquired after incubation with unwashed gold nanoparticle conjugate **8** showed that these silica precipitates were still composed of spherical particles, but they were partly covered or enveloped in film-like structures. Additionally, needle-like structures could also be observed (Figure 17 D), which was not the case for the precipitations of the same peptides prior to incubation with **8** (Figures 15 and 16). Figure 18 depicts the TEM images obtained from the precipitates with **4** or **7** after incubation with once washed gold nanoparticle conjugate **8,** which show that the conjugate attached to both types of silica particles. In order to confirm that the binding was mediated by streptavidin-biotin interactions, a negative control (silica particles containing non-biotinylated peptide **3**) had to be introduced.

In the first set of experiments including a negative control (TEM images in Figures 19 (peptide **3**), 20 (peptide **4**) and 21 (peptide **7**)), biomimetic precipitations with **4**, **7** or **3** were carried out as described in section 2.2.4. Incubation of the washed precipitates with once washed and resuspended gold nanoparticle conjugate **8** and TEM/SEM sample preparation was carried out as described for the experiment associated with Figure 18, using twice the amount of conjugate **8.**

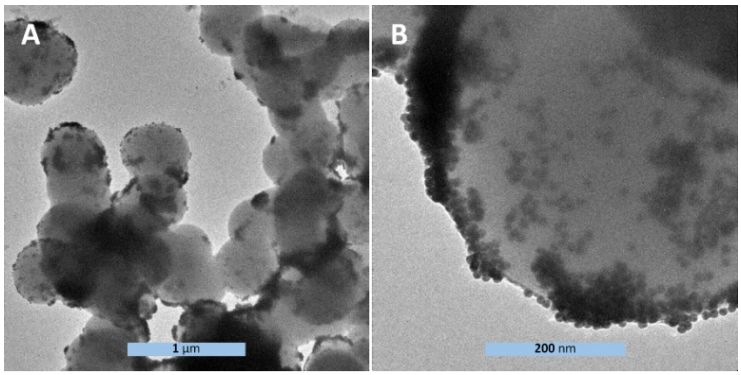

*Figure 19: TEM images of silica particles containing **3** after incubation with 20 µl washed and resuspended gold nanoparticle conjugate **8** for one hour at RT*

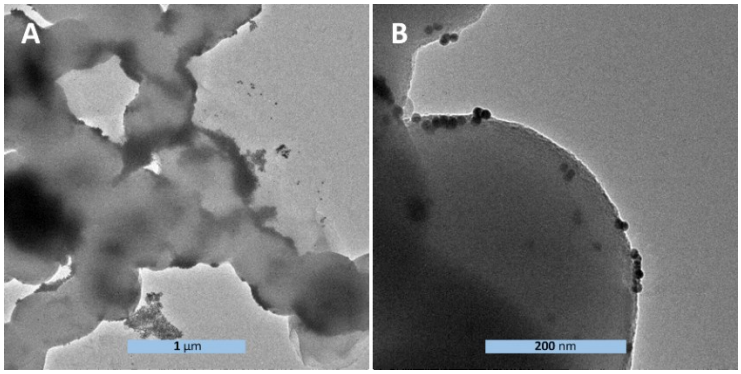

Figure 20: *TEM images of silica particles containing **4** after incubation with 20 µl washed and resuspended gold nanoparticle conjugate **8** for one hour at RT*

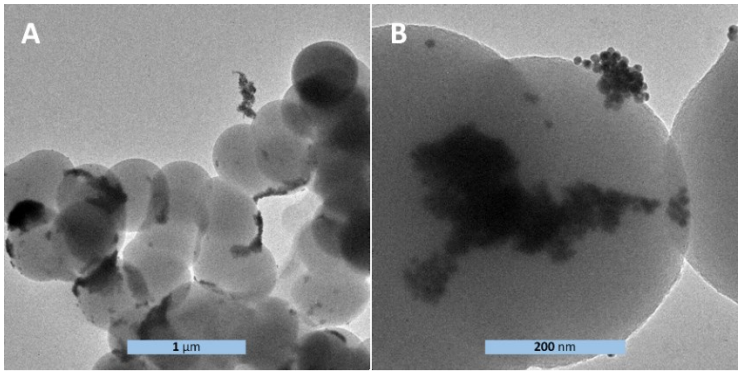

Figure 21: *TEM images of silica particles containing **7** after incubation with 20 µl washed and resuspended gold nanoparticle conjugate **8** for one hour at RT*

The TEM images depicted in Figures 19 to 21 show that compound **8** attached to all three types of silica particles (containing **3**, **4** or **7**). It is clear from these images that the distribution of the aggregates formed by gold nanoparticle conjugate **8** that bound to the silica particles was very inhomogeneous. As the aggregates of compound **8** also bound to the negative control (the silica particles containing non-biotinylated peptide **3**), it is impossible to deduce that attachment of compound **8** arose from streptavidin-biotin interactions.

In the second set of experiments with gold nanoparticle conjugate **8,** the precipitates with peptides **3**, **4** or **7** (0.02 mg (Figures 22 and 23), 0.04 mg or 0.08 mg precipitate (data not shown)) were not washed and isolated from the precipitation mixture. Instead, they were immediately incubated with 10 µl of compound **8** (washed four times) for 10 minutes at RT. The resulting particles were washed with H_2O and prepared for TEM (Figure 23) and SEM (Figure 22) imaging as described in section 2.2.5.

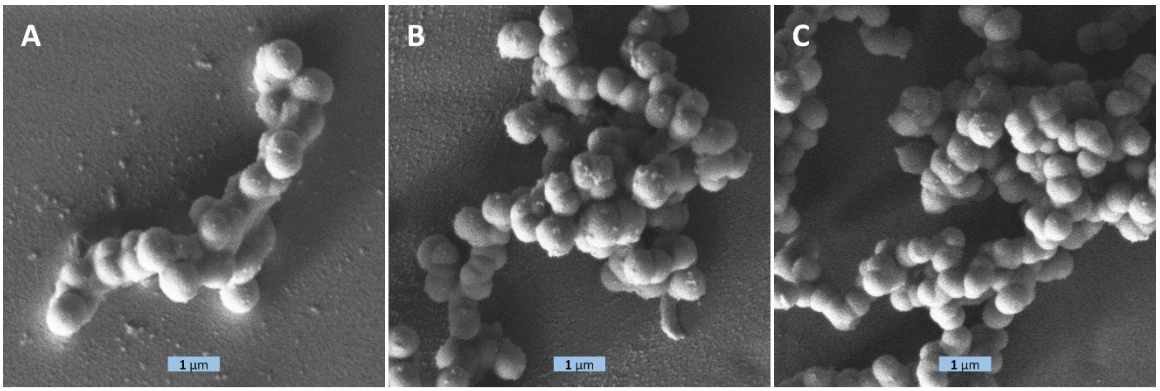

*Figure 22: SEM images obtained from the incubation of 0.02 mg unwashed silica particles containing **3** (A), **4** (B) and **7** (C) with 10 µl (four times) washed and resuspended gold nanoparticle conjugate **8** for 10 min at RT*

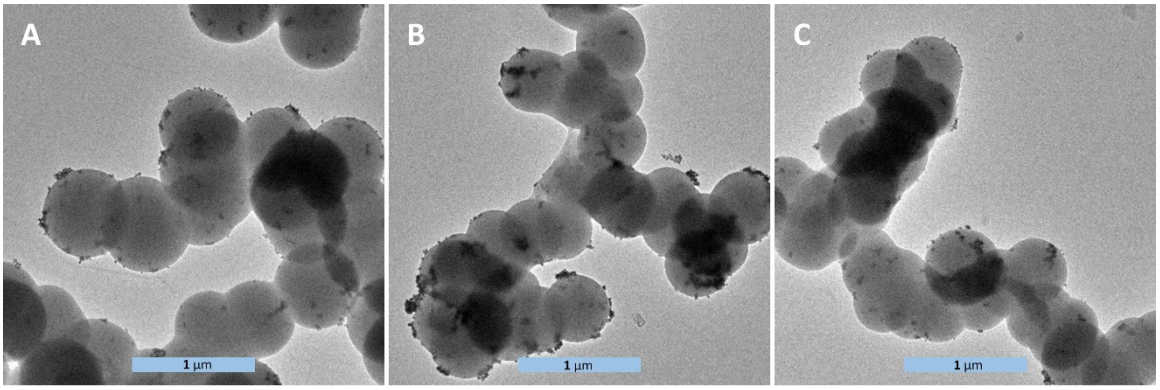

*Figure 23: TEM images obtained from the incubation of 0.02 mg unwashed silica particles containing **3** (A), **4** (B) and **7** (C) with 10 µl (four times) washed and resuspended gold nanoparticle conjugate **8** for 10 min at RT*

All 3 precipitates in Figure 22 contain spherical particles, which indicates that the addition of the gold nanoparticle conjugate **8**, which was carried out before the precipitation process was terminated, did not affect the shape of the particles. The SEM images in Figure 22 show that, while the particles are spherical as in the precipitations with peptide **7** (Figure 15 C and D), peptide **4** (Figure 15 A and B) and peptide **3** (Figure 34 A) prior to addition of gold nanoparticle conjugate **8**, they exhibit uneven surfaces. Further investigation of the precipitates using TEM imaging (Figure 23) revealed that the uneven surface is probably a result of aggregates of compound **8** being attached to the silica particles containing peptide **3** (Figure 23 A), peptide **4** (Figure 23 B) or peptide **7** (Figure 23 C). TEM images (not shown) acquired from the addition of 10 µl conjugate **8** to 0.04 mg or 0.08 mg of silica particles containing peptide **3**, **4** or **7** showed that the amount of conjugate bound to the surface of the silica particles decreased as the ratio silica particles : conjugate **8** increased, as would be expected.

In a third set of experiments with gold nanoparticle conjugate **8**, precipitations with **3**, **4** and **7** were performed as described in section 2.2.4 and the washed precipitates (0.04 mg) were incubated with 10 µl of compound **8** (washed 5 times) for one hour at RT as described in section 2.2.5. In contrast to previous experiments, TEM (Figure 25) and SEM (Figure 24) samples were prepared afterwards without prior centrifugation and washing of the samples to avoid possible attachment of conjugate **8** to the silica particles caused by centrifugation. Instead, the samples were washed with H_2O directly on the Thermanox™ coverslips or copper grids.

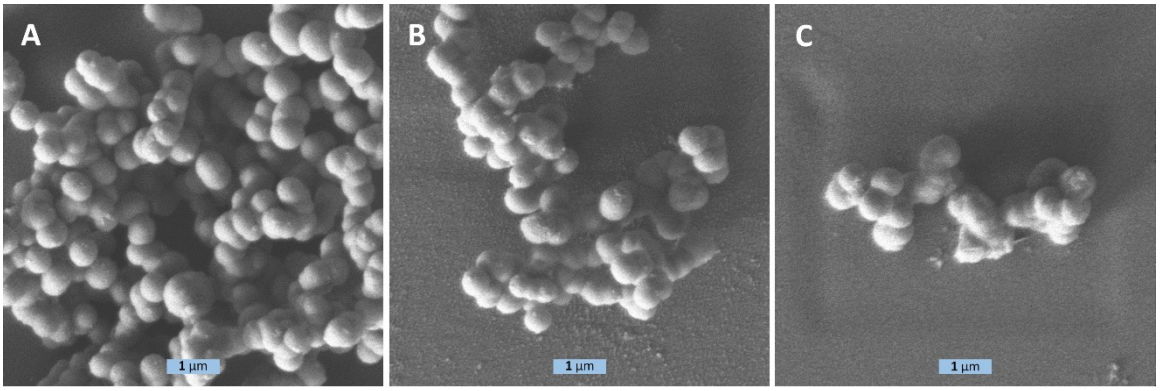

*Figure 24: SEM images obtained from the silica precipitates (0.04 mg) with **3** (A), **4** (B) or **7** (C) after incubation with 10 µl (five times) washed and resuspended compound **8** for one hour at RT, with washing performed after instead of before sample application to the Thermanox™ coverslip*

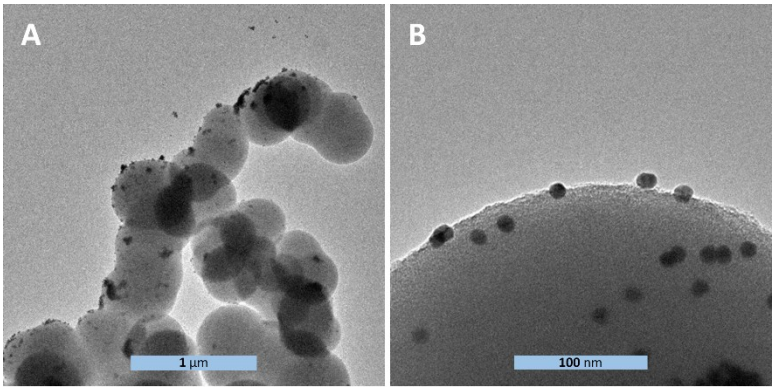

*Figure 25: TEM images obtained from the silica precipitate (0.04 mg) with **3** after incubation with 10 µl (five times) washed and resuspended compound **8** for one hour at RT, with washing performed after instead of before sample application to the copper grid*

The SEM images of the precipitates containing peptide **3** (Figure 24 A), **4** (Figure 24 B) and **7** (Figure 24 C) revealed that they were all composed of spherical silica particles with bumps on the surface, which were identified as aggregates of streptavidin gold nanoparticle conjugate **8** that had attached to the silica particles via TEM imaging (Figure 25). Again, it is not possible from the TEM images depicted in Figure 25 to deduce that the gold nanoparticle conjugate **8** bound to the silica particles via streptavidin-biotin interactions, as the conjugate attached to silica particles containing non-biotinylated peptide **3**.

Overall, SEM and TEM images of all experiments described in this section demonstrate that gold nanoparticle conjugate **8** did not only bind to silica particles containing peptides **4** or **7** but also to the particles with non-biotinylated peptide **3.** While the incubation of particles containing peptides **4** or **7** with unwashed compound **8** led to the formation of needle-like structures (Figure 17 D) and a film covering the particles, these results could be avoided by washing of compound **8** (and thereby removing glycerol from the gold nanoparticle conjugate **8** which might have caused these abnormalities in observed silica structure) in all experiments following the first one. Incubation of washed precipitates containing peptide **4**, **7** or **3** with washed compound **8** for one hour led to the

attachment of the conjugate **8** to all three types of silica particles (Figures 19-21), which was also observed when washed gold nanoparticle conjugate **8** was added to particles containing **4**, **7** or **3** for 10 minutes before they were washed and isolated from the precipitation mixture (Figures 22 and 23). When the particles with peptides **4**, **7** and **3** were incubated with washed conjugate **8** for one hour without subsequent centrifugation (Figures 24 and 25), gold nanoparticle conjugate **8** still did not only bind to the particles containing peptides **4** or **7** but also to the negative control containing non-biotinylated peptide **3**, indicating that the observed unspecific attachment of conjugate **8** to particles containing **3** did not arise from centrifugation. These observations suggest that the binding of conjugate **8** to the different types of silica particles containing biotinylated or non-biotinylated peptides was not based on streptavidin-biotin interactions. Therefore, it was not possible to draw any conclusions about whether or not the *N*- or *C*-terminus of peptide **3** is exposed on the silica surface and accessible for binding. Instead of via streptavidin-biotin-interactions, conjugate **8** possibly attached unspecifically to the silica particles via interaction of streptavidin or the conjugated gold nanoparticles with the silica material or peptide **3** itself. Affinity of streptavidin to silica material itself based on electrostatic interactions should be ruled out as colloidal silica particles have been shown to exhibit negative surface charges at pH 3-13 [116] and the pI of streptavidin is between 5 and 6, which means that the protein should overall be negatively charged at pH 7 [32]. Although the utilization of streptavidin-gold nanoparticle conjugates for the investigation of the accessibility of the *N*- and *C*-terminus of the R5 peptide on the silica particle surface was not successful in this project, such conjugates have been successfully used in other studies of the accessibility or location of biomolecules such as proteins. An example is the successful determination of the accessibility, location and distribution of biotinylated bacteriorhodopsin membrane proteins in lipid membranes on solid supports via attachment of streptavidin-gold nanoparticle conjugates by Puu *et al.* [117]. This demonstrates that, in principle, the utilization of the (strept)avidin-biotin interaction can be a suitable method for the investigation of the location or accessibility of biomolecules such as proteins.

As the gold nanoparticles in gold nanoparticle conjugate **8** themselves might have been responsible for binding to the silica particles, the same strategy for the investigation of the display and accessibility of the *N*- and *C*-terminus of peptide **3** on the surface of the silica particles was further investigated based on possible avidin-biotin interaction between avidin-sulforhodamine 101 conjugates (compound **9**, purchased as a lyophilized powder from Sigma Aldrich, MW approx. 66 kDa) and peptides **4** and **7**.

3.1.6 Investigation of silica particle binding to avidin-sulforhodamine 101 conjugate 9

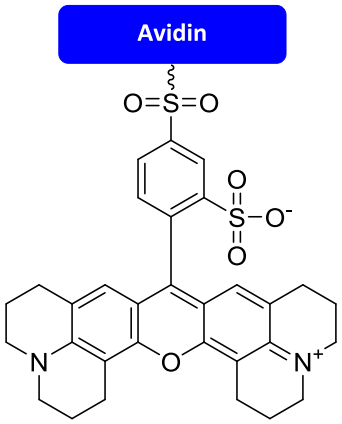

*Figure 26: Structure of compound **9** (sulforhodamine 101 structure available from supplier [118])*

The second strategy for the investigation of the accessibility of the *N*- and *C*-terminus of peptide **3** on the silica particle surface employed the determination of binding of avidin-sulforhodamine 101 conjugate **9** to the particles. The investigation of the binding of fluorescent conjugate **9** (Figure 26) to silica particles containing biotinylated peptides **4** or **7** was carried out as described in section 2.2.6 based on the determination of the difference in concentration of compound **9** in the solutions prior to and after incubation with the silica precipitates. In order to establish a relationship between the concentration of compound **9** and the absorbance at 592 nm, calibrations were performed in H_2O (Figure 27) and 50 mM potassium phosphate buffer (pH 7, Figure 28) as described in section 2.2.6 using concentrations of compound **9** between 0.1 and 0.01 mg/ml (Tables 4 and 5) and the corresponding absorbances of the solutions at 592 nm.

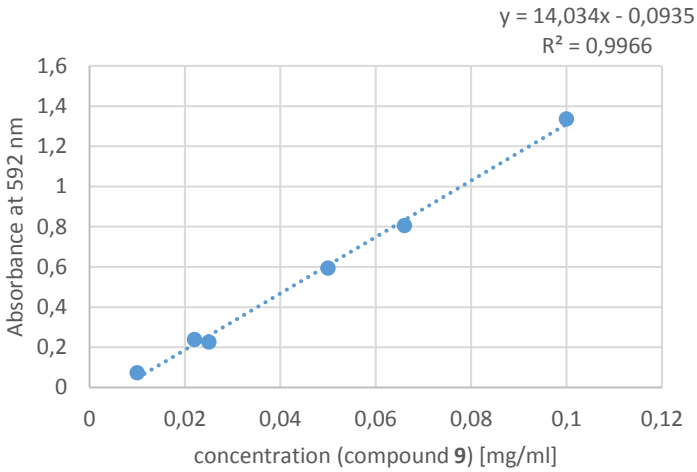

*Figure 27: Calibration for compound **9** in H_2O obtained by plotting the absorbances of the standard solutions at 592 nm against the corresponding concentrations*

*Table 4: Concentrations and corresponding absorbances (at 592 nm) of the standard solutions of compound **9** used for the calibration in H_2O*

concentration (compound 9) [mg/ml]	Absorbance at 592 nm
0.1	1.336
0.066	0.805
0.05	0.593
0.025	0.226
0.022	0.238
0.01	0.072

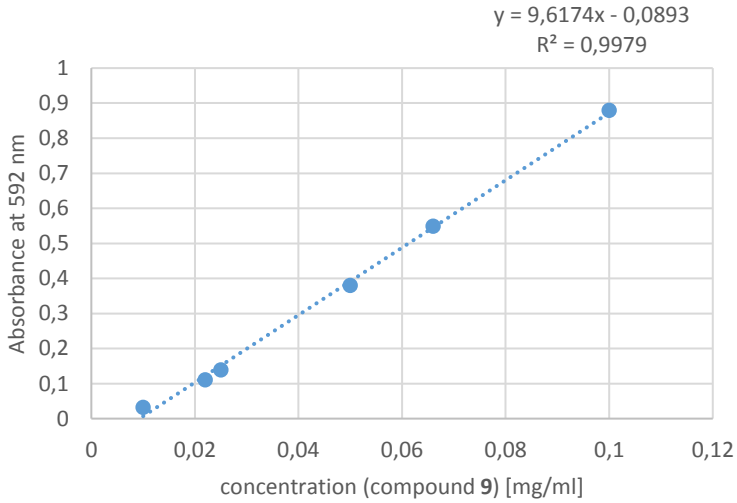

*Figure 28: Calibration for compound **9** in 50 mM potassium phosphate buffer (pH 7) obtained by plotting the absorbances of the standard solutions at 592 nm against the corresponding concentrations*

*Table 5: Concentrations and corresponding absorbances (at 592 nm) of the standard solutions of compound **9** used for the calibration in 50 mM potassium phosphate buffer (pH 7)*

concentration (compound 9) [mg/ml]	Absorbance at 592 nm
0,1	0,879
0,066	0,549
0,05	0,38
0,025	0,139
0,022	0,111
0,01	0,032

For the determination of the binding of compound **9** to the particles containing **4**, **7** or **3** (as a negative control), the first set of experiments involved biomimetic precipitations with these 3 peptides as described in section 2.2.4. After washing of the precipitates with H_2O, they were incubated in solutions with different concentrations of compound **9** in H_2O (section 2.2.6, exact conditions in table caption for Table 6, exact concentrations were determined by UV-Vis measurements, termed "initial conjugate solutions" in Table 6) for 1.5 hours at RT. Following incubation with **9**, particles were washed 5 times with 100 µl H_2O and concentrations of **9** in the washing solutions were determined via UV-Vis measurements. The absorbance data used to calculate the percentages of conjugate **9** attached to the silica particles after their incubation with solutions of compound **9** and the percentage of **9** removed from the particles (calculation explained in section 2.2.6) after the first wash is given in the supplementary information (section 6, Tables S1 to S8).

*Table 6: Percentages of compound **9** bound to silica particles containing peptide **3**, **4** or **7** after incubation in aqueous solutions of compound **9** with concentrations ranging from 0.025 to 0.1 mg/ml for 1.5 hours at RT at particle concentrations of 1 mg/ml, followed by centrifugation (3 min, RT, 14 000 rpm). Precipitates were then washed 5 times with 100 µl H_2O (section 2.2.6, 3 min, RT, 14 000 rpm) and the percentages of compound **9** washed off the silica particles after the first wash are shown.*

Concentration of initial conjugate solution [mg/ml]	**Percentage of compound 9 bound to the particles [%]**			**Percentage of compound 9 washed off after first wash [%]**		
	peptide 3	**peptide 4**	**peptide 7**	**peptide 3**	**peptide 4**	**peptide 7**
0.025	58.4	58.6	57.6	24.0	24.6	25.3
0.05	57.0	62.0	61.9	14.9	16.8	13.7
0.073	32.7±3.9	35.2±3.4	38.3±3.2	29.2±3.8	25.3±3.2	21.4±5.3
0.1	33.3±3.2	34.8±3.1	43.1±5.1	28.0±6.7	28.4±5.5	20.8±5.1

Table 6 shows the percentages of conjugate **9** bound to the silica particles (with peptides **3**, **4** and **7**) for the experimental conditions explained in the table caption. It is evident from Table 6 that the percentage of the initial amount of the fluorescent conjugate **9** that becomes attached to the particles does not differ significantly between the three types of silica particles (containing peptide **3**, **4** or **7**) investigated at all initial concentrations of compound **9** (0.025, 0.05, 0.073 or 0.1 mg/ml) used in the experiments. Tables 6 also demonstrates that the percentages of compound **9** washed off after the first wash also do not significantly differ between the three types of silica particles. In general, the results show that the particles containing peptide **3** (negative control) bind relatively high percentages of the initial amount of compound **9** (between 33 % and 58 %, depending on the initial concentration of conjugate **9** used in each experiment), which indicates that this binding is not caused by streptavidin-biotin interactions but could be a general feature of silica particles made with such peptides. This theory is supported by the observation that the amount of conjugate washed off the silica particles containing peptide **3** is not significantly higher than for the particles containing peptide **4** or **7** in any of the experiments described above. Based on these data, no conclusion can be drawn about the display and accessibility of the *N*- and *C*-terminus of the R5 peptide on the surface of the particles. Data for the removal of conjugate **9** from the silica particles is only shown for the first wash, as the data for the subsequent washes were unreliable and suggested that more compound **9** was washed off the particles than had previously bound to them.

TEM (Figure 30) and SEM (Figure 29) samples (1 mg/ml particle concentration) were prepared according to section 2.1.2. and 2.1.1 after incubation of the silica particles containing peptide **3**, **4** or **7** in a 0.1 mg/ml solution of compound **9** in H_2O at RT for 1.5 hours and subsequent washing (5 times with 100 µl H_2O).

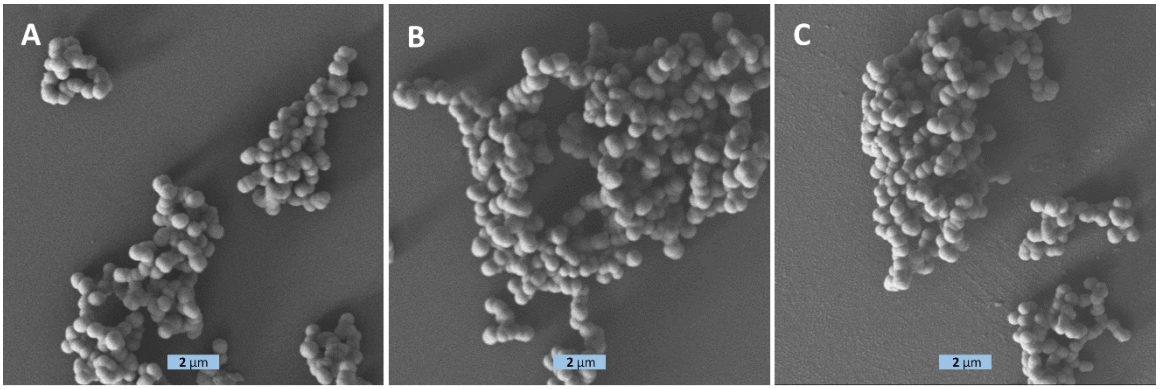

*Figure 29: SEM images acquired after incubation of particles containing **3** (A), **4** (B) or **7** (C) in a 0,1 mg/ml solution of compound **9** in H_2O for 1.5h at RT, centrifugation (3 min, RT, 14 000 rpm) and washing 5 times with 100 µl H_2O (3 min, RT, 14 000 rpm)*

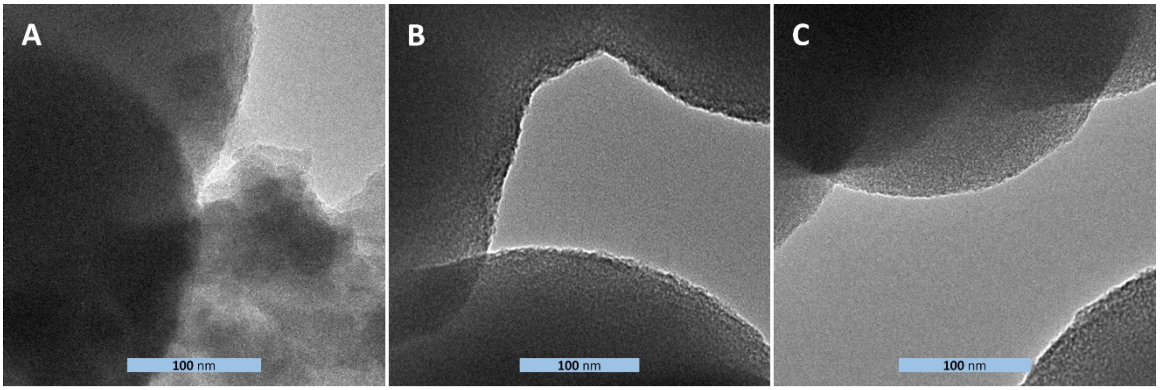

*Figure 30: TEM images acquired after incubation of particles containing **3** (A), **4** (B) or **7** (C) in a 0,1 mg/ml solution of compound **9** in H_2O for 1.5h at RT, centrifugation (3 min, RT, 14 000 rpm) and washing 5 times with 100 µl H_2O (3 min, RT, 14 000 rpm)*

The SEM images in Figure 29 and TEM images in Figure 30 demonstrate that the structure and morphology of the particles containing peptide **3**, **4** or **7** were still mostly the same after incubation in a 0.1 mg/ml aqueous solution of the conjugate **9** with the exception of rarely observed inhomogeneous structures attached to the surface of the different types of particles as shown in Figure 30 A.

In order to investigate the release of **9** in 50 mM potassium phosphate buffer (pH 7) from the particles with peptide **3**, **4** or **7,** which had previously been incubated with conjugate **9** and washed 5 times with 100 µl H_2O (conditions in table caption of Table 7), the particles were incubated in 50 mM potassium phosphate buffer (pH 7) for one hour at RT at a particle concentration of 2 mg/ml. The amount of compound **9** released (Table 7) was determined via UV-Vis measurements of the supernatants at 592 nm and the calculation of the concentration of compound **9** from the calibration (carried out in 50 mM potassium phosphate buffer (pH 7)) following equation 2 in section 2.2.6.1. From the concentration of the solutions of compound **9,** the amount and percentage of conjugate **9** released from the particles in 50 mM potassium phosphate buffer (pH 7) was determined according to equations 3, 4 and 5 from section 2.2.6.1.

*Table 7: Determination of the percentage of compound **9** released from silica particles containing peptide **3**, **4** or **7** (previously incubated for 1.5 hours at RT in 0.073 mg/ml compound **9** in H_2O and washed 5 times with 100 µl H_2O), incubated in 50 mM potassium phosphate buffer (pH 7) for 1 hour at RT, followed by centrifugation (3 min, RT, 14 000 rpm) and UV-Vis absorbance measurement of the supernatant at 592 nm*

Peptide	Amount of compound 9 bound to the particles [mg]	Absorbance of supernatant at 592 nm after 1 hour incubation at pH 7	Concentration of compound 9 in supernatant [mg/ml]	Amount of compound 9 in supernatant [mg]	Percentage of compound 9 released* after incubation at pH 7 for 1 hour [%]
3	0.00478±0.00061	0.033±0.014	0.0128±0.0015	0.00128±0.00015	28.3±0.7
4	0.00513±0.00055	0.06±0.018	0.0155±0.0018	0.00155±0.00018	31.6±0.5
7	0.00560±0.00053	0.108±0.029	0.0205±0.0027	0.00205±0.00027	37.9±2.0

*percentage was determined as percentage of conjugate **9** initially bound before washing with H_2O

Table 7 demonstrates that incubation of the particles in 50 mM potassium phosphate buffer at pH 7 after binding of compound **9** and washing with H_2O led to further release of compound **9** suggesting that even after washing with 100 µl H_2O 5 times, there was still conjugate bound to all 3 types of particles (containing peptide **3**, **4** or **7**). The highest percentage was released from the particles containing peptide **7** followed by the particles with peptide **4** and finally **3**.

After incubation of the particles in 50 mM potassium phosphate buffer (pH 7) for one hour as described above, they were resuspended in H_2O at a concentration of 0.4 mg/ml and viewed on the fluorescence microscope as described in section 2.1.4, in order to visualize residual fluorescence caused by still attached compound **9**. The images were acquired using 2 channels: sulforhodamine 101 and bright field.

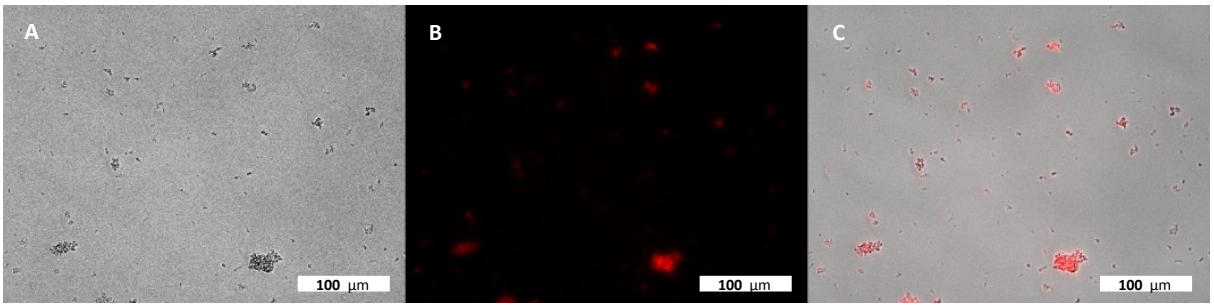

*Figure 31: Fluorescence microscopy images obtained from the particles containing peptide **3** after incubation in 0.073 mg/ml compound **9** (in H_2O), 5 times washing with 100 µl H_2O and one hour incubation in 50 mM potassium phosphate buffer (pH 7) at RT, A: bright field, B: sulforhodamine 101, C: composite of A and B*

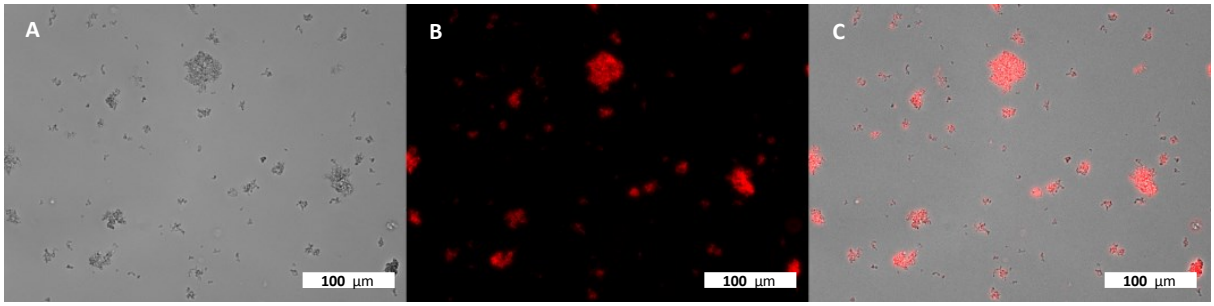

*Figure 32: Fluorescence microscopy images obtained from the particles containing peptide **4** after incubation in 0.073 mg/ml compound **9** (in H_2O), 5 times washing with 100 µl H_2O and one hour incubation in 50 mM potassium phosphate buffer (pH 7) at RT, A: bright field, B: sulforhodamine 101, C: composite of A and B*

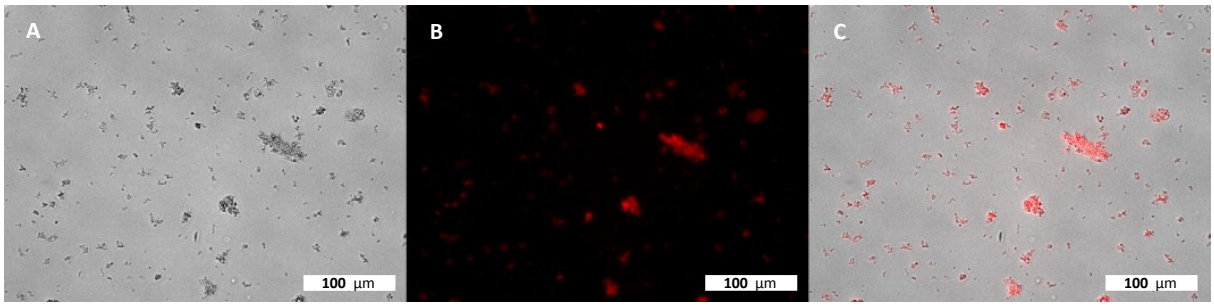

*Figure 33: Fluorescence microscopy images obtained from the particles containing peptide **7** after incubation in 0.073 mg/ml compound **9** (in H_2O), 5 times washing with 100 µl H_2O and one hour incubation in 50 mM potassium phosphate buffer (pH 7) at RT, A: bright field, B: sulforhodamine 101, C: composite of A and B*

The fluorescence microscopy images depicted in Figures 31 to 33 demonstrate that even after extensive washing with H_2O and incubation in 50 mM potassium phosphate buffer (pH 7), all three types of particles still had sufficient amounts of compound **9** bound to them to cause detectable fluorescence signals.

Another set of experiments was carried out similarly to the experiment associated with Table 6, but the particles containing peptides **3**, **4** or **7** were first incubated in 50 mM potassium phosphate buffer (pH 4 or 7), to promote release of the peptides, (2 mg/ml particle concentration) at RT for 24 hours and washed twice with 100 µl 50 mM potassium phosphate buffer (pH 7) before they were incubated in solutions of compound **9** in 50 mM potassium phosphate buffer (pH 7) (exact concentrations given in Tables 8 and 9, 1 mg/ml particle concentration) for 1.5 hours at RT. Subsequent centrifugation and washing was carried out as in the experiments associated with Table 6, using 50 mM potassium phosphate buffer (pH 7) instead of H_2O. Determination of compound **9** bound to the particles was carried out as described in section 2.2.6 (equations 3-5) using the calibration established for compound **9** in 50 mM potassium phosphate buffer (pH 7).

As the absorbance data from the supernatants obtained from washing of the silica particles (after they had been incubated with compound **9**) with 50 mM potassium phosphate buffer (pH 7) in these experiments were not reliable (strong baseline drifts in the absorbance curves), they are not shown.

*Table 8: Data for the calculation of the percentage of compound **9** bound to the silica particles containing peptide **3**, **4** or **7** after incubation in 50 mM potassium phosphate buffer (pH 4) for 24 hours at RT and washing with 50 mM potassium phosphate buffer (pH 7) followed by incubation in a 0.083 mg/ml solution of compound **9** in 50 mM potassium phosphate buffer (pH 7) for 1.5 hours at RT with subsequent centrifugation (3 min, RT, 14 000 rpm)*

Peptide	Concentration of compound 9 in initial conjugate solution [mg/ml]	Amount of compound 9 in initial conjugate solution [mg]	Absorbance of initial supernatant	Concentration of compound 9 in initial supernatant [mg/ml]	Amount of compound 9 in initial supernatant [mg]	Percentage of compound 9 bound to the particles [%]
3	0.083	0.0166	0.542	0.0656	0.01312	**20.9**
4	0.083	0.0166	0.491	0.0603	0.01206	**27.3**
7	0.083	0.0166	0.478	0.0590	0.01180	**28.9**

*Table 9: Data for the calculation of the percentage of compound **9** bound to the silica particles containing peptide **3**, **4** or **7** after incubation in 50 mM potassium phosphate (pH 7) for 24 hours at RT and washing with 50 mM potassium phosphate buffer (pH 7) followed by incubation in a 0.083 mg/ml solution of compound **9** in 50 mM potassium phosphate buffer (pH 7) for 1.5 hours at RT with subsequent centrifugation (3 min, RT, 14 000 rpm)*

Peptide	Concentration of compound 9 in initial conjugate solution [mg/ml]	Amount of compound 9 in initial conjugate solution [mg]	Absorbance of initial supernatant	Concentration of compound 9 in initial supernatant [mg/ml]	Amount of compound 9 in initial supernatant [mg]	Percentage of compound 9 bound to the particles [%]
3	0.088	0.0176	0.447	0.0558	0.01116	**36.5**
4	0.088	0.0176	0.371	0.0479	0.00958	**45.5**
7	0.088	0.0176	0.331	0.0437	0.00874	**50.3**

Although the percentages of conjugate bound to the silica particles (containing the different biotinylated and non-biotinylated peptides) obtained from the experiments corresponding to Tables 8 and 9 do differ between the 3 peptides, the differences are still not big enough to be able to draw a conclusion about the display of the *N*- or *C*-terminus of the R5 peptide on the surface of the biomimetically generated silica particles. As the particles containing the non-biotinylated R5 variant **3** still bind at least 21 % (Table 8) of conjugate **9** it can be assumed that the binding of the conjugate does not (only) arise from biotin-avidin interaction.

The results in this section demonstrate that the display and accessibility of the *N*- and *C*-terminus of the R5 peptide variant **3** on the surface of biomimetically generated silica particles could not be determined using compound **9**, which not only attached to particles containing peptide **4** or **7** but also to silica particles containing non-biotinylated peptide **3** with percentages of attached compound **9** in the same range as observed for particles with peptide **4** and **7** (Table 6). The percentage of bound compound **9** washed off the silica particles containing peptide **3** was also in the same range as for the silica particles containing peptide **4** or **7** (Table 6). In addition, Table 7 shows that a significant amount of conjugate **9** was still bound to all types of investigated particles after extensive washing with H_2O and could partially be released after incubation of the particles in 50 mM potassium phosphate buffer (pH 7), following which the particles containing **4**, **7** or **3** all still exhibited detectable fluorescence (Figures 31-33). These results suggest, that the binding of compound **9** to the investigated silica particles was not (only) mediated by avidin-biotin-interaction but rather via unspecific interaction of avidin with the silica material or non-biotinylated peptide **3** itself. The results listed in Tables 8 and 9 show that in general, more conjugate **9** is bound to the particles with peptides **3**, **4** and **7** that had been incubated in 50 mM potassium phosphate buffer (pH 7, Table 9) prior to incubation with **9** than to the corresponding particles that had been incubated at pH 4 (Table 8). As it has been shown that at lower pH, more R5 peptide is released from such particles [5], this could potentially mean that the presence of the R5 peptide variants **3**,**4** and **7** does influence the interaction of the silica particles with conjugate **9** and the observed loading of conjugate **9** onto the silica particles.

Loading procedures of cargo molecules onto silica particles normally depend on the type of particle. The surfaces of nonporous silica nanoparticles can be functionalized with anchor functionalities (such as amine or thiol groups) that allow for the attachment of various biomolecules to the silica particles using a method involving co-condensation of TEOS with appropriately functionalized alkoxysilanes or the post coating-method, which involves deposition of an additional layer of silica containing the desired functional group onto silica particles post synthesis. Biomolecules can then be loaded onto the surface-modified silica particles via covalent attachment (e.g. oligonucleotides are attached to thiol

groups via disulfide-coupling chemistry, amine containing biomolecules such as proteins can be linked to amine groups on silica surfaces via homobifuctional crosslinkers that show a high reactivity towards amines, such as glutaraldehyde). [32] Loading of cargo molecules onto mesoporous silica particles, which are potential delivery vehicles for a variety of biomolecules, is mediated via physical adsorption on the surface and diffusion of the cargo molecules into the pores of the particles when they are incubated in a solution of the cargo molecules. Loading and release of the cargo is thereby dependent on diffusion rates of the molecules into and from the pores, which depends on pore size and structure. [55] In the case of silica particles derived from the biomimetic approach using the R5 peptide or its variant containing a cysteine on the *N*-terminus (peptide **3**), the incorporation of cargo molecules is normally achieved via covalent attachment of the cargo molecule to the *N*-terminus of the peptide. Another method is the binding of cargo molecules to the thiol group of the *N*-terminal cysteine residue with the possibility of controlled cargo release by cleavage of the disulfide bond using reducing conditions. When the silica precipitation is carried out using a modified form of the R5 peptide, the peptide containing the cargo is encapsulated in the particles [5]. The experiments described in this and the previous section demonstrate that the gold nanoparticle conjugate **8** or the fluorescent conjugate **9** were attached to silica particles derived from peptide **3** post synthesis by incubation of the silica particles in a solution of **8** or **9.** Binding of these conjugates to silica particles was achieved without attaching them to peptide **3,** which might also be possible for other proteins apart from streptavidin and avidin, if proteins in general unspecifically attach to silica particles derived from **3**. If this is the case, silica particles derived from peptide **3** possibly can not only bind proteins via attachment to peptide **3** but also through simple incubation of the particles with these molecules, similar to mesoporous silica particles [55]. If such silica particles show the ability to bind proteins in general, they might also randomly attach to proteins in a physiological environment, which could alter surface properties of the particles and influence their interaction with, for example, cells. It has previously been shown that, when different types of nanoparticles (such as gold or silica nanoparticles) are exposed to physiological environments, an immediate coating of the nanoparticles with proteins (generating a “protein-shell” termed protein-corona) occurs. [119] Protein-coating of nanoparticles can indeed alter their interaction with cells, as it takes place between the protein-coated nanoparticle and the cell rather than between the bare particle surface and the cell. It has been reported for nanoparticles derived from different materials (including gold and silica nanoparticles) that the generated protein corona can, depending on corona composition and the nanoparticle materials, sizes and shapes, lead to facilitated [120] or hindered [121] uptake of nanoparticles by cells compared to the bare particles. [119] Therefore, it is important to investigate the possible formation of a protein corona on silica particles derived from R5 peptide variants in physiological environments and how this affects uptake of the particles by cells.

3.2 Investigation of the effect of different precipitation parameters on the morphologies of silica particles derived from 3 with TMOS or TEOS

Biomimetic silica precipitations with the R5 peptide variant **3** as a silica precipitating agent were carried out with variations in different parameters such as the pH as well as concentrations of **3** and TEOS to investigate the effects that these parameters have on the morphologies of the resultant silica precipitates and to optimize the conditions for the production of spherical silica particles with smooth morphologies and uniform size distributions using a biomimetic approach with TMOS or TEOS and peptide **3**.

3.2.1 Biomimetic silica precipitations with **3** and TMOS at different pH values

The biomimetic silica precipitations with **3** (1 mg/ml) and TMOS as a silica precursor (25 mM final concentration of silicic acid) were carried out as described in section 2.3.1 in 50 mM potassium phosphate buffer with pH values ranging from 4 to 9 in order to investigate the influence of the pH value on the morphology of the obtained precipitates. The precipitates were viewed on SEM (Figure 34) and TEM (Figure 35) as described in section 2.1.1 and 2.1.2 At pH values below 7, no precipitate was observed.

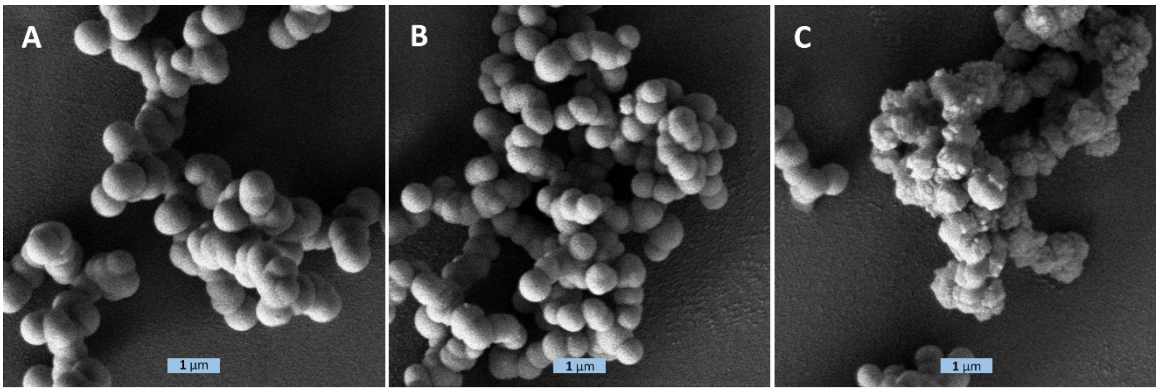

*Figure 34: SEM images of the silica precipitates obtained from precipitations with 1 mg/ml **3** and 25 mM silicic acid at pH values of 7 (A), 8 (B) and 9 (C)*

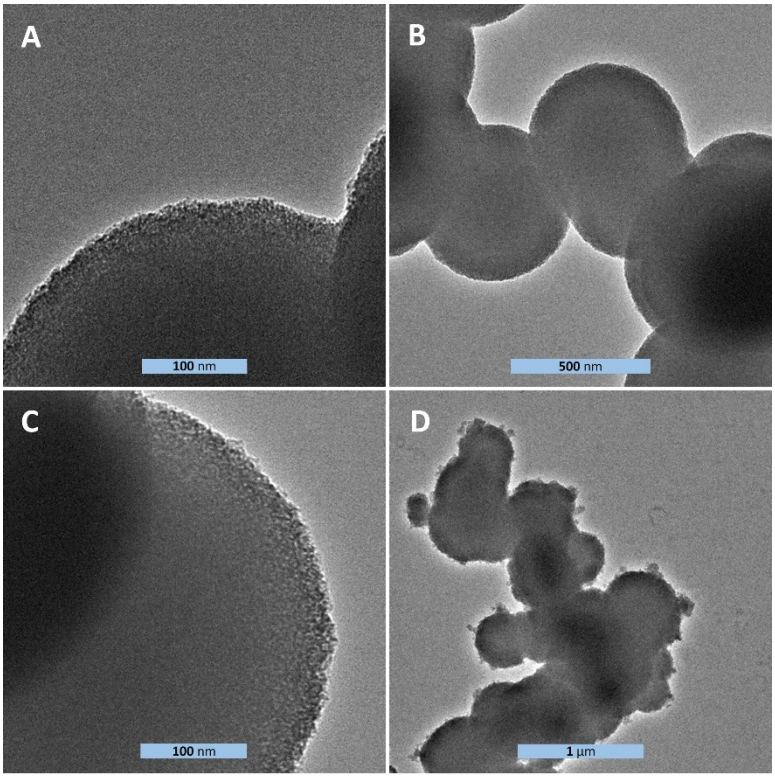

*Figure 35: TEM images of the silica precipitates obtained from precipitations with 1 mg/ml **3** and 25 mM silicic acid at pH 8 (A and B) and pH 9 (C and D)*

The investigation of the morphology of silica precipitates revealed that, while at pH 7 and 8 (Figure 34 A and B) the silica precipitates are composed of aggregated spherical silica particles with diameters of slightly less than one µm with smooth surfaces, the precipitate obtained at pH 9 contained aggregates of silica particles with rough surfaces (Figure 34 C). Further investigation via TEM was carried out for the precipitates obtained at pH 8 (Figure 35 A and B) and pH 9 (Figure 35 C and D), which confirmed that the surfaces of the particle aggregates obtained at pH 8 were relatively smooth (Figure 35 A/B), while most of the particles derived from precipitations at pH 9 exhibited rough surfaces (Figure 35 D).

Based on these observations, the morphology of the silica precipitates does seem to be dependent on the specific pH value the precipitations were carried out at. The spherical structure and smooth morphology obtained for precipitations at pH 7 is in agreement with the structures of silica precipitates obtained for peptide **3** under the same conditions by Lechner and Becker in 2012 [108]. Furthermore, similar to our observation that no silica precipitate is formed below neutral pH when peptide **3** is used as a silica precipitating agent, it has been reported previously that the R5 peptide (peptide **3** without the *N*-terminal cysteine residue) has no silica precipitating activity below pH 7 [75]. This has been assumed to be a result of the missing lysine modifications (methylations and polyamine modifications) present in native silaffins. These modifications normally probably assist self-assembly of native silaffin peptides, and silaffin-1A (containing the mentioned lysine modifications but lacking phosphorylations present in native silaffin-1A) exhibits silica precipitating activity (under addition of polyvalent phosphate anions) at pH values as low as 5. [75] In the case of peptide **3**, the formation of disulfide bonds between cysteines of the individual peptides might (in addition to ε-amino groups carrying positive charges that interact with phosphate anions from the buffer, which act as crosslinks between individual peptides) assist self-assembly of the peptide and formation of the aggregates that serve as templates for the polycondensation of silicic acid. It has been suggested that affecting self-assembly of the R5 peptide can influence the morphology of silica precipitates. [122] This implies that the variation in pH possibly affects self-assembly of peptide **3,** which then causes changes in the morphology of the precipitates obtained at pH 9 compared to pH 7/8. (Figure 34/35).

3.2.2 Biomimetic silica precipitations with 3 and TEOS at different pH values

Biomimetic precipitations with **3** (1 mg/ml) and TEOS (45 mM) were performed as described in section 2.3.2 in 50 mM potassium phosphate buffer at pH 4 to 9 to investigate a possible connection between the pH the precipitations were carried out at and the morphologies of the resultant silica precipitates. The precipitates were viewed and imaged via SEM (Figure 36) and TEM (Figure 37) as described in section 2.1. No precipitate was observed at pH values below 6.

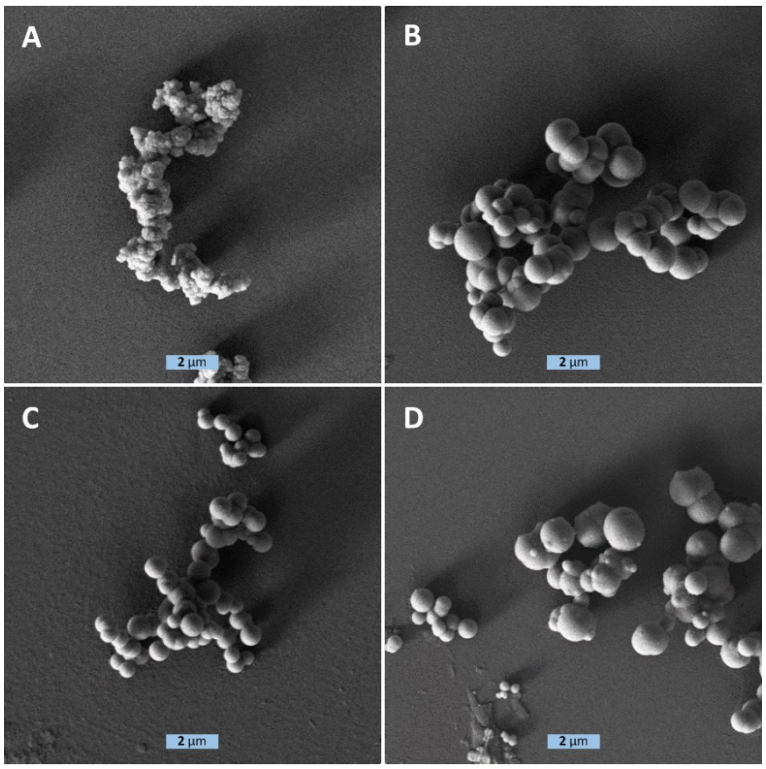

*Figure 36: SEM images of the precipitates obtained from biomimetic silica precipitation with **3** (1 mg/ml) and TEOS (45 mM) in 50 mM potassium phosphate buffer at pH 6 (A), 7 (B), 8 (C), and 9 (D)*

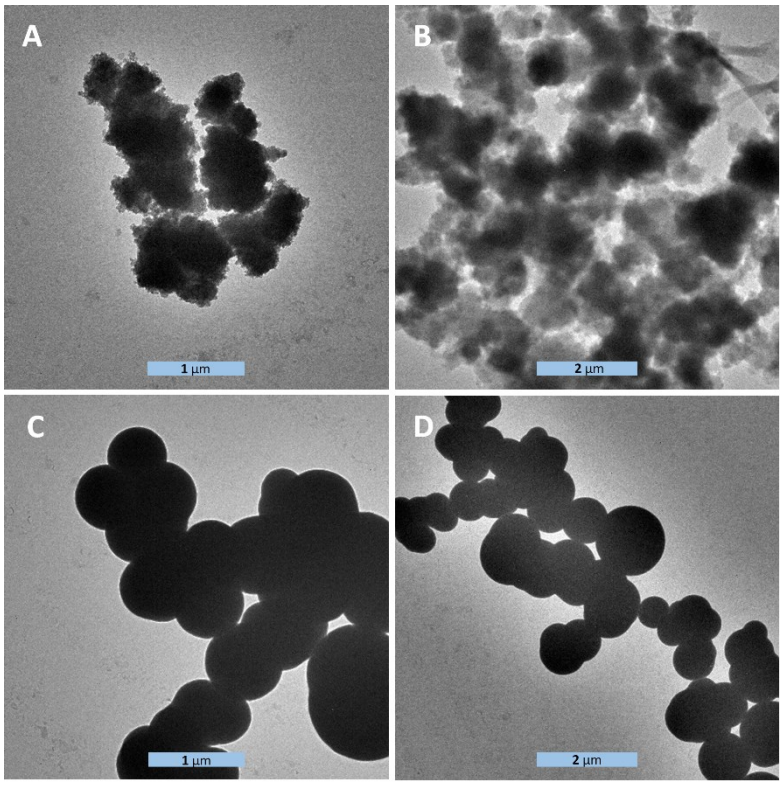

*Figure 37: TEM images of the precipitates obtained from biomimetic silica precipitation with **3** (1 mg/ml) and TEOS (45 mM) in 50 mM potassium phosphate buffer at pH 6 (A and B) and pH 7 (C and D)*

The SEM images in Figure 36 show that the precipitates obtained at pH values of 7 (Figure 36 B) or 8 (Figure 36 C) comprise aggregated silica particles with diameters in the micrometer range with spherical shapes and smooth surfaces. In contrast, in the precipitate obtained at pH 9, occasionally particles with rougher surfaces can be observed (Figure 36 D). In contrast to precipitates at pH 7,8 and 9, the SEM image of the precipitate obtained at pH 6 shows that it is composed of silica particles with very rough surfaces. This observation was further confirmed by investigation of the precipitates obtained at pH 6 (Figure 37 A and B) and pH 7 (Figure 37 C and D) via TEM, which confirmed the rough surfaces of the inhomogeneous particle aggregates formed at pH 6 compared to the aggregates consisting of spherical silica particles with smooth surfaces at pH 7. In addition, from Figure 36 as well as Figure 37 C and D it is apparent that the sizes of the spherical particles are not completely uniform and diameters range from approximately 500 nm to 1.5 µm.

To sum up, the results shown for TEOS precipitations with peptide **3** at different pH values indicate that the morphology of the silica precipitates is influenced by changes in the pH. As mentioned for TMOS precipitations previously, it has been suggested that affecting self-assembly of silaffin peptides can influence the morphology of silica precipitates [122]. Therefore, the differences in morphologies could be attributed to the effect that the pH value has on the formation of the aggregates of peptide **3** that act as templates for polycondensation of silicic acid. Based on this suggestion and the assumption that disulfide-bond formation between cysteines in peptide **3** plays an important role in self-aggregation of the peptide, the rough morphology of the precipitate obtained at pH 6 (Figure 36 A and 37 A and B) compared to precipitates obtained at pH 7, 8 or 9 could be explained as a result of a lower tendency of the cysteines in peptide **3** to form disulfide bonds at lower pH values. However, this can only remain a hypothesis, as the degree of disulfide bond formation and dimerization of peptide **3** was not determined and compared at different pH values in this project. Therefore, a higher tendency for disulfide bond generation at higher pH values was not proven for peptide **3**.

3.2.3 Biomimetic silica precipitations with different concentrations of **3** and TEOS at pH 6 and 7

Biomimetic precipitations with different concentrations of **3** and TEOS at pH 6 or 7 were carried out as explained in section 2.3.3 in order to identify possible connections between the peptide or TEOS concentrations at pH 6 (Figure 38) or 7 (Figure 39) and the morphology of the resultant silica precipitates. Viewing and imaging of the precipitates was performed on SEM (section 2.1.1)

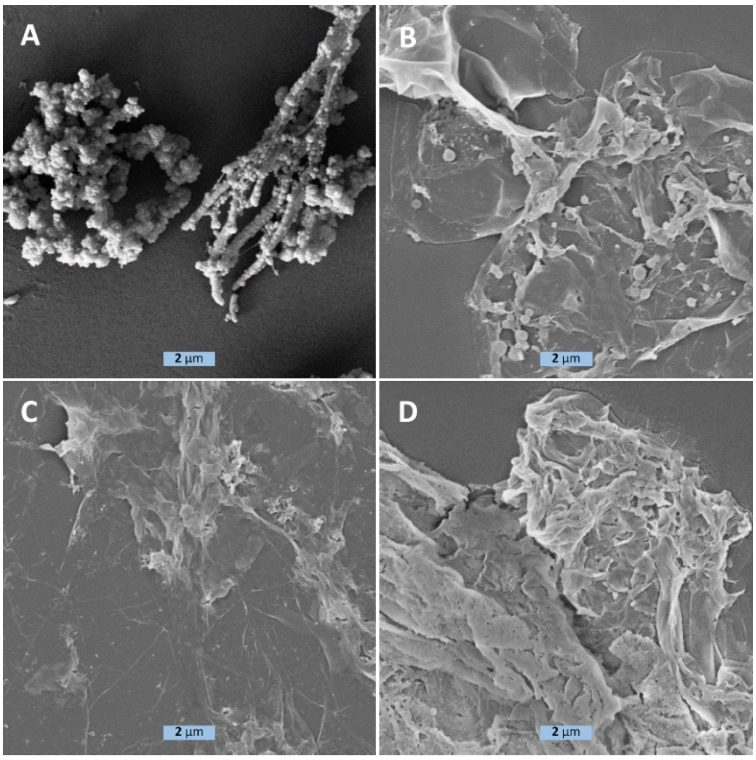

*Figure 38: SEM images obtained from biomimetic silica precipitations with **3** (1 mg/ml for A and B, 0.5 mg/ml for C and D) and TEOS (45 mM for A and C, 22.5 mM for B and D) in 50 mM potassium phosphate buffer at pH 6*

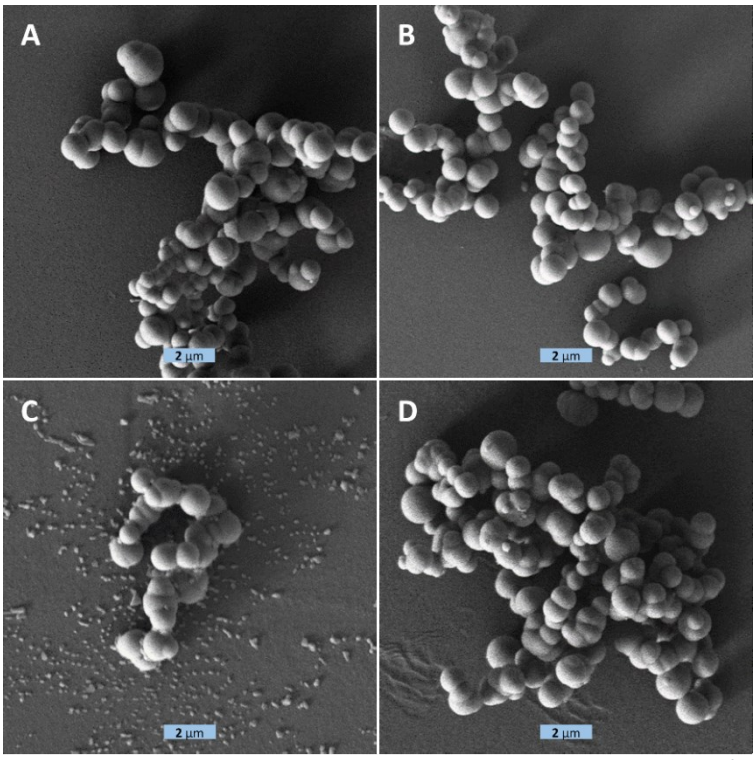

*Figure 39: SEM images obtained from obtained from biomimetic silica precipitations with **3** (1 mg/ml for A and B, 0.5 mg/ml for C and D) and TEOS (45 mM for A and C, 22.5 mM for B and D) in 50 mM potassium phosphate buffer at pH 7*

Figure 38 depicts the morphologies of the silica precipitates obtained from biomimetic silica precipitations at pH 6 with variations in the concentrations of peptide **3** and TEOS. While the precipitate derived from the precipitation at a peptide concentration of 1 mg/ml and a TEOS concentration of 45 mM (Figure 38 A) is mainly composed of aggregates of silica particles possessing rough surfaces, fibrillar structures could also be observed (right half of Figure 38 A) in these samples. In contrast, at pH 6, all other precipitates, obtained from 1 mg/ml peptide and 22.5 mM TEOS (Figure 38 B), 0.5 mg/ml peptide and 45 mM TEOS (Figure 38 C) or 0.5 mg/ml peptide and 22.5 mM TEOS (Figure 38 D), mainly comprised film-like silica structures with only a few single spherical silica particles visible in Figure 38 B.

In Figure 39, the SEM images acquired from biomimetic precipitations at pH 7 using different concentrations of **3** and TEOS are pictured. On the contrary to the morphologies observed for the same combinations of concentrations of **3** and TEOS at pH 6, the precipitates obtained from precipitations in 50 mM potassium phosphate buffer (pH 7) with a combination of 1 mg/ml peptide and 45 mM TEOS (Figure 39 A), 1 mg/ml peptide and 22.5 mM TEOS (Figure 31 B), 0.5 mg/ml peptide with 45 mM TEOS (Figure 39 C) as well as 0.5 mg/ml peptide with 22.5 mM TEOS (Figure 39 D) are all composed of spherical silica particles with relatively smooth surfaces and non-uniform sizes.

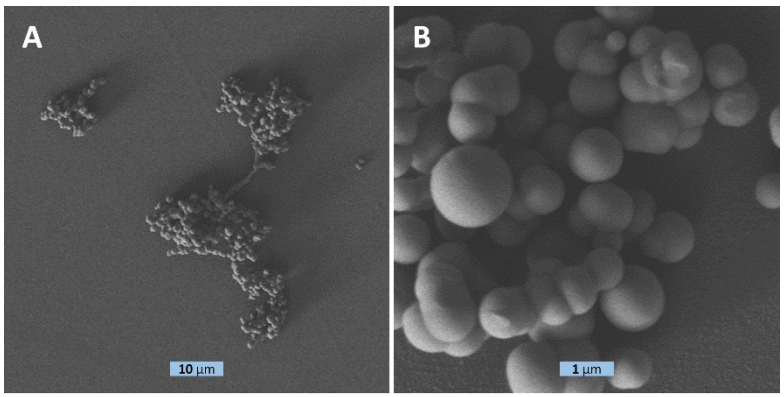

*Figure 40: SEM images obtained from biomimetic silica precipitations with 2 mg/ml **3** and 45 mM TEOS in 50 mM potassium phosphate buffer (pH 7)*

The morphology of the precipitate obtained from 2 mg/ml **3** and 45 mM TEOS in 50 mM potassium phosphate buffer (pH 7) was investigated via SEM (Figure 40 A and B) and was revealed to be composed of aggregates of spherical particles exhibiting smooth surfaces and non-uniform sizes ranging from about 500 nm to 1.5 µm.

The results shown in Figures 38-40 indicate that at pH 6, the concentrations of peptide **3** and TEOS seem to influence the morphology of the silica precipitates while at pH 7, the precipitates obtained from different concentrations of peptide **3** and TEOS largely exhibit the same structure and morphology. This suggests (in combination with the results in Figures 36 and 37) that the pH, which possibly influences the formation of the aggregates of peptide **3** (potentially by influencing the formation of disulfide bonds between the cysteine residues and the charge states of side chain amine groups in peptide **3**) that function as templates for silicic acid polycondensation, is the main factor among the varied precipitation parameters influencing the morphology of the obtained precipitates. Only at a pH as low as 6, an effect of the concentrations of peptide **3** and TEOS on precipitate structures can be observed.

Overall, for both the precipitations with peptide **3** using TMOS as a silica precursor (Figures 34 and 35) as well as the precipitations with peptide **3** using TEOS as a silica precursor (Figures 36 and 37), the pH

influences the structure and morphology of the resultant precipitates (when the concentrations of peptide **3** and the silica precursor are held constant). This is possibly caused by affecting the formation of self-assemblies of peptide **3** (which are possibly facilitated by the formation of disulfide bonds between cysteine residues of the individual peptides [122]). For precipitations with peptide **3** using TEOS as a silica precursor, when the pH was held constant at 6, different concentrations of peptide **3** and TEOS (Figure 38) did influence the structure and morphology of the resultant precipitates with only a combination of 1 mg/ml **3** and 45 mM TEOS leading to the formation of silica particles (with rough surfaces). Lower concentrations of peptide **3** and/or TEOS resulted in the formation of silica films instead of particles possibly resulting from the combination of an impaired ability of **3** to self-aggregate at this pH with low peptide and/or TEOS concentrations. On the contrary, at pH 7 (Figure 39/40), all investigated concentrations of peptide **3** and TEOS led to spherical silica particles with relatively smooth surfaces, suggesting that conditions at pH 7 are the most convenient for the generation of smooth spherical silica particles with peptide **3** and TEOS or TMOS.

3.3 Synthesis of doubly fluorescent modified silica particles

Bifunctional silica particles derived from the R5 peptide could potentially be used for several applications (depending on the types of modifications introduced) including the possible combination of delivery of (bio)molecules with imaging, delivery of two different cargo molecules or vaccine adjuvants. Therefore, we aimed at the development of a convenient method for the simultaneous introduction of two modifications into such particles. The synthesis of silica particles with two fluorescent modifications was carried out employing a biomimetic synthesis approach and introducing one of the modifications via attachment to the *N*-terminus of peptide **3** (resulting in peptide **17**), while the second modification was incorporated using a fluorescein-modified silica precursor (compound **10**). This method allows for the simultaneous introduction of two modifications, as the modified peptide co-precipitates with the silica [5], which is formed under incorporation of the modified silica precursor. As the second modification is incorporated directly into the silica material, it is, in contrast to the modification attached to the *N*-terminus of peptide **3**, independent from R5 peptide release.

3.3.1 Biomimetic silica precipitation with peptide 3 and TMOS using silane 10

3.3.1.1 Precipitations

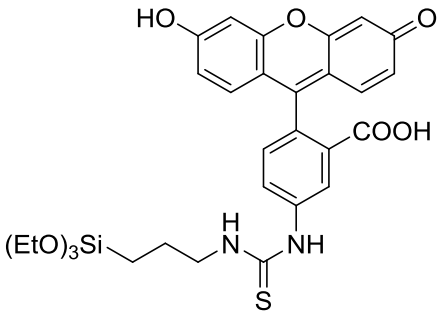

Figure 41: Structure of silane 10 [123]

The synthesis of silica particles with peptide **3** and TMOS under incorporation of fluorescein (using silane **10** as a silica precursor) was generally carried out as described in section 2.4.1.1. Generally, the synthesis of spherical fluorescein modified silica particles with smooth morphologies via the biomimetic synthesis approach presented a challenge and many different combinations of conditions were tested before the desired precipitates were obtained. All precipitations were carried out in 50 mM potassium phosphate buffer at pH 7, based on the observation from the previous section that this pH seemed most suitable for the production of smooth spherical silica particles.

First, the effect of different concentrations of **10** on the particle morphology was studied. Aliquots of compound **10** were dissolved in MeOH and added to the mixture of 270 mM TMOS in 1 mM HCl at the beginning or end of 4 minute TMOS hydrolysis at RT (with concentrations of **10** of 1 mg/ml, 2.9 mg/ml, 4.8 mg/ml and 9.1 mg/ml). The individual mixtures were then added to the solutions of peptide **3** (1 mg/ml)**.** The final concentrations of compound **10** were 0.09 mg/ml, 0.26 mg/ml, 0.44 mg/ml and 0.8 mg/ml, while the final silicic acid concentration was 25 mM. Following precipitation as described in section 2.4.1.1, TEM samples were prepared and imaged (Figure 42).

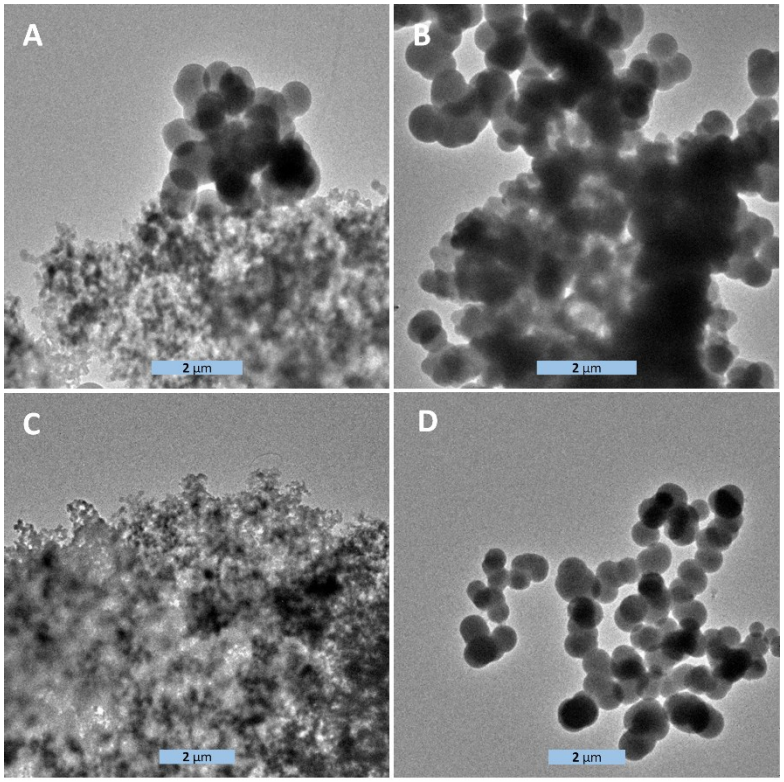

*Figure 42: TEM images of precipitates with 1 mg/ml **3** and different amounts of **10** dissolved in MeOH. Final concentrations of **10**: 0.8 mg/ml (A), 0.09 mg/ml (B) and 0.26 mg/ml (C and D). **10** was added at the beginning (A and B) or the end of 4 minute TMOS hydrolysis (C and D). Precipitates for final concentrations of **10** of 0.44 mg/ml and 0.26 mg/ml (addition at the beginning of TMOS hydrolysis) are not shown as they showed the same structure as (B)*

The precipitate in Figure 42 A shows the (rare) presence of the desired spherical silica particles with smooth morphologies and diameters of less than one µm, but the majority of the precipitate is composed of inhomogeneous aggregates of smaller silica particles. Similarly, the silica precipitate depicted in Figure 42 B is constituted by largely disordered silica aggregates (of larger particles than the precipitate in Figure 42 A) with occasionally occuring spherical silica particles in the micrometer size-range, suggesting that the variation in final concentration of **10** does not significantly change the structure of the precipitate. The precipitate depicted in Figure 42 C and D shows the same composition as the precipitate in Figure 42 A. Overall, the results in Figure 42 demonstrate that the addition of compound **10** at the beginning or end of the 4 minute TMOS hydrolysis and the final concentration of **10** does not make a difference concerning the structure and morphology of the resulting precipitates.

Next, we attempted to prolog the hydrolysis time of compound **10.** Aliquots of **10** were dissolved in MeOH and hydrolyzed in 1 mM HCl (concentration of **10** of 1 mg/ml or 3 mg/ml), and incubated at RT for different time periods (1h, 3h, 6h, and 24h). TMOS was afterwards added to the mixtures at a concentration of 270 mM. The mixtures were further incubated at RT for 4 minutes prior to addition to the solutions of peptide **3** (1 mg/ml). The final concentrations of compound **10** were 0.09 mg/ml

and 0.27 mg/ml while the final silicic acid concentration was 25 mM. The precipitation was then continued as described in section 2.4.1.1 and SEM or TEM images were acquired according to section 2.1.1 and 2.1.2 (Figure 43).

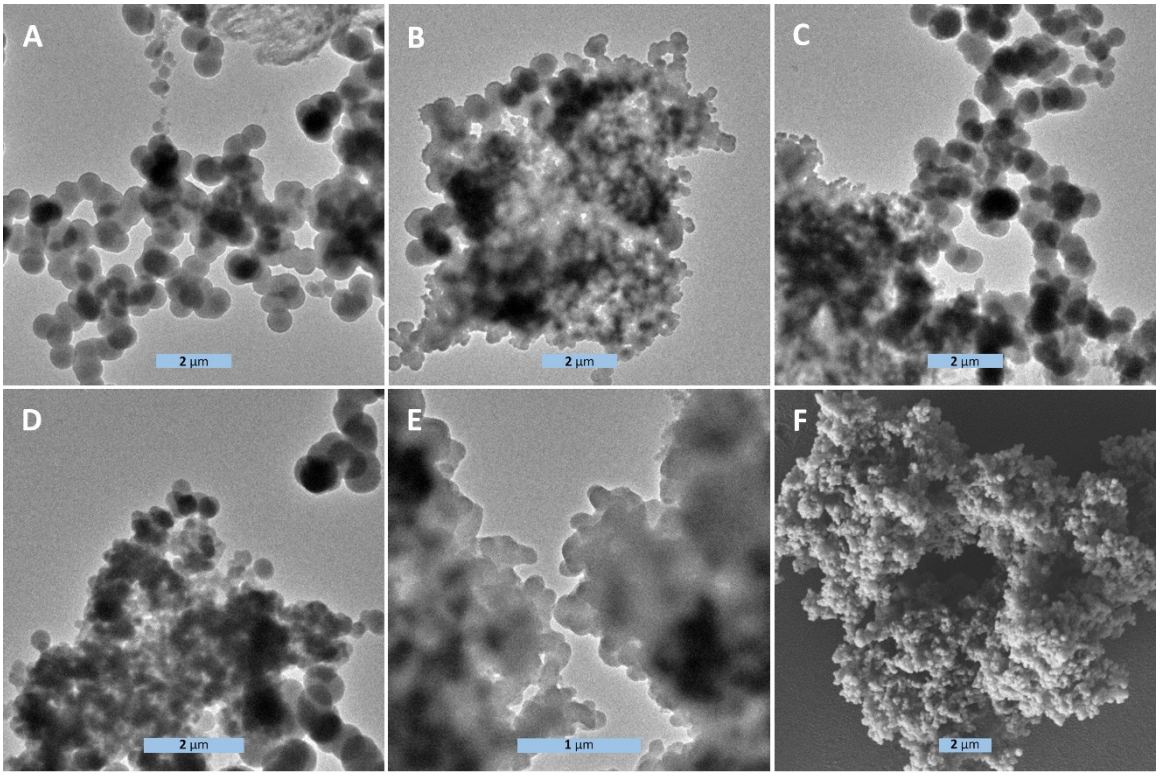

*Figure 43: A-E: TEM images of the silica precipitates obtained with 1 mg/ml **3** and final concentrations of 0.09 mg/ml (A and B) or 0.27 mg/ml (C, D and E) compound **10** with incubation times in 1 mM HCl of 1 hour (A and C), 3 hours (B), 6 hours (D) or 24 hours (E) before addition of TMOS (270 mM) to the mixture. F: SEM image of the silica precipitate derived from 0.27 mg/ml **10** with 3 hours incubation time in 1 mM HCl*

The precipitates obtained from biomimetic precipitations with different concentrations and incubation times of compound **10** in 1 mM HCl (Figure 43) show the presence of disordered silica aggregates in all cases dominating over the rarely observed spherical silica particles in the micrometer size range visible in Figure 43 A, C and D, which means that even a hydrolysis time of 24 hours of in MeOH dissolved compound **10** in 1 mM HCl did not lead to the desired precipitates composed of spherical silica particles with a smooth morphology.

As all precipitations using MeOH as a solvent for compound **10** resulted in the formation of disordered aggregates of small silica particles, conditions were developed using different organic solvents. Aliquots of compound **10** were dissolved in EtOH, 1-PrOH or iso-PrOH. These solutions were then added to 1 mM HCl at concentrations of compound **10** of 1 mg/ml and incubated at RT for 3 hours. TMOS was subsequently added to the mixture at a concentration of 270 mM and incubated for 4 minutes at RT prior to addition of the solution to peptide **3** (1 mg/ml) resulting in a final concentration of compound **10** of 0.09 mg/ml and 25 mM silicic acid. The residual steps of the precipitation were carried out as described in section 2.4.1.1 and SEM samples were prepared according to section 2.1.1 (Figure 44).

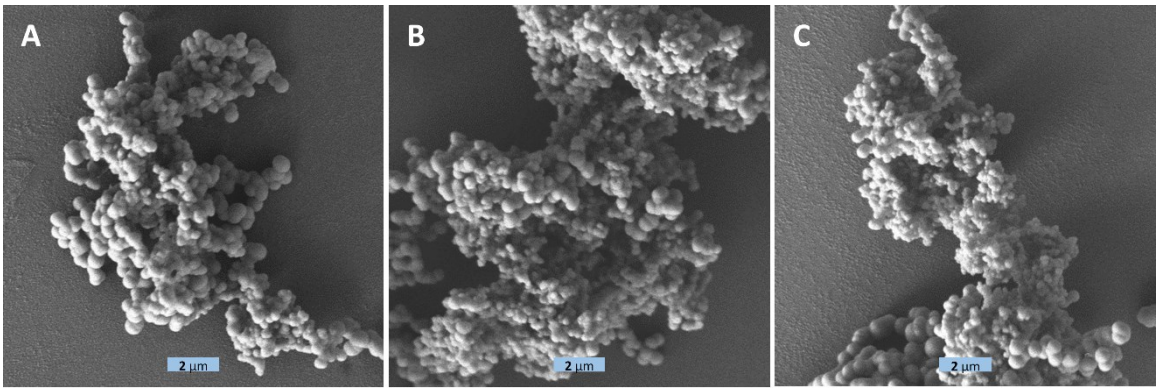

*Figure 44: SEM images obtained from the biomimetic precipitations using EtOH (A), 1-PrOH (B) or iso-PrOH (C) as a solvent for compound **10** with final concentrations of compound **10** of 0.09 mg/ml in 1 mg/ml **3***

The SEM images in Figure 44 show that the precipitates derived from EtOH, 1-PrOH and i-PrOH as solvents for **10** were again composed of rather disordered aggregates of small silica particles with a few spherical particles with diameters in the micrometer range occurring occasionally.

Therefore, further experiments were carried out with the same procedure as in the experiment associated with Figure 44, trying BuOH and t-BuOH as solvents for compound **10,** with final concentrations of **10** of 0.045 mg/ml (BuOH) or 0.023 mg/ml (t-BuOH) in the precipitation mixture.

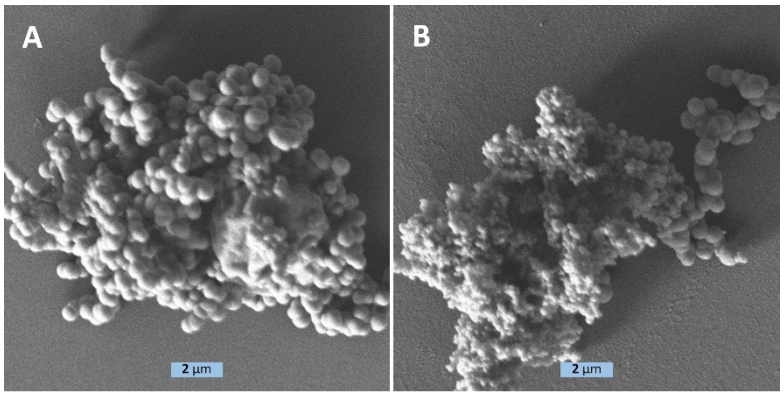

*Figure 45: SEM images obtained from the biomimetic precipitations using BuOH (A) or tBuOH (B) as a solvent for compound **10** with final concentrations of compound **10** of 0.045 mg/ml (A) or 0.023 mg/ml (B) in 1 mg/ml **3***

Figure 45 shows that the precipitations with BuOH and tBuOH as solvents for **10** resulted in the formation of the same disordered aggregates of small silica particles with occasional occurrence of spherical silica particles in the micrometer size-range as observed for EtOH, 1-PrOH and i-PrOH.

In order to find suitable conditions leading to the exclusive formation of spherical fluorescein modified silica particles with smooth surfaces, another experiment was performed: Conditions avoiding the use of organic solvents and involving hydrolysis of compound **10** in an alkaline environment were attempted. The solubility of compound **10** was higher in 100 mM K_2HPO_4 (pH 9) than in 1 mM HCl and the hydroxide-ion is a better nucleophile than H_2O, which might contribute to a better hydrolysis of the sterically bulky modified silica precursor **10** compared to hydrolysis in 1 mM HCl. Compound **10** was dissolved in 100 mM K_2HPO_4 (pH 9) (0.4 mg/ml **10**), incubated at RT for 3 hours and then added to a 1.25 mg/ml solution of **3** at a final concentration of **10** of 0.04 mg/ml. Silicic acid wash freshly generated from a solution of 270 mM TMOS in 1 mM HCl and added to the peptide solution after 4 minutes of TMOS hydrolysis simultaneously with the solution of compound **10** with a final concentration of silicic acid of 27 mM. The rest of the precipitation procedure was carried out as

described in section 2.4.1.1, SEM and TEM samples were prepared according to section 2.1.1 and 2.1.2 (Figure 46 A and Figure 47).

A second experiment was performed under the same conditions but with incubation of **10** in 100 mM K_2HPO_4 for 24 hours (Figure 46 B).

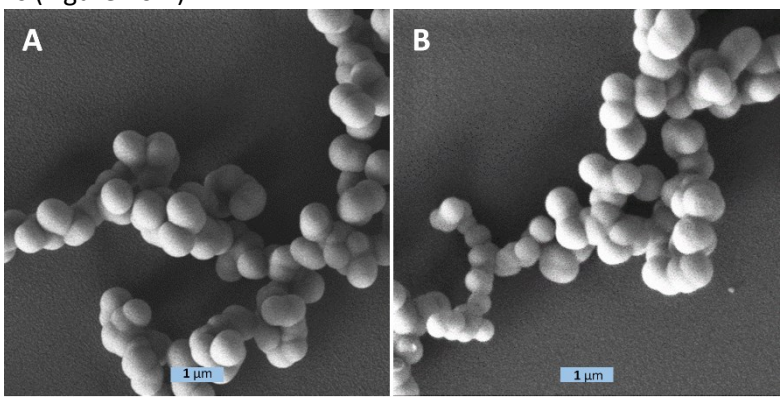

*Figure 46: SEM images obtained from the precipitations with incubation of compound **10** in 100 mM K_2HPO_4 (pH 9) at RT for 3 hours (A) or 24 hours (B) (0.4 mg/ml **10**) before addition of the solution of compound **10** to the solution of peptide **3** (1.25 mg/ml) (B). Silicic acid (25 mM) was added to peptide **3** simultaneously with the solutions of compound **10** (final concentration 0.04 mg/ml)*

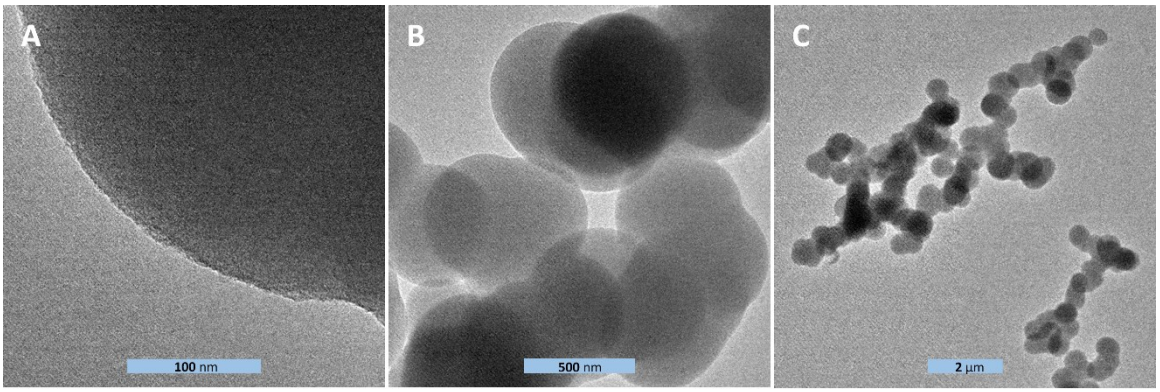

*Figure 47: TEM images obtained from the precipitation with incubation of compound **10** in 100 mM K_2HPO_4 (pH 9) at RT for 3 hours (0.4 mg/ml) before addition to the solution of peptide **3** (1.25 mg/ml) (B). Silicic acid (25 mM) was added to peptide **3** simultaneously with the solution of compound **10** (final concentration 0.04 mg/ml)*

The SEM images in Figure 46 demonstrate that the resultant silica precipitates are composed of spherical silica particles with a smooth morphology. Thus, the conditions used for the precipitate shown in Figure 46 A were deemed suitable for the synthesis of smooth spherical silica particles modified with **10** and chosen as the standard conditions for the preparation of fluorescein modified silica particles. They led to the exclusive formation of spherical silica particles with smooth morphologies and involved a shorter incubation time for compound **10** in 100 mM K_2HPO_4 (pH 9) than the conditions used for the precipitate shown in Figure 46 B. Further investigation via TEM (Figure 47) confirmed the spherical structure and smooth morphology of the particles shown in Figure 46 A.

The results in this section demonstrate that the precipitations with **10** dissolved in organic solvents did not lead to the desired spherical particles with smooth morphologies under any of the described conditions but rather to large inhomogeneous aggregates of smaller silica particles. This might have been caused by incomplete hydrolysis of silane **10** (dissolved in organic solvents) in 1 mM HCl. Incompletely hydrolyzed **10** might have inhibited the polycondensation process (section 1.1.1) involving silicic acid and **10** and thereby caused the formation of mainly very small particles. It is rather unlikely that the morphology of the precipitate was a result of the organic solvents disturbing the aggregates of peptide **3,** which act as templates for the polycondensation, as they had already been

preformed during the 24 hour incubation of **3** in 50 mM potassium phosphate buffer (pH 7) and the fraction of organic solvent in the precipitation mixture was very small (approximately 0.003%).

The synthesis of silica particles surface-modified with small molecules such as fluorescent dyes (as obtained here via a biomimetic approach using peptide **3**) has been described before using a non-biomimetic approach based on the Stöber [13] synthesis method for silica (nano)particles under alkaline conditions involving co-condensation of TEOS with appropriately modified silica precursors such as APTES (ensuring covalent binding of the fluorescent dye to the silica matrix) in a mixture of EtOH, H_2O, ammonium hydroxide and an appropriately modified fluorescent dye [124]. Disadvantages of this method for the preparation of surface functionalized silica particles (when compared to the biomimetic approach established in this section) include relatively long reaction times (overnight) and more complex synthesis procedures. While both methods enable the incorporation of the fluorescent dye (or other cargo molecules) during the synthesis of the silica particles and do not require post-synthetic modification procedures, the method established in this section additionally allows for the simultaneous introduction of sensitive biomolecules such as proteins [125]. They can be introduced via covalent attachment to peptide **3**, owing to the mild synthesis conditions (neutral pH) in contrast to the strongly alkaline conditions required for Stöber-inspired syntheses. The biomimetic synthesis approach with peptide **3** could potentially be used to generate differently modified particles when differently modified silica precursors are used apart from **10**. However, it has to be kept in mind that the method established in this project requires the hydrolysis of **10** at pH 9 for 3 hours and base-sensitive cargo molecules cannot be introduced into the silica material using this procedure.

*3.3.1.2 Determination of the percentage of compound **10** incorporated into and released from the particles*

After the appropriate conditions for the formation of spherical fluorescein modified silica particles had been established, the percentage of compound **10** incorporated during synthesis and released afterwards was determined. 50 mM potassium phosphate buffer (pH 4 or pH 7, Tables 11 and 12) was used as a release buffer (for exact conditions see section 2.4.1.2) and the release of **10** after a week of incubation at RT was determined as described in section 2.4.1.2. A calibration was first performed to establish a relationship between the absorbance of a solution of compound **10** and the corresponding concentration of silane **10**. The absorbance of standard solutions with concentrations of compound **10** between 0.005 mg/ml and 0.08 mg/ml (Table 10) at 495 nm was plotted against the corresponding concentration of compound **10** to obtain the calibration shown in Figure 48.

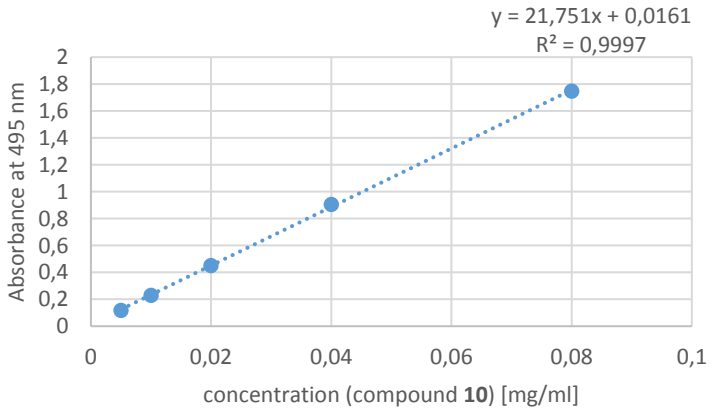

*Figure 48: Calibration for compound **10** obtained by plotting the absorbance of the standard solutions at 495 nm against the corresponding concentrations*

*Table 10: Concentrations and corresponding absorbance (at 495 nm) of the standard solutions of compound **10** used for the calibration*

concentration (compound 10) [mg/ml]	Absorbance at 495 nm
0,08	1,747
0,04	0,906
0,02	0,452
0,01	0,23
0,005	0,117

*Table 11: Data for the calculation of the percentage of compound **10** incorporated into the silica particles*

Concentration of initial solution of compound 10 [mg/ml]	Amount of compound 10 in initial solution [mg]	Absorbance of initial supernatant	Concentration of compound 10 in initial supernatant [mg/ml]	Amount of compound 10 in initial supernatant [mg]	Percentage of compound 10 incorporated into the particles [%]
0.049	0.0049	0.144	0.0059	0.00059	88.0

*Table 12: Data for the calculation of the percentage of compound **10** released from the particles after 1 week of incubation in 50 mM potassium phosphate buffer (pH 4 or pH 7) at RT*

pH	Amount of compound 10 incorporated into the particles* [mg]	Absorbance of supernatant after 1 week incubation	Concentration of compound 10 in supernatant after 1 week incubation [mg/ml]	Amount of compound 10 in supernatant after 1 week incubation [mg]	Percentage of compound 10 released after 1 week incubation [%]
4	0.00215	0.016	0	0	0
7	0.00215	0.081	0.0030	0.00030	14.0

*The precipitate was divided into 2 aliquots, therefore the total amount of fluorescein incorporated (0.0043 mg) had to be divided by 2

Tables 11 and 12 show that the majority of compound **10** (88 %) was incorporated into the particles and that, while none of it was released after one week of incubation in 50 mM potassium phosphate buffer (pH 4), 14 % of the incorporated compound **10** was released after incubation in 50 mM potassium phosphate buffer (pH 7) for one week. Additionally, TEM samples were prepared for the particles after one week of incubation in 50 mM potassium phosphate buffer (pH 4 (Figure 49 A and B) or pH 7 (Figure 49 C and D)) as described in section 2.4.1.2.

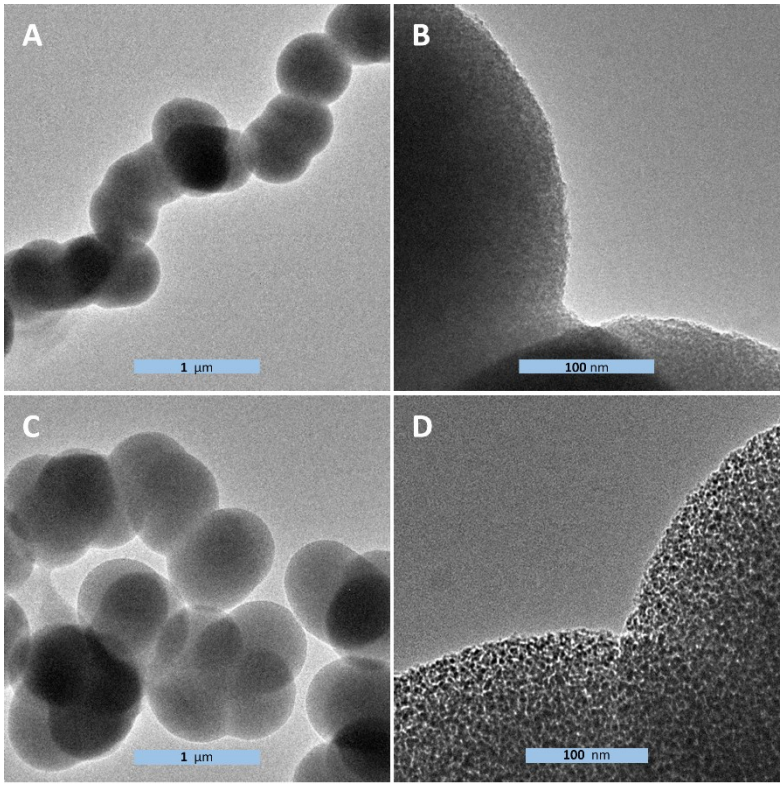

*Figure 49: TEM images obtained for the silica particles modified with compound **10** after one week of incubation in 50 mM potassium phosphate buffer (pH 4 (A and B) or pH 7 (C and D))*

The particles incubated at pH 4 did not release any detectable amount of fluorescein after one week of incubation (Table 12) and the surface of these particles (Figure 49 A and B) looks similar to the surface of the particles prior to incubation (Figure 47 A). In contrast, the particles incubated for one

week at pH 7 released about 14 % of the amount of compound **10** that had been incorporated into the particles during the precipitation and the surfaces of these particles (Figure 49 C and D) changed in comparison to the particles before incubation in 50 mM potassium phosphate buffer (pH 7). The particles exhibit a very porous morphology post incubation (Figure 49 D).

The porosity observed after incubation of the particles might be caused by hydrolytic release of compound **10** from the silica material at pH 7, as there is no increased porosity visible after incubation of the particles at pH 4 where no release of compound **10** was detected. Additionally,it has been reported that the release of R5 peptide variants in biomimetically generated silica particles is pH dependent and that higher release rates are observed at pH 5 than at pH 7.4 [5] This suggests that the pores are not (solely) generated as a result of the release of peptide **3,** as, based on these results, more peptide **3** must have been released at pH 4 than at pH 7, which should create a more porous morphology for the particles incubated at pH 4, if the pores were an exclusive result of peptide **3** release.

3.3.1.3 Fluorescence microscopy

Fluorescence microscopy images (acquired as described in section 2.4.1.3, Figure 50) of silica particles modified with **10** show that they exhibit detectable fluorescence and confirm that the incorporation of fluorescein into the silica particles derived from peptide **3** via compound **10** was successful.

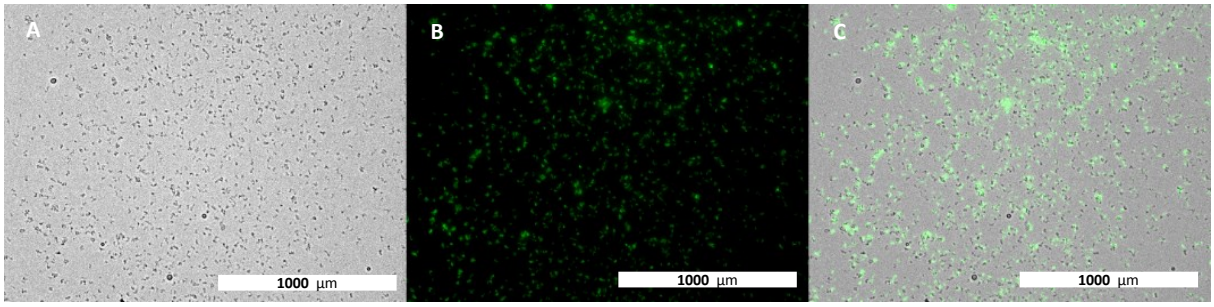

*Figure 50: Bright field (A) and fluorescein (B) images of silica particles modified with compound **10** (0.00625 mg/ml particle concentration) synthesized according to section 2.4.1.2*

3.3.1.4 Cell study A

Cell study A was performed as described in section 2.4.1.3. Imaging of the cells that had been treated with particles modified with compound **10** at was carried out (section 2.1.4) 1.5 hours after the addition of particles (0.0125 mg/ml, Figure 51) and after staining of the cells with DNA and lysosome stains (Hoechst 33258 and Alexa Fluor 594 respectively, Figure 52, stained 24 hours after incubation of the cells with the particles at 37 °C and 5% CO_2). Images acquired from cells treated with particles at concentrations of 0.1 mg/ml, 0.05 mg/ml, 0.025 mg/ml are not shown, as these concentrations were too high to enable a good visualization of particle uptake by THP-1 cells.

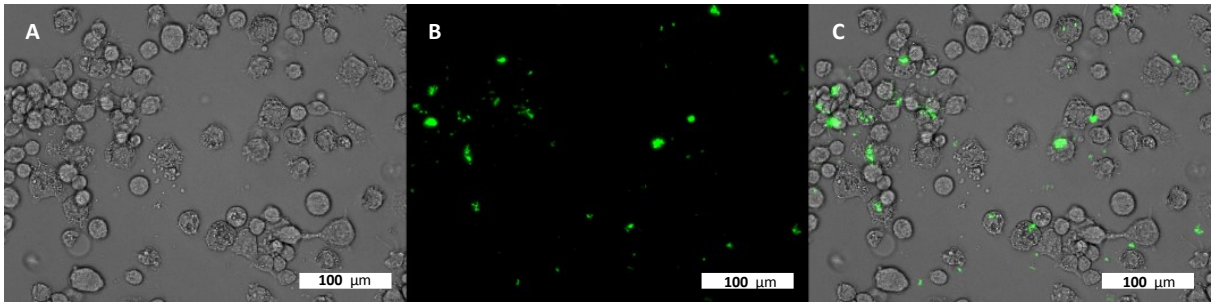

*Figure 51: Images acquired 1.5 hours after incubation of THP-1 cells with particles modified with compound **10** at a concentration of 0.0125 mg/ml; A: bright field channel, B: fluorescein channel, C: composite of bright field and fluorescein channels*

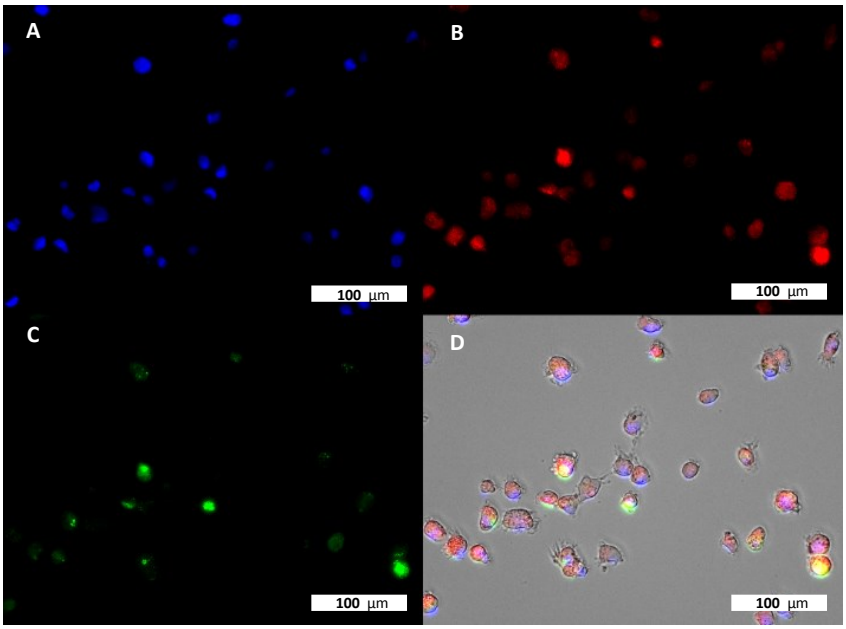

*Figure 52: Images acquired after staining of the cells with Hoechst 33258 (DNA) and Alexa Fluor 594 (Lysosomes), carried out 24 hours after incubation of the THP-1 cells with 0.0125 mg/ml silica particles modified with compound **10**; A: Hoechst 33258 channel, B: Alexa Fluor 594 channel, C: fluorescein channel, D: composite of channels shown in A-C and the bright field channel*

The overlay of the bright field (Figure 51 A) and fluorescein channel (Figure 51 B) shown in Figure 51 C indicates that the majority of the silica particles modified with compound **10** was already located inside the cells, which means that the cells already started take-up of the particles after 1.5 hours of incubation with them.

From Figure 52 D, which shows an overlay of the four images (channels: Hoechst 33258 (DNA), Alexa Fluor 594 (lysosomes), the fluorescein channel to visualize compound **10** in the silica particles and the bright field channel for imaging of the cells themselves) acquired after staining of the cells, it can be concluded that at 24 hours after the incubation of the THP-1 cells with silica particles modified with compound **10** (at a concentration of 0.0125 mg/ml), all particles were located inside the cells. As the staining was performed after the treatment of the cells with the particles, this does not necessarily mean that the entire amount of particles was taken up by the cells, as particles that were still outside the cells might have been removed during the removal of the medium prior to staining. The particles that were possibly still present in the medium removed from the cells after 24 hour incubation of the cells with particles were not isolated and the percentage of particles taken up by the cells was therefore not determined and will have to be investigated in the future.

3.3.1.5 Cell study B

Cell study B was carried out as described in section 2.4.1.3 and was performed not only with particles modified with **10**, but simultaneously with particles modified with **17** (section 3.3.2.7) or **10** and **17** (section 3.3.3.5). Images of the cells were acquired immediately, 2 hours or 24 hours after DNA staining (Hoechst 33258) and treatment of the THP-1 cells with particles modified with **10** at a concentration of 0.01 mg/ml. 4 channels were used for imaging: Hoechst 33258, fluorescein for visualization of compound **10** incorporated into the silica particles, cyanine-5 to rule out cross-contamination with particles containing peptide **17**, and bright field.

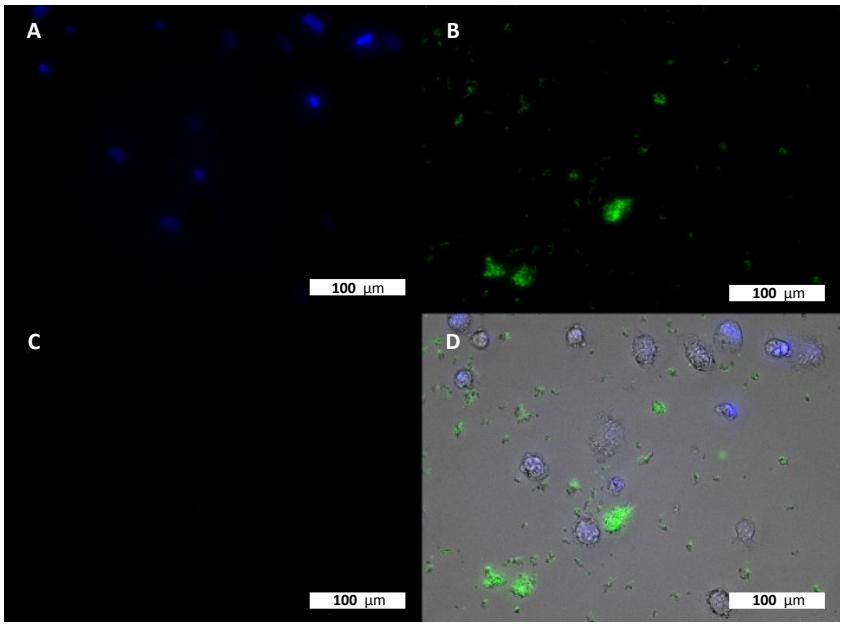

*Figure 53: Images of stained (Hoechst 33258 DNA stain) THP-1 cells immediately after incubation of the cells with silica particles modified with compound **10** (0.01 mg/ml), A: Hoechst 33258 channel, B: fluorescein channel, C: cyanine-5 channel, D, composite of channels shown in A-C with the bright field channel*

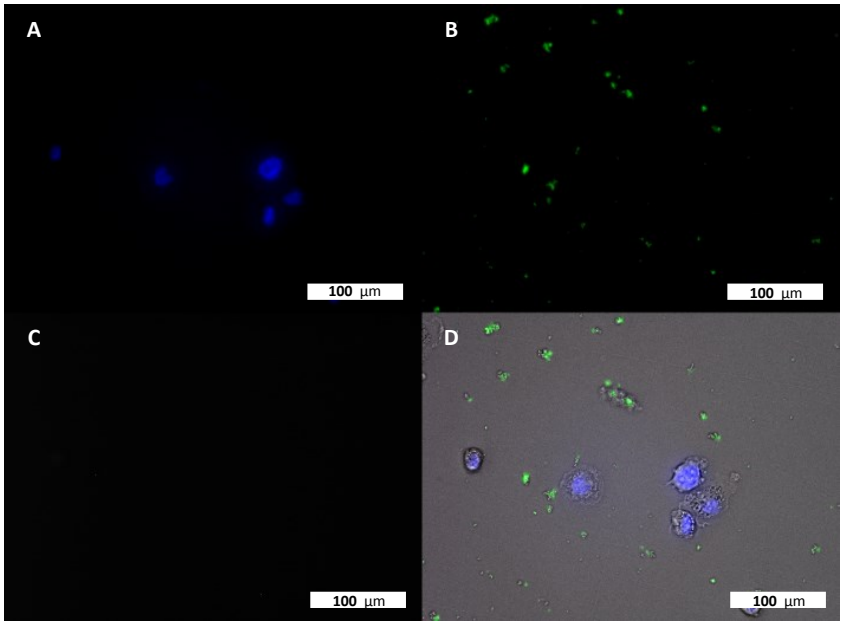

*Figure 54: Images of stained (Hoechst 33258 DNA stain) THP-1 cells 2 hours after incubation of the cells with silica particles modified with compound **10** (0.01 mg/ml), A: Hoechst 33258 channel, B: fluorescein channel, C: cyanine-5 channel, D, composite of channels shown in A-C with the bright field channel*

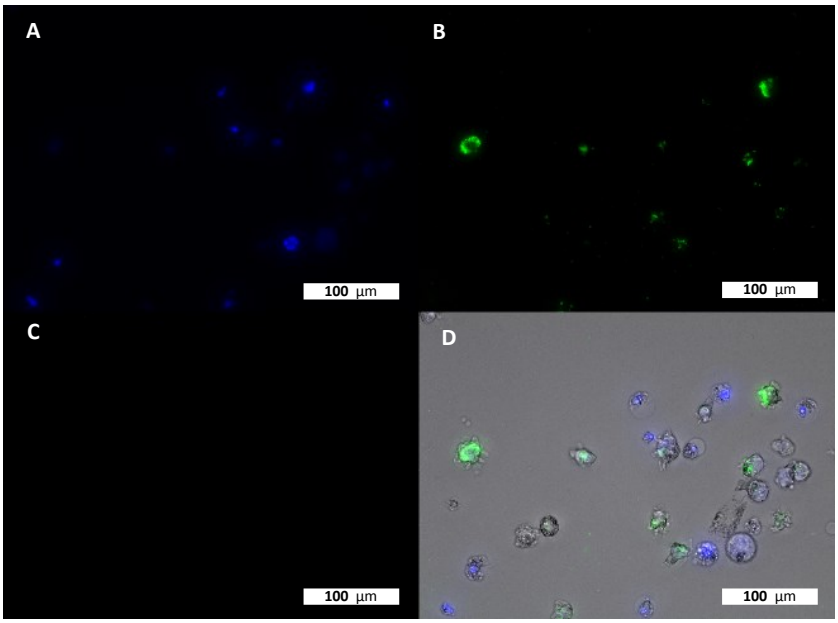

*Figure 55: Images of stained (Hoechst 33258 DNA stain) THP-1 cells 24 hours after incubation of the cells with silica particles modified with compound **10** (0.01 mg/ml), A: Hoechst 33258 channel, B: fluorescein channel, C: Cyanine-5 channel, D, composite of channels shown in A-C with the bright field channel*

Figures 53 D and 54 D show that the majority of silica particles modified with compound **10** was still located outside the cells and had not been taken up immediately and 2 hours after treatment of the cells with the particles. In contrast, Figure 55 D shows that after 24 hours, almost all of the particles had been taken up by the cells. Figure 53 C, Figure 54 C and Figure 55 C confirm that the particles imaged were solely modified with compound **10** and cross-contamination with particles containing peptide **17** can be ruled out (cell study B was simultaneously carried out with silica particles containing peptide **17**).

Overall, all precipitations with peptide **3** and TMOS using compound **10** as an additional silica precursor that are associated with Figures 42-45 (using organic solvents) led to the formation of disordered silica aggregates. In contrast, precipitates obtained after hydrolysis of silane **10** in 100 mM K_2HPO_4 (pH 9) for 3 hours (Figure 46 A and 47) or 24 hours (Figure 46 B) prior to addition to peptide **3** were composed of spherical silica particles with smooth surfaces. Fluorescence microscopy imaging (Figure 50) confirmed that compound **10** had been successfully incorporated into the silica particles. Therefore, these conditions seem to be suitable for the introduction of a further modification (in addition to cargo molecules such as fluorescent dyes or proteins that can be covalently attached to the *N*-terminus or *N*-terminal cysteine residue of peptide **3** [5, 125]) into silica particles derived from peptide **3** and TMOS using compound **10** as a silica precursor. Silane **10** is efficiently incorporated into the particles: Tables 11 and 12 demonstrate that the majority of compound **10** (88 %) is incorporated into the silica particles in the course of the precipitation and the release is pH-dependent with 14 % of the incorporated amount of compound **10** being released at pH of 7 after a week, while at pH 4, compound **10** does not seem to be released after a week. This means that compound **10** exhibits different release behavior compared to R5 variants, which show enhanced release at lower pH values [5]. Compound **10** has previously been used to synthesize fluorescein modified silica particles via the water-in-oil micro-emulsion method by Ciccione *et al*. [123] using TEOS as a silica precursor. The results in this section demonstrate that compound **10** can also be introduced into silica particles using the biomimetic synthesis approach, which is less complex and time-consuming than the micro-emulsion method. However, in this section, TMOS was used as a silica precursor, which is more volatile and toxic [126]

than TEOS [127] and therefore, a biomimetic approach using compound **10** and TEOS as silica precursors would be preferred. The cell studies showed that the particles were taken up by macrophages derived from THP-1 cells within 24 hours. In general, the uptake of silica particles by cells has been reported before and has been attributed to the interaction of silica particles with cell walls mediated by the head-groups of phospholipids. The resultant association of silica particles to the cell walls eventually leads to the uptake of the particles via endocytosis [3, 128]. However, the cell studies in this section were the first ones to confirm that such doubly modified silica particles are taken up by macrophages derived from THP-1 cells.

3.3.2 Biomimetic silica precipitations with 3, 17 and TMOS

In the biomimetic approach for the synthesis of silica particles using peptide **3** as a silica precipitating agent, modifications can be introduced into the particles not only via derivatized silica precursors such as silane **10**, but also via the attachment of a cargo molecule to the *N*-terminus of **3.** Attachment of cyanine-5 to **3** can be especially useful as it provides information about encapsulation of **3** into and release of **3** from the silica particles via fluorescence microscopy imaging (section 3.3.2.6 and 3.3.2.7) and UV-Vis absorbance measurements (section 3.3.2.4).

*3.3.2.1 Synthesis of **16***

The synthesis of compound **16** was carried out as described in section 2.4.2.1. After purification of crude **16** via silica column chromatography, a yield of 255.4 mg of purified product was obtained (20 % of the theoretical yield of 1,27 g). The NMR analysis (section 2.4.2.1) is in moderate agreement with previously reported NMR data for cyanine-5 [129].

*3.3.2.2 Synthesis and purification of **17***

Peptide **17** (Structure in Figure 57) was synthesized and purified according to section 2.4.2.2. Prior to purification, the crude yield obtained for peptide **17** was 24.5 mg, which decreased to 1.2 mg after double HPLC purification (5% of the theoretical yield of 25.7 mg for 0.01 mmol peptide).

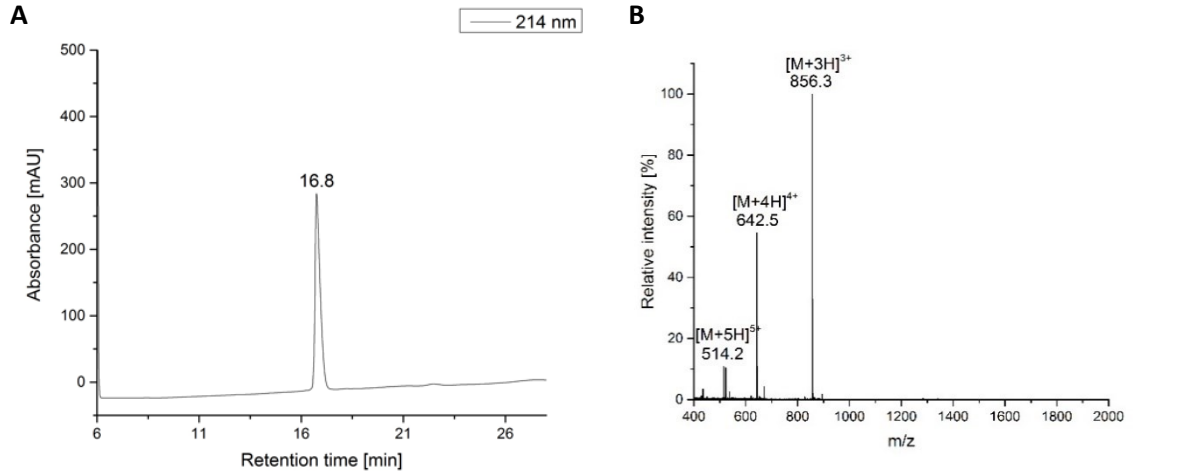

*Figure 56: A: HPLC chromatogram of purified peptide **17**, B: Mass spectrum obtained from a direct injection of purified peptide **17** on the Thermo Fisher HPLC-MS system*

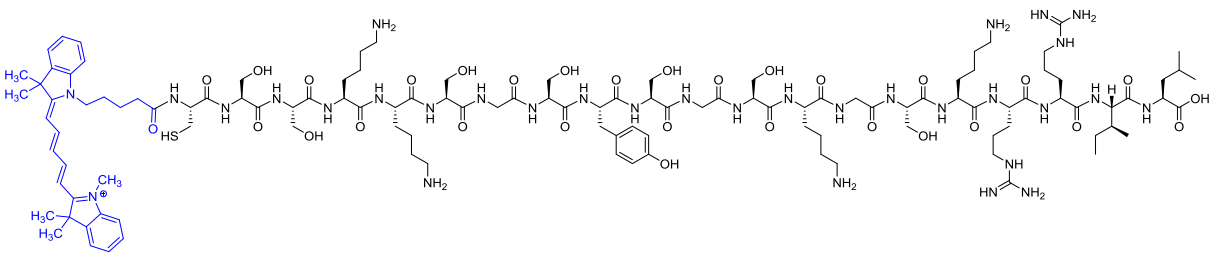

*Figure 57: Structure of peptide **17***

Figure 56 A shows the RP-HPLC-chromatogram obtained from the final analysis of purified peptide **17** with the elution of the peptide occurring at a retention time of 16.8 minutes. The corresponding mass spectrum with a charge pattern corresponding to an observed mass of 2566 Da, which is in agreement with the expected mass for peptide **17** (2566.4 Da), is depicted in Figure 56 B. The mass spectrum obtained for purified peptide **17** in combination with the corresponding RP-HPLC chromatogram indicates high purity of the peptide.

3.3.2.3 Precipitations

The precipitations for the production of silica particles containing peptide **17** were carried out according to section 2.4.2.3 using a solution of 1 mg/ml peptide **3** containing 1 % (w/w) (Figure 58 A and 59 A and B) or 4.8 % (w/w) (Figure 58 B and 59 C and D) peptide **17** in 50 mM potassium phosphate buffer (pH 7). Samples of the precipitates for SEM and TEM were prepared as described in section 2.1.1 and 2.1.2.

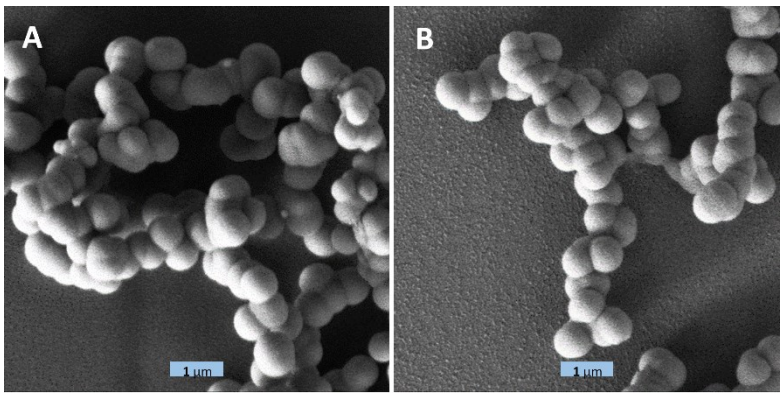

*Figure 58: SEM images obtained from the precipitate resulting from the biomimetic precipitation using peptide **3** (1 mg/ml) with 1 % peptide **17** (w/w) (A) or 4.8 % peptide **17** (w/w) (B)*

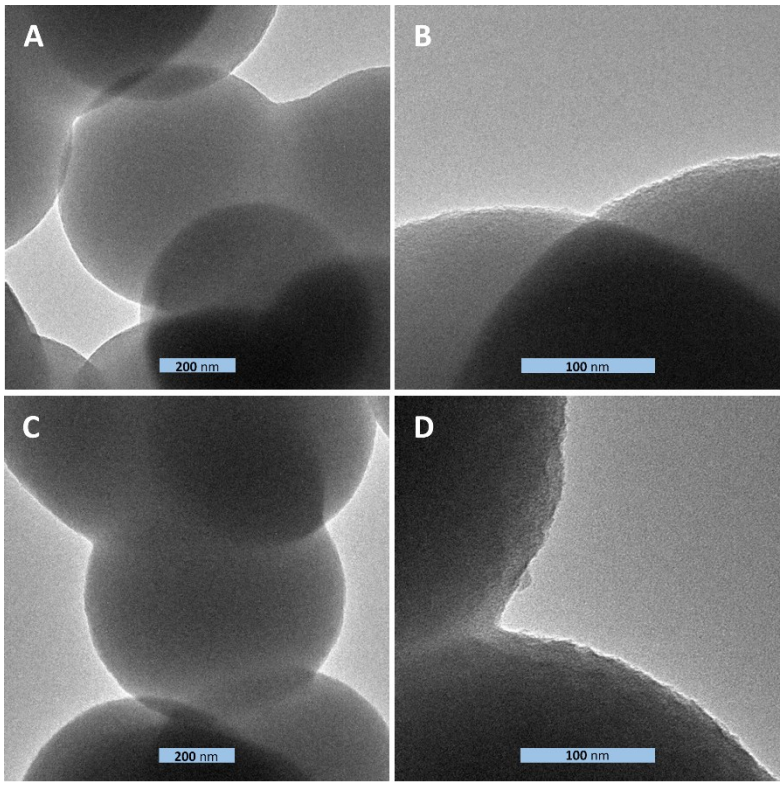

*Figure 59: TEM images obtained from the precipitate resulting from the biomimetic precipitation using peptide **3** (1 mg/ml) with 1 % peptide **17** (w/w) (A and B) or 4.8 % peptide **17** (w/w) (C and D)*

SEM (Figure 58) and TEM (Figure 59) images for both precipitates show that they consist of spherical silica particles with diameters in the micrometer range similar to the precipitates obtained under the same conditions without the presence of peptide **17** (Figure 34 A). This demonstrates that the addition of these small quantities of peptide **17** did not influence the structure and morphology of the resultant silica precipitates compared to the precipitates obtained from non-modified peptide **3**.

*3.3.2.4 Determination of the percentage of peptide **17** incorporated into the particles*

In order to determine the percentage of peptide **17** incorporated into the particles in the course of the precipitation carried out in a solution of 1 mg/ml peptide **3** containing 4.8% peptide **17** (w/w), a calibration was performed to establish a relationship between the absorbance of the investigated solutions of peptide **17** at 641 nm and the corresponding concentration of peptide **17**. The calibration was carried out as described in section 2.4.2.4 in 50 mM potassium phosphate buffer (pH 7) with standard solutions containing between 0.1 mg/ml and 0.01 mg/ml peptide **17** (Figure 60 and Table 13)

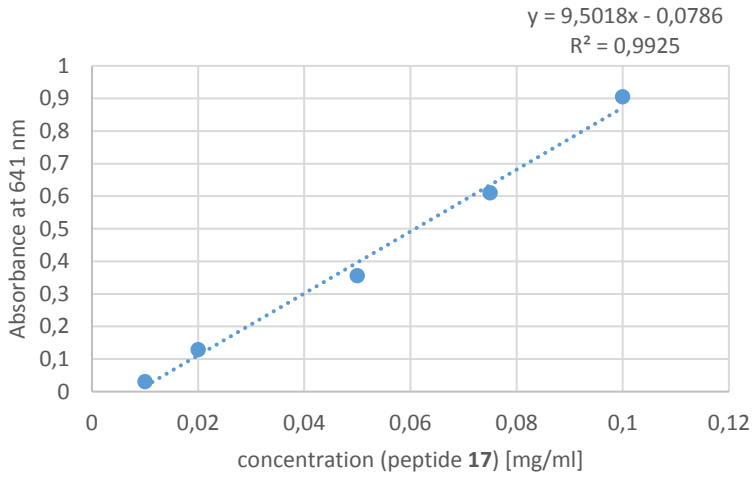

*Figure 60: Calibration for peptide **17** obtained by plotting the absorbance of the standard solutions at 641 nm against the corresponding concentrations of peptide **17***

*Table 13: Concentrations and corresponding absorbance (at 641 nm) of the standard solutions of peptide **17** used for the calibration*

concentration (peptide 17) [mg/ml]	Absorbance at 641 nm
0,1	0,905
0,075	0,61
0,05	0,356
0,02	0,129
0,01	0,03

The percentage of peptide **17** incorporated into the particles was then determined according to section 2.4.2.4 via comparison of the concentration of **17** in the initial precipitation mixture and in the supernatant obtained after 30 minutes of precipitation.

*Table 14: Percentage of peptide **17** incorporated into the particles derived from a solution of 1 mg/ml peptide **3** containing 4.8 % peptide **17** (w/w)*

Concentration of the initial solution of peptide 17 [mg/ml]	Amount of peptide 17 in initial solution [mg]	Absorbance of initial supernatant	Concentration of peptide 17 in initial supernatant [mg/ml]	Amount of peptide 17 in initial supernatant [mg]	Percentage of peptide 17 incorporated into the particles [%]
0.044	0.0177	0.001	0.0084	0.0034	80.8

The results listed in Table 14 show that the majority (80.8 %) of peptide **17** from the precipitation mixture (4.8% (w/w) peptide **17** in peptide **3**) was incorporated into the particles in the course of the precipitation.

*3.3.2.5 Release of peptide **17** from the particles*

The morphology of the precipitate derived from a solution of 4.8 % (w/w) peptide **17** in peptide **3** was investigated after release of peptide **17** (and **3**) from the silica particles with 50 mM potassium

phosphate buffer at pH 4 and 7 as release buffers (incubation of the particles in the release buffers for one week at RT) as described in section 2.4.2.5 and the corresponding TEM images are depicted in Figure 61.

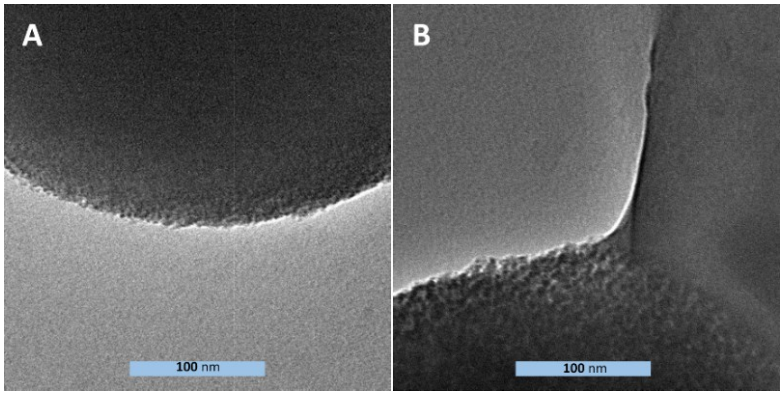

*Figure 61: TEM images obtained after incubation of particles derived from 4.8 % peptide **17** in peptide **3** in 50 mM potassium phosphate buffer at pH 4 (A) and pH 7 (B) for one week at RT*

Figure 61 shows that the particles incubated for a week in 50 mM potassium phosphate buffer at RT at pH 4 (Figure 61 A) as well as those incubated at pH 7 (Figure 61 B) both show a porous morphology compared to the corresponding particles before incubation (Figure 59 C and D). In addition, the porosity seems more pronounced in the particles incubated at pH 7. As this porosity is not observed in the particles before incubation in 50 mM potassium phosphate buffer for a week, this change in morphology could be a result of the release of peptide **17** and peptide **3** from the particles.

3.3.2.6 Fluorescence microscopy

Fluorescence microscopy images of particles derived from 1 % (w/w) **17** and 4.8 % **17** (w/w) in **3** were acquired at a particle concentration of 0.01 mg/ml to confirm that they exhibited detectable fluorescence (see section 2.4.2.6, cyanine-5 channel, Figure 62).

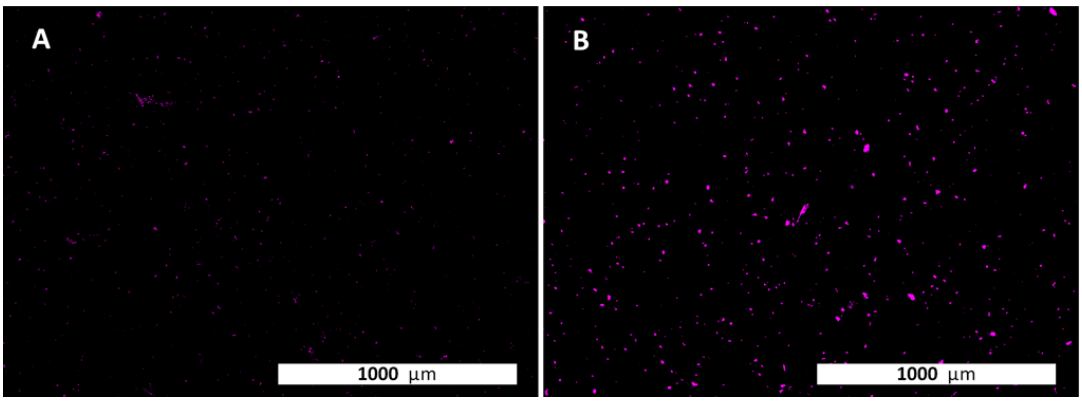

*Figure 62: Fluorescence microscopy images obtained from the particles derived from (A) 1% peptide **17** in **3** and (B) 4.8% peptide **17** in **3** (cyanine-5 channel)*

Figure 62 demonstrates that both the particles derived from 1% (w/w) **17** and 4.8% (w/w) **17** in **3** exhibited detectable fluorescence on the cyanine-5 channel. The particles derived from 4.8% (w/w) **17** in **3** show a more intense signal as would be expected for a higher content of **17** in the particles.

3.3.2.7 Cell study

The cell study was carried out with particles derived from a solution of 4.8 % peptide **17** in peptide **3** as described in section 2.4.2.6 simultaneously with the cell studies of particles containing **10** (section 3.3.1.5) or **10** and **17** (section 3.3.3.5). DNA staining of the cells (Hoechst 33258, section 2.1.4) was

performed before addition of the particles to the cells. The cells were imaged immediately, 2 hours and 24 hours after treatment of the cells with particles containing **17** at concentrations of 0.01 mg/ml using 4 channels: Hoechst 33258, cyanine-5 for visualization of peptide **17** incorporated into the particles, fluorescein to rule out cross-contaminations with particles modified with compound **10** and bright field.

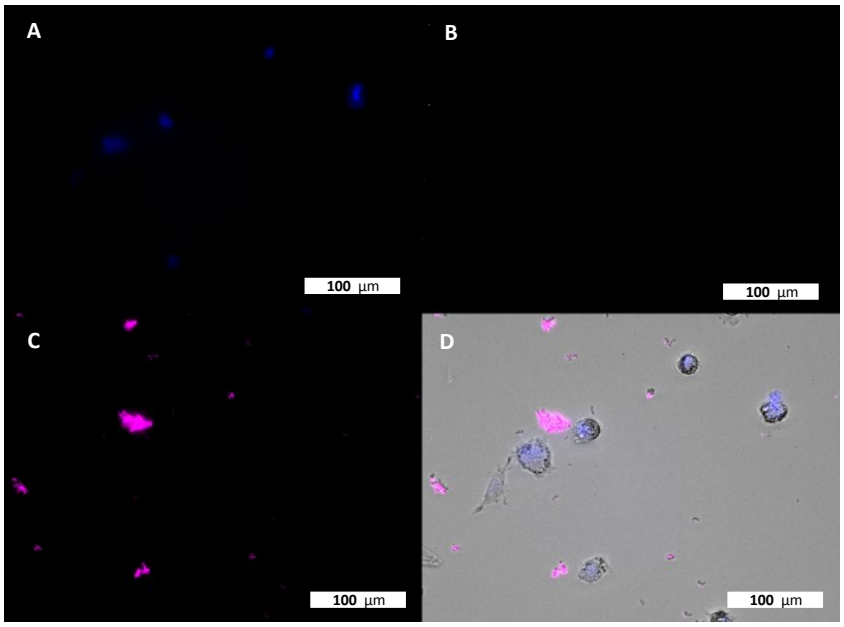

*Figure 63: Images of stained (Hoechst 33258 DNA stain) THP-1 cells immediately after incubation of the cells with silica particles containing peptide **17** (0.01 mg/ml), A: Hoechst 33258 channel, B: fluorescein channel, C: cyanine-5 channel, D, composite of channels shown in A-C with the bright field channel*

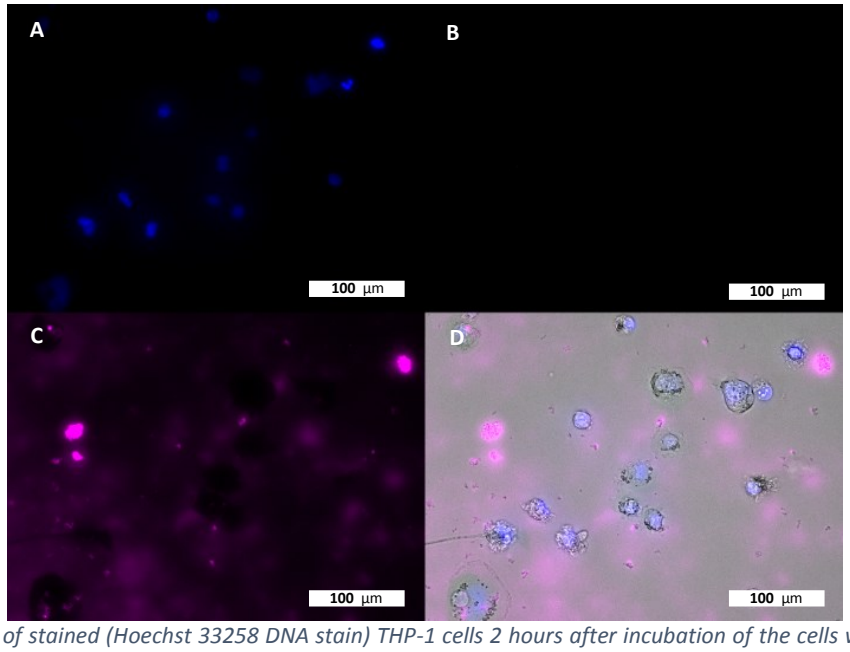

*Figure 64: Images of stained (Hoechst 33258 DNA stain) THP-1 cells 2 hours after incubation of the cells with silica particles containing peptide **17** (0.01 mg/ml), A: Hoechst 33258 channel, B: fluorescein channel, C: cyanine-5 channel, D, composite of channels shown in A-C with the bright field channel*

Figure 63, which shows the images acquired immediately after treatment of the cells with silica particles containing peptide **17**, demonstrates that at this time point, the particles are outside the cells and have not been taken up by them. Two hours after incubation of the cells with silica particles, peptide **17** seems to have been released to a certain extent, as the cyanine-5 channel in Figure 64 does not only show a cyanine-5 signal that is restricted to the particle aggregates (as in Figure 63), but

visualizes a cyanine-5 signal also in the medium surrounding the particles. At this time point, the majority of the particles is still localized outside of the THP-1 cells. 24 hours after treatment of the cells with silica particles, the cyanine-5 channel (Figure 65) indicates that most of peptide **17** has been released from the particles. Therefore, it is difficult to make a statement from the overlay of the cyanine-5, Hoechst and bright field channel (Figure 65 D) about whether or not the particles have been taken up by the cells after 24 hours, as the cyanine-5 signal is not restricted to the particles.

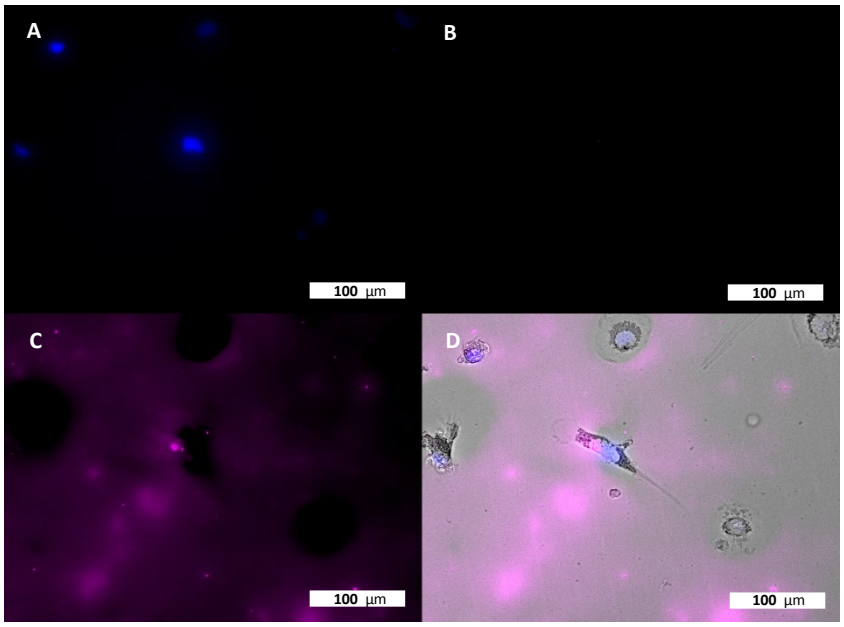

*Figure 65: Images of stained (Hoechst 33258 DNA stain) THP-1 cells 24 hours after incubation of the cells with silica particles containing peptide **17** (0.01 mg/ml), A: Hoechst 33258 channel, B: fluorescein channel, C: cyanine-5 channel, D, composite of channels shown in A-C with the bright field channel*

The results in this section demonstrate that peptide **17** could successfully be incorporated into silica particles using the biomimetic approach with TMOS as a silica precursor and a solution of 1 % (w/w) or 4.8 % (w/w) peptide **17** in **3**. This led to the formation of spherical silica particles with smooth morphologies and the successful incorporation of the fluorescent dye cyanine-5 (via peptide **17,** see cell study in Figures 63-65 and fluorescence microscopy in Figure 62) into the particles. While in this experiment, cyanine-5 was attached to the *N*-terminus of peptide **3,** resulting in peptide **17**, the introduction of another fluorescent dye via this method, NBD, via attachment to the *N*-terminus of peptide **3** has already been reported by Lechner and Becker [108] and also led to a homogeneous incorporation of the fluorescent probe into the particles as the peptide co-precipitates with the silica. The data in Table 14 suggest that the majority of peptide **17** (80.8 %) was efficiently incorporated into the silica particles derived from a solution of 4.8 % (w/w) peptide **17** in **3** during the biomimetic precipitation. Attachment of small molecules to the *N*-terminus of peptide **3** therefore seems to be a suitable method to incorporate them into silica particles derived from modified peptide **3**. From the cell studies in Figures 63-65 it can be seen that the peptide with its cargo can be released again from the particles over time, suggesting that these particles could potentially be used as delivery agents for various cargo molecules that can be attached to peptide **3**. Interestingly, the fluorescence microscopy images in Figures 64 and 65 show that the peptide is released from the particles into the medium, but taken up by the cells only to a small extent. Release of an R5 peptide variant from such biomimetically generated particles has been reported before [5] in PBS at pH 7.4 and, with higher percentages of peptide released, in sodium acetate buffer at pH 5. While native silaffins show an extremely tight and stable association with biogenic silica, requiring treatment of biosilica from diatoms with HF or acidic

ammonium fluoride to achieve release of these peptides, the facilitated release of synthetic R5 peptide variants has been attributed to the weaker association of this peptide with the silica as it lacks any PTMs that are present in native silaffins and contribute to their strong association to biogenic silica. [5] Due to such release of peptide **17** from the particles in the cell study shown in Figures 63-65, it is difficult to say whether or not the particles were taken up by the cells as they are difficult to localize after the release of peptide **17**. Apart from the release of cargo molecules from these particles through the release of the R5 peptide variant itself, another method has been reported [5] involving the attachment of cargo molecules to the *N*-terminal cysteine residue of the R5 peptide variant via a disulfide bond. This technique allows for the release of the cargo molecule when the disulfide linkage is cleaved under reducing conditions. Encapsulation of proteins in silica particles derived from **3** has been reported via the attachment of proteins to the *N*-terminal cysteine residue in **3** using EPL, demonstrating the versatility of R5 peptide modification as a method to encapsulate cargo in such particles [125]. While biomimetically produced particles with R5 peptide variants such as **3** and **17** could potentially be used as delivery vehicles for various cargo molecules such as fluorescent dyes or proteins [125], mesoporous silica particles have also been suggested as delivery vehicles for different types of molecules including drugs [55] and proteins [130] and have been reported to be taken up efficiently by different cell types including human cancer cells [131]. However, silica particles derived from silaffin peptides such as **3** or variants of **3** modified with proteins or fluorescent dyes provide advantages over mesoporous delivery vehicles such as less elaborate and quicker synthesis under mild conditions (neutral pH, ambient temperature) and entrapment of the cargo proteins during silica particle synthesis instead of loading of the cargo post synthesis. [125]

3.3.3 Biomimetic silica precipitations with 3, 17, TMOS and 10

3.3.3.1 Precipitations

The precipitations for the generation of bifunctional silica particles modified with compound **10** containing peptide **17** were carried out as described in section 2.4.1.2 in a solution of peptide **3** (0.1 mg, 1.25 mg/ml) with 1 % (w/w) peptide **17** or 4.8 % (w/w) peptide **17** in 50 mM potassium phosphate buffer (pH 7). SEM (Figure 66) and TEM (Figure 67) samples were prepared according to section 2.1.1 and 2.1.2.

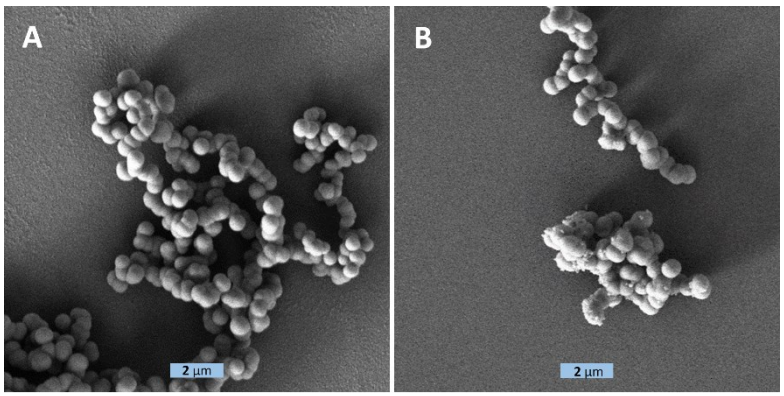

*Figure 66: SEM images acquired from the precipitates obtained from precipitations in a solution of peptide **3** (1.25 mg/ml) with 1 % (w/w) peptide **17** (A) and 4.8 % (w/w) peptide **17** (B)*

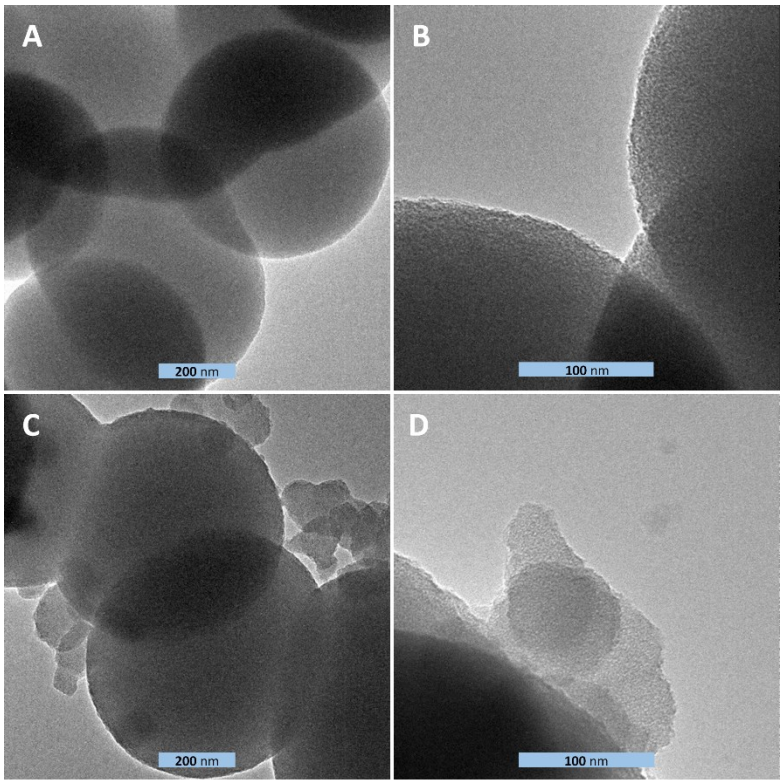

*Figure 67: TEM images acquired from the precipitates obtained from precipitations carried out in a solution of peptide **3** (1.25 mg/ml) with 1 % (w/w) peptide **17** (A and B) or 4.8 % (w/w) peptide **17** (C and D)*

SEM and TEM images of the fluorescein modified silica particles containing 1 % peptide **17** (Figure 66 A and Figure 67 A and B) demonstrate that this precipitate is composed of spherical silica particles possessing a smooth morphology and diameters in the micrometer range. In contrast, the precipitates obtained for the precipitations with 4.8 % peptide **17** (Figure 66 B and 67 C and D) consist of spherical silica particles in the same size-range with rougher surfaces. A higher percentage of peptide **17** seems to influence the morphology of the silica particles modified with compound **10** which was not the case for particles that were not modified with compound **10** (section 3.3.2.3).

*3.3.3.2 Determination of the percentage of peptide **17** and compound **10** incorporated into the particles*

The percentages of compound **10** and peptide **17** incorporated was determined according to section 2.4.3.2 for the precipitation in a solution of 4.8 % peptide **17** in peptide **3**, which was carried out as described in section 2.4.3.1. As described in section 2.4.3.2, the comparison of the concentrations of **10** and **17** in the initial precipitation mixture with the corresponding concentrations in the supernatant obtained after 30 minutes of precipitation was employed to determine the percentages of **10** and **17** incorporated.

*Table 15: Data for the calculation of the percentage of compound **10** and peptide **17** incorporated into the particles*

Compound	Concentration in initial solution [mg/ml]	Amount of compound in initial solution [mg]	Absorbance of initial supernatant	Concentration of compound in initial supernatant [mg/ml]	Amount of compound in initial supernatant [mg]	Percentage of compound incorporated into the particles [%]
Compound 10	0.0406	0.0149	0.073	0.0041	0.0015	89.9
Peptide 17	0.0376	0.0138	0.003	0.0086	0.0032	76.8

From the data shown in Table 15 it is evident that the majority of compound **10** (89.9 %) and peptide **17** (76.8 %) is incorporated into the silica particles in the course of the precipitations. Furthermore, the percentages are similar to the percentages obtained for the particles modified with compound **10** without peptide **17** (88 % of compound **10** were incorporated, section 3.3.1.2) and for the silica particles not modified with compound **10** derived from 4.8 % peptide **17** in **3** (80.8 % of peptide **17** were incorporated, section 3.3.2.4), suggesting that the two modifications are independent from each other concerning the extent of incorporation.

*3.3.3.3 Release of peptide **17** and compound **10** from the particles*

The influence of the release of peptide **17** and compound **10** on the morphology of silica particles modified with compound **10** derived from a solution of 4.8 % (w/w) peptide **17** in **3** after incubation of the particles in 50 mM potassium phosphate buffer at pH 4 or 7 at RT for one week was investigated employing the experimental procedure described in section 2.4.3.3 and the corresponding TEM images are depicted in Figure 68.

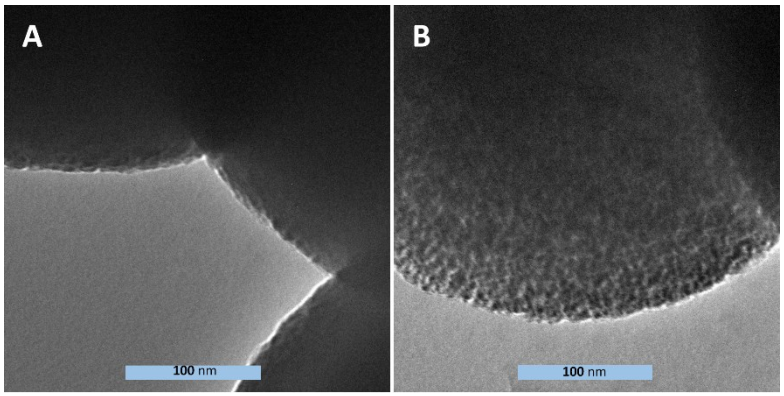

*Figure 68: TEM images obtained after incubation of silica particles modified with compound **10** (derived from 4.8 % peptide **17** in **3**) in 50 mM potassium phosphate buffer at pH 4 (A) and pH 7 (B) at RT for one week*

Figure 68 demonstrates that the particles incubated in 50 mM potassium phosphate buffer at pH 7 show a more pronounced porosity than the particles incubated at pH 4, which do not show a significantly more visible porosity compared to the corresponding particles prior to incubation (Figure 67 C and D). If more compound **10** is released at pH 7 than at pH 4, which was observed for silica particles modified with compound **10** containing peptide **3** (section 3.3.1.2), this observation could mean that the porosity is dependent on the release of compound **10**.

3.3.3.4 Fluorescence microscopy

Prior to the cell studies, the silica particles modified with compound **10** derived from 1 % and 4.8 % peptide **17** in **3** (Figure 69 and 70) were viewed on the fluorescence microscope at a particle concentration of 0.01 mg/ml as described in section 2.4.3.4 to confirm that they exhibited detectable fluorescence and compare their fluorescence intensities using the fluorescein and cyanine-5 channels.

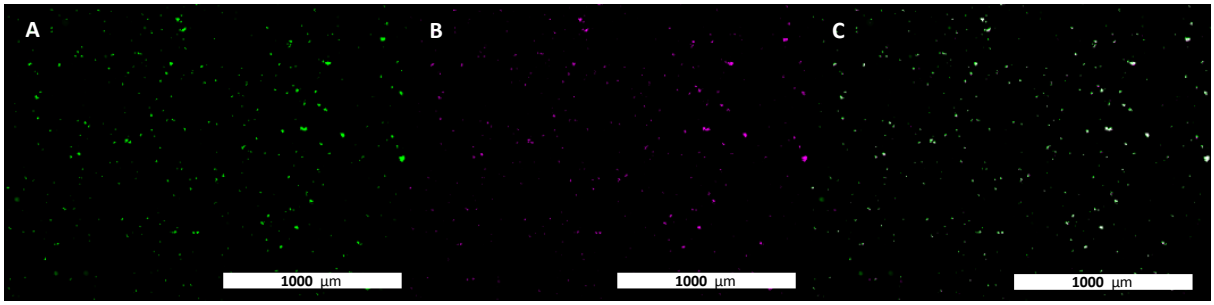

*Figure 69: Fluorescence microscopy images obtained from the particles (0.01 mg/ml) modified with compound **10** derived from 4.8 % peptide **17** in **3** A: fluorescein channel, B: cyanine-5 channel, C: overlay of fluorescein and cyanine-5 channels*

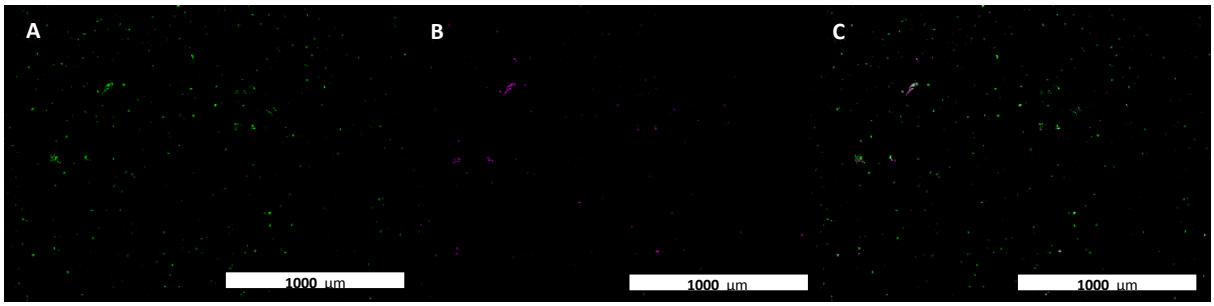

*Figure 70: Fluorescence microscopy images obtained from the particles (0.01 mg/ml) modified with compound **17** derived from 1 % peptide **17** in **3**, A: fluorescein channel, B: cyanine-5 channel, C: overlay of fluorescein and cyanine-5 channels*

Figure 69 confirms the presence of compound **10** (Figure 69 A) and peptide **17** (Figure 69 B) in the investigated particles and the overlay in Figure 69 C confirms that both fluorescent modifications are located on the same particles. Similar results were obtained for the silica particles modified with compound **10** derived from 1 % peptide **17** in **3** but with a weaker signal for the cyanine-5 channel (when comparing both signals to their corresponding fluorescein signal) due to the lower percentage of **17** (Figure 70).

3.3.3.5 Cell study

The cell study was performed with silica particles modified with compound **10** derived from 4.8 % peptide **17** in **3** as described in section 2.4.3.4 simultaneously with the cell studies of particles containing **17** (section 3.3.2.7) or **10** (section 3.3.1.5). The stained cells (Hoechst 33258) were treated with particles (0.01 mg/ml) and imaged immediately, 2 hours and 24 hours after treatment using 4 channels: Hoechst 33258, cyanine-5 for visualization of peptide **17** incorporated into the particles, fluorescein to show that the particles were simultaneously modified with compound **10** and bright field.

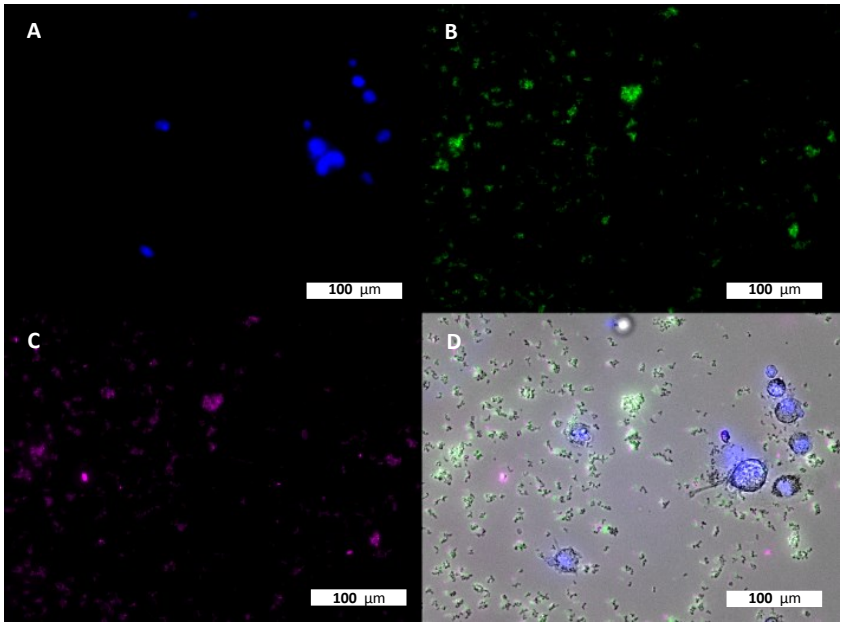

Figure 71: Images of stained (Hoechst 33258 DNA stain) THP-1 cells acquired immediately after incubation of the cells with silica particles (0.01 mg/ml) modified with compound **10** derived from 4.8 % peptide **17** in **3**, A: Hoechst 33258 channel, B: fluorescein channel, C: cyanine-5 channel, D, composite of channels shown in A-C with the bright field channel

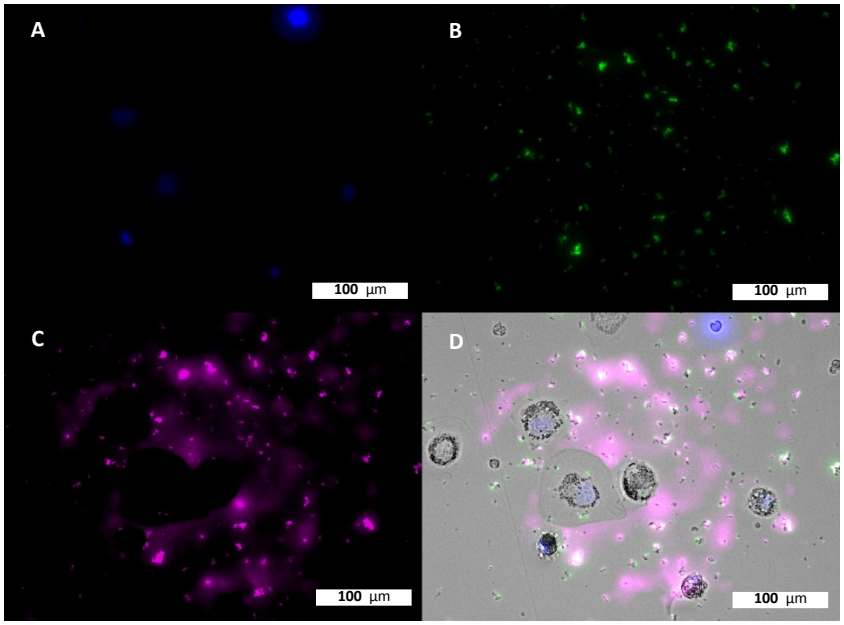

Figure 72: Images of stained (Hoechst 33258 DNA stain) THP-1 cells acquired 2 hours after incubation of the cells with silica particles (0.01 mg/ml) modified with compound **10** derived from 4.8 % peptide **17** in **3**, A: Hoechst 33258 channel, B: fluorescein channel, C: cyanine-5 channel, D, composite of channels shown in A-C with the bright field channel

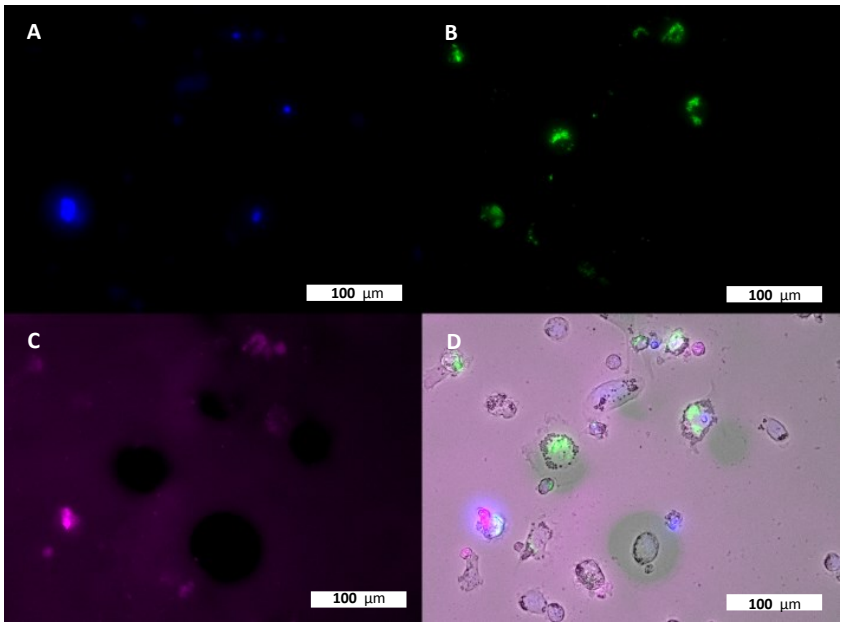

Figure 73: Images of stained (Hoechst 33258 DNA stain) THP-1 cells acquired 24 hours after incubation of the cells with silica particles (0.01 mg/ml) modified with compound **10** derived from 4.8 % peptide **17** in **3**, A: Hoechst 33258 channel, B: fluorescein channel, C: cyanine-5 channel, D, composite of channels shown in A-C with the bright field channel

Figure 71 B and C confirm that, immediately after treatment of the cells, the particles investigated carry peptide **17** and compound **10** simultaneously. The overlay of the Hoechst 33258, cyanine-5, fluorescein and bright field channels (Figure 71 D) shows that the particles are located outside the cells. Peptide **17** has not been visibly released at this time point. 2 hours after treatment of the cells with particles, they are still mostly located outside the cells (Figure 72 D) and have started to release peptide **17** (Figure 72 C). 24 hours post treatment the majority of the particles has been taken up the cells (Figure 73 D) and even more peptide **17** has been released (Figure 73 C). Fluorescence microscopy shows that peptide **17** has been released into the medium surrounding the cells and has partly also

been taken up by the cells themselves (Figure 73 D). In contrast to the release of **17**, compound **10** has not been visibly released from the particles within 24 hours after incubation.

Overall, the results in this section demonstrate that two modifications can simultaneously be introduced into silica particles using the biomimetic approach with a mixture of peptide **17** (carrying a cyanine-5 modification on the *N*-terminus) and peptide **3** with compound **10** (carrying a fluorescein modification) as a silica precursor in addition to TMOS. Figures 66 and 67 demonstrate that the doubly modified silica precipitates are composed of spherical silica particles with smooth (1 % peptide **17** in **3**) or rough (4.8 % peptide **17** in **3**) surfaces depending on the percentage of **17** incorporated. Investigation of the particles via fluorescence microscopy (Figures 69/70) confirmed that the obtained silica particles simultaneously carry the cyanine-5 modification introduced via peptide **17** and the fluorescein modification incorporated through compound **10**.

The results in Tables 11 and 14 show that compound **10** or peptide **17** are efficiently incorporated into the silica particles during the precipitation with percentages of incorporated silane **10** of 88 % and encapsulated **17** of 80.8 % (from a solution of 4.8% (w/w) **17** in **3**). While the homogeneous incorporation of a fluorescent dye into biomimetically produced silica particles via attachment to the *N*-terminus of an R5 peptide variant has been reported before [108], in this project it was combined with the simultaneous introduction of a fluorescein modification using a mixture of TMOS and silane **10** as silica precursors. This method for a simultaneous incorporation of two modifications into silica particles derived from R5 peptide variants is a new approach that combines a functionality (in this case the cyanine-5 fluorescent dye) introduced via attachment to an R5 peptide variant with a modification (fluorescein) incorporated into the silica material itself via an appropriately modified silica precursor. Therefore, this method is a very convenient technique for the simultaneous introduction of two functionalities into silica particles during the precipitation without requiring post synthetic modification of the particles. When peptide **17** and silane **10** are simultaneously used in a biomimetic precipitation with peptide **3**, the incorporated percentages of these compounds are in the same range (Table 15, 89.9 % for **10** and 76.8 % for **17**) as observed when only one of them is introduced into silica particles derived from **3** (Tables 11 and 14). While the incorporation of fluorescent dyes into silica particles via the alkaline Stöber process [124] and the introduction of compound **10** into silica particles via the micro-emulsion approach [123] have previously been reported, the technique developed in this project provides (in addition to the incorporation of a second modification) advantages such as a shorter and less elaborate synthesis procedure and milder precipitation conditions (neutral pH), which allows for the production of hybrid materials of silica with biomolecules. The cell studies in Figures 71-73 support the assumption that the two functionalities are attached to the silica particles in different manners as a release of the cyanine-5 modification (via release of peptide **17**) is observed 2 and 24 hours after particle incubation in cell culture medium (pH 7.2-7.4), while the fluorescein modification introduced via compound **10** is not visibly released under these conditions within 24 hours when the particles are located inside the cells. The release of peptide **17** is in agreement with previously reported release of R5 variants from silica particles in PBS at pH 7.4 [5]. Release studies for compound **10** in 50 mM potassium phosphate buffer (pH 7 or 4) showed that, while release at pH 4 is not detectable even after one week of incubation, 14 % of compound **10** is released after one week of incubation at pH 7. This indicates that release of compound **10**, which has been incorporated into the silica material itself, occurs at a slower rate and/or to a lesser extent than the release of R5 peptide variants from the silica particles, which has been reported to be 12 % for peptide **3** after one hour of incubation at pH 7.4 (37°C) and 84 % at pH 5 (37°C)[5]. In addition, the different nature of release of compound **10** and

peptide **17** is underlined by the observation that, while more R5 has been shown to be released at lower pH values, more compound **10** is released at higher pH values [5].

If the method for double modification of silica particles employed in this section can also be performed using different types of molecules attached to the *N*-terminus of peptide **3** and different modifications on the silica precursor, the particles could potentially be useful for a variety of applications, including delivery vehicles for 2 different cargo molecules, vaccine adjuvants or imaging purposes (depending on the types of modifications introduced). It has been demonstrated in this project that particles with a cyanine-5 fluorescent modification attached to the R5 peptide variant **3** and a fluorescein modification incorporated into the silica material itself can be used in cell studies of R5 peptide derived silica particles to image the modified R5 peptide variant and the silica material independently from one another at different time points after incubation of the particles with cells. This provides simultaneous information about the location of the R5 peptide variant and the silica particles at each time point. Further potential applications of these doubly modified particles include the combination of delivery vehicles for cargo molecules such as proteins, peptides or drugs (attached to the R5 peptide variant) with imaging of the particles via a fluorescent modification introduced into the silica material (through an appropriately modified silica precursor such as **10**). Other applications of such bifunctional silica particles include targeted drug delivery (when a targeting agent is incorporated into the silica material) or vaccine adjuvants. For the use as vaccine adjuvants, the particles could be modified with a pathogen-associated signature molecule designed to trigger an innate immune response, that could be introduced via an appropriately modified silica precursor, and simultaneously act as a depot for antigenic peptides attached to the R5 peptide variant **3**, thereby enhancing the immune response and efficiency of the vaccine.

4 Conclusion and Outlook

One of the aims of this project was the investigation of the display and binding accessibility of the *N*- or *C*-terminus of the R5 peptide in silica particles derived from this peptide utilizing the (strept)avidi-biotin interaction. For this strategy, *N*- and *C*-terminally biotinylated versions of an R5 peptide variant carrying an *N*-terminal cysteine were used to generate silica particles via a biomimetic synthesis approach. Streptavidin-gold nanoparticle as well as avidin-sulforhodamine 101 conjugates were incubated with the silica particles, assuming that, if the *N*- or *C*-terminal biotin moieties of the peptides were accessible on the surface, the conjugates would bind to the silica particles and binding would be detectable via TEM or UV-Vis absorbance measurements. While no conclusion about the surface display and accessibility of the *N*- and *C*-terminus of the R5 peptide could be made, it was observed that the streptavidin-gold nanoparticle and avidin-sulforhodamine 101 conjugates could also attach to the silica particles containing a non-biotinylated R5 variant and at least a fraction of the protein conjugates was still attached to the particles after thorough washing with H_2O and 1 hour incubation in 50 mM potassium phosphate buffer (pH 7). As this attachment cannot have occurred via biotin-streptavidin interactions, this could mean that attachment of proteins to R5 peptide derived silica particles might generally be achieved by simple incubation of the particles with proteins, if other proteins unspecifically adsorb to the surface as well. These particles might then also randomly bind, for example, proteins present in physiological environments and this so-called protein-corona might change their surface properties and interaction with cells, facilitating or hindering particle uptake, as it has been observed for nanoparticles composed of many different materials including gold and non-biomimetically generated silica [119]. Therefore, this feature will have to be investigated further, in order to determine if and how different proteins attached to the surface interfere with uptake of R5 peptide derived particles by cells.

In order to optimize the synthesis conditions of such silica particles derived from the R5 peptide for the formation of spherical particles with smooth surfaces, the influence of the pH, peptide concentrations and TEOS concentrations on the morphology of silica particles derived from biomimetic precipitations with the R5 peptide and TMOS or TEOS was investigated. It was shown that the morphologies are in fact dependent on the pH of the 50 mM potassium phosphate buffer the precipitations are carried out in. For TMOS precipitations, spherical silica particles possessing the smoothest morphologies were obtained at pH 7 or 8, while particles at pH 9 exhibited rougher surfaces and no silica precipitates were formed at pH values lower than 7. For TEOS precipitations, no precipitate was observed below pH 6 and particles with smooth morphologies were obtained at pH 7, 8 and 9, while precipitates at pH 6 exhibited rougher surfaces. The particle morphologies were shown to be dependent on peptide and TEOS concentration for TEOS precipitations at pH 6, while at pH 7, all tested peptide and TEOS concentrations led to the formation of spherical and smooth silica particles. Based on the observation that in 50 mM potassium phosphate buffer at pH 7, smooth and spherical particles were generated in TMOS and TEOS precipitations independently of peptide and TEOS concentrations, similar synthesis conditions for spherical and smooth doubly fluorescent modified silica particles were developed using TMOS and **10** (a fluorescein modified derivative of TEOS) as silica precursors and peptide **17** (an R5 peptide variant with an *N*-terminal cyanine-5 modification) in 50 mM potassium phosphate buffer at pH 7, involving hydrolysis of **10** at pH 9. Such doubly modified silica particles generated via this biomimetic synthesis method provide advantages over Stöber and micro-emulsion syntheses of functionalized silica particles such as an easy and quick synthesis procedure and mild conditions with neutral pH and ambient temperature, which allow for the introduction of protein modifications while maintaining protein activity. This method could potentially be used to synthesize

doubly modified silica particles carrying other types of modifications such as proteins and small molecules, providing a great versatility of the particles that can then potentially be used for a variety of applications such as delivery vehicles for proteins or other cargo molecules in combination with imaging, targeted drug delivery or vaccine adjuvants. The doubly modified particles were shown to be taken up by THP-1 cells within 24 hours. As the cyanine-5 modification was introduced via attachment to the *N*-terminus of the R5 peptide variant **3** and the incorporation of fluorescein into the silica material itself was achieved via the use of fluorescein-modified silica precursor **10**, the two modifications were associated with the particles in different manners which manifested in different release behaviours of **17** and **10** observed in these cell studies. The cell studies showed that, while peptide **17** was visibly released into the medium (pH 7.2-7.4) after 24 hours, no release of **10** could be observed within this timeframe.

While we discovered that avidin and streptavidin conjugates can attach to silica particles derived from the R5 peptide variant **3** by simple incubation of the particles with the conjugates, no conclusion could be made for the binding accessibility and display of the *N*- and *C*-terminus of the R5 peptide. Therefore, another method will have to be developed to provide an answer to this question. Additionally, it will have to be investigated if the observation, that (strept)avidin conjugates can be attached to silica particles derived from the R5 peptide via simple incubation with the particles, is valid for other proteins and molecules as well and if this simple method can generally be used to load cargo molecules onto this type of silica particles.

In addition, the applicability of the method developed in this project for double modification of silica particles derived from R5 peptide variants for the introduction of other modifications via attachment to the R5 peptide and the use of an appropriately modified silica precursor will have to be tested. Furthermore, release studies for compound **10** and peptide **17** from the doubly modified silica particles synthesized in this project will have to be carried out at continuous time points in order to assess how the release of these compounds progresses over time, how it is dependent on release buffer conditions (pH) and how the release profiles of compound **10** and peptide **17** differ from each other. While it was shown in the cell studies performed in this project that the doubly modified silica particles were taken up by THP-1 cells within 24 hours, in order to determine the specific effects that the particles have on these cells, an investigation of, for example, cytotoxicity of the particles or the release of cytokines from the cells will have to be carried out. Additionally, in this project, the doubly modified silica particles were synthesized using TMOS as a silica precursor, which is volatile and highly toxic [126]. Therefore, the development of a suitable method for the synthesis of such particles using TEOS as a silica precursor, which is less volatile and less toxic [127] than TMOS, would be desirable.

5 References

1. **Mugica, L.C., et al.**, *Surface functionalization of silica particles for their efficient fluorescence and stereo selective modification.* Colloids and Surfaces A: Physicochemical and Engineering Aspects, 2016. **500**: p. 79-87.
2. **Bergna, H.E. and W.O. Roberts**, *Colloidal Silica: Fundamentals and Applications*. 2005: CRC Press.
3. **Slowing, I.I., et al.**, *Mesoporous silica nanoparticles as controlled release drug delivery and gene transfection carriers.* Advanced drug delivery reviews, 2008. **60**(11): p. 1278-1288.
4. **Henstock, J.R., L.T. Canham, and S.I. Anderson**, *Silicon: The evolution of its use in biomaterials.* Acta Biomaterialia, 2015. **11**(Supplement C): p. 17-26.
5. **Lechner, C.C. and C.F. Becker**, *Modified silaffin R5 peptides enable encapsulation and release of cargo molecules from biomimetic silica particles.* Bioorganic & medicinal chemistry, 2013. **21**(12): p. 3533-3541.
6. **Kang, K.-K., et al.**, *Synthesis of silica nanoparticles using biomimetic mineralization with polyallylamine hydrochloride.* Journal of Colloid and Interface Science, 2017. **507**: p. 145-153.
7. **Singh, L.P., et al.**, *Sol-Gel processing of silica nanoparticles and their applications.* Advances in colloid and interface science, 2014. **214**: p. 17-37.
8. **Brinker, C.J. and G.W. Scherer**, *Sol-gel science: the physics and chemistry of sol-gel processing*. 2013: Academic press.
9. **Rahman, I.A. and V. Padavettan**, *Synthesis of Silica Nanoparticles by Sol-Gel: Size-Dependent Properties, Surface Modification, and Applications in Silica-Polymer Nanocomposites—A Review.* Journal of Nanomaterials, 2012. **2012**: p. 15.
10. **Suryanarayana, C.**, *Mechanical alloying and milling.* Progress in materials science, 2001. **46**(1): p. 1-184.
11. **Hench, L.L. and J.K. West**, *The sol-gel process.* Chemical Reviews, 1990. **90**(1): p. 33-72.
12. **Coradin, T. and P.J. Lopez**, *Biogenic Silica Patterning: Simple Chemistry or Subtle Biology?* ChemBioChem, 2003. **4**(4): p. 251-259.
13. **Stöber, W., A. Fink, and E. Bohn**, *Controlled growth of monodisperse silica spheres in the micron size range.* Journal of colloid and interface science, 1968. **26**(1): p. 62-69.
14. **Guo, J., et al.**, *Size-controllable synthesis of monodispersed colloidal silica nanoparticles via hydrolysis of elemental silicon.* Journal of colloid and interface science, 2008. **326**(1): p. 138-142.
15. **Liberman, A., et al.**, *Synthesis and surface functionalization of silica nanoparticles for nanomedicine.* Surface Science Reports, 2014. **69**(2–3): p. 132-158.
16. **Tang, F., L. Li, and D. Chen**, *Mesoporous silica nanoparticles: synthesis, biocompatibility and drug delivery.* Advanced Materials, 2012. **24**(12): p. 1504-1534.
17. **Cai, Q., et al.**, *The preparation of highly ordered MCM-41 with extremely low surfactant concentration.* Microporous and Mesoporous Materials, 1999. **32**(1): p. 1-15.
18. **Radu, D.R., et al.**, *Fine-tuning the degree of organic functionalization of mesoporous silica nanosphere materials via an interfacially designed co-condensation method.* Chemical Communications, 2005(10): p. 1264-1266.
19. **Yokoi, T., H. Yoshitake, and T. Tatsumi**, *Synthesis of amino-functionalized MCM-41 via direct co-condensation and post-synthesis grafting methods using mono-, di- and tri-amino-organoalkoxysilanes.* Journal of Materials Chemistry, 2004. **14**(6): p. 951-957.
20. **Kresge, C., et al.**, *Ordered mesoporous molecular sieves synthesized by a liquid-crystal template mechanism.* nature, 1992. **359**(6397): p. 710-712.
21. **Grün, M., I. Lauer, and K.K. Unger**, *The synthesis of micrometer- and submicrometer-size spheres of ordered mesoporous oxide MCM-41.* Advanced Materials, 1997. **9**(3): p. 254-257.
22. **Jambhrunkar, S., et al.**, *Stepwise Pore Size Reduction of Ordered Nanoporous Silica Materials at Angstrom Precision.* Journal of the American Chemical Society, 2013. **135**(23): p. 8444-8447.

23. **Trewyn, B.G., C.M. Whitman, and V.S.Y. Lin**, *Morphological Control of Room-Temperature Ionic Liquid Templated Mesoporous Silica Nanoparticles for Controlled Release of Antibacterial Agents.* Nano Letters, 2004. **4**(11): p. 2139-2143.
24. **Bao, Y.Z., et al.**, *Influences of individual and composed poly (vinyl alcohol) suspending agents on particle morphology of suspension poly (vinyl chloride) resin.* Journal of applied polymer science, 2003. **90**(14): p. 3848-3855.
25. **Teeguarden, J.G., et al.**, *Particokinetics in vitro: dosimetry considerations for in vitro nanoparticle toxicity assessments.* Toxicological Sciences, 2006. **95**(2): p. 300-312.
26. **Huang, X., et al.**, *The effect of the shape of mesoporous silica nanoparticles on cellular uptake and cell function.* Biomaterials, 2010. **31**(3): p. 438-448.
27. **Decuzzi, P., et al.**, *Size and shape effects in the biodistribution of intravascularly injected particles.* Journal of Controlled Release, 2010. **141**(3): p. 320-327.
28. **Kim, S., et al.**, *Surface modification of silica nanoparticles by UV-induced graft polymerization of methyl methacrylate.* Journal of colloid and interface science, 2005. **292**(1): p. 93-98.
29. **Cauda, V., C. Argyo, and T. Bein**, *Impact of different PEGylation patterns on the long-term bio-stability of colloidal mesoporous silica nanoparticles.* Journal of Materials Chemistry, 2010. **20**(39): p. 8693-8699.
30. **He, Q., et al.**, *In vivo Biodistribution and Urinary Excretion of Mesoporous Silica Nanoparticles: Effects of Particle Size and PEGylation.* Small, 2011. **7**(2): p. 271-280.
31. **Techniques, B**., *Hermanson, GT, Ed*. 1996, Academic Press: San Diego, CA.
32. **Knopp, D., D. Tang, and R. Niessner**, *Bioanalytical applications of biomolecule-functionalized nanometer-sized doped silica particles.* Analytica chimica acta, 2009. **647**(1): p. 14-30.
33. **Wang, H., et al.**, *Novel immunoassay for Toxoplasma gondii-specific immunoglobulin G using a silica nanoparticle-based biomolecular immobilization method.* Analytica chimica acta, 2004. **501**(1): p. 37-43.
34. **An, Y., et al.**, *Preparation and self-assembly of carboxylic acid-functionalized silica.* Journal of colloid and interface science, 2007. **311**(2): p. 507-513.
35. **Qhobosheane, M., et al.**, *Biochemically functionalized silica nanoparticles.* Analyst, 2001. **126**(8): p. 1274-1278.
36. **Blasi, L., et al.**, *Formation and characterization of glutamate dehydrogenase monolayers on silicon supports.* Biosensors and Bioelectronics, 2005. **21**(1): p. 30-40.
37. **Han, L., et al.**, *Synthesis of carboxylic group functionalized mesoporous silicas (CFMSs) with various structures.* Journal of Materials Chemistry, 2007. **17**(12): p. 1216-1221.
38. **Peng, J., et al.**, *Identification of live liver cancer cells in a mixed cell system using galactose-conjugated fluorescent nanoparticles.* Talanta, 2007. **71**(2): p. 833-840.
39. **Hiramatsu, H. and F.E. Osterloh**, *pH-Controlled Assembly and Disassembly of Electrostatically Linked CdSe−SiO2 and Au−SiO2 Nanoparticle Clusters.* Langmuir, 2003. **19**(17): p. 7003-7011.
40. **Lei, Z., S. Bi, and H. Yang**, *Chitosan-tethered the silica particle from a layer-by-layer approach for pectinase immobilization.* Food chemistry, 2007. **104**(2): p. 577-584.
41. **Hilliard, L.R., X. Zhao, and W. Tan**, *Immobilization of oligonucleotides onto silica nanoparticles for DNA hybridization studies.* Analytica Chimica Acta, 2002. **470**(1): p. 51-56.
42. **Park, J.T., et al.**, *Surface modification of silica nanoparticles with hydrophilic polymers.* Journal of Industrial and Engineering Chemistry, 2010. **16**(4): p. 517-522.
43. **Laruelle, G., et al.**, *Block copolymer grafted-silica particles: a core/double shell hybrid inorganic/organic material.* Polymer, 2004. **45**(15): p. 5013-5020.
44. **Ueda, J., et al.**, *Cationic graft polymerization onto silica nanoparticle surface in a solvent-free dry-system.* Polymer Bulletin, 2008. **60**(5): p. 617-624.
45. **Zhou, Q., et al.**, *Living anionic surface-initiated polymerization (LASIP) of a polymer on silica nanoparticles.* Langmuir, 2002. **18**(8): p. 3324-3331.
46. **Jordi, M.A. and T.A. Seery**, *Quantitative Determination of the Chemical Composition of Silica–Poly (norbornene) Nanocomposites.* Journal of the American Chemical Society, 2005. **127**(12): p. 4416-4422.

47. **Ueda, J., et al.**, *Scale-up synthesis of vinyl polymer-grafted nano-sized silica by radical polymerization of vinyl monomers initiated by surface initiating groups in the solvent-free dry-system.* European polymer journal, 2005. **41**(2): p. 193-200.
48. **Stenzel, M.H., L. Zhang, and W.T. Huck**, *Temperature-Responsive Glycopolymer Brushes Synthesized via RAFT Polymerization Using the Z-group Approach.* Macromolecular rapid communications, 2006. **27**(14): p. 1121-1126.
49. **Pyun, J., T. Kowalewski, and K. Matyjaszewski**, *Synthesis of polymer brushes using atom transfer radical polymerization.* Macromolecular Rapid Communications, 2003. **24**(18): p. 1043-1059.
50. **Luckarift, H.R., et al.**, *Enzyme-encapsulated silica monolayers for rapid functionalization of a gold surface.* Colloids and Surfaces B: Biointerfaces, 2007. **58**(1): p. 28-33.
51. **Jain, T.K., et al.**, *Nanometer silica particles encapsulating active compounds: a novel ceramic drug carrier.* Journal of the American Chemical Society, 1998. **120**(43): p. 11092-11095.
52. **Gelman, F., J. Blum, and D. Avnir**, *One-pot sequences of reactions with sol-gel entrapped opposing reagents: an enzyme and metal-complex catalysts.* Journal of the American Chemical Society, 2002. **124**(48): p. 14460-14463.
53. **Wang, Y., et al.**, *The investigation of MCM-48-type and MCM-41-type mesoporous silica as oral solid dispersion carriers for water insoluble cilostazol.* Drug Development and Industrial Pharmacy, 2014. **40**(6): p. 819-828.
54. **Mellaerts, R., et al.**, *Increasing the oral bioavailability of the poorly water soluble drug itraconazole with ordered mesoporous silica.* European Journal of Pharmaceutics and Biopharmaceutics, 2008. **69**(1): p. 223-230.
55. **Wang, Y., et al.**, *Mesoporous silica nanoparticles in drug delivery and biomedical applications.* Nanomedicine: Nanotechnology, Biology and Medicine, 2015. **11**(2): p. 313-327.
56. **Diamandis, E.P. and T.K. Christopoulos**, *The biotin-(strept)avidin system: principles and applications in biotechnology.* Clinical Chemistry, 1991. **37**(5): p. 625.
57. **Lowenstam, H.A. and S. Weiner**, *On biomineralization*. 1989: Oxford University Press on Demand.
58. **Kretsinger, R.H.**, *A Comparison of the Roles of Calcium in Biomineralization and in Cytosolic Signalling*, in *Biomineralization and Biological Metal Accumulation: Biological and Geological Perspectives Papers presented at the Fourth International Symposium on Biomineralization, Renesse, The Netherlands, June 2–5, 1982*, P. Westbroek and E.W. de Jong, Editors. 1983, Springer Netherlands: Dordrecht. p. 123-131.
59. **Addadi, L. and S. Weiner**, *Control and Design Principles in Biological Mineralization.* Angewandte Chemie International Edition in English, 1992. **31**(2): p. 153-169.
60. **Simpson, T. and B. Volcani**, *Silicon and siliceous structures in biological systems*. 1981, New York: Springer-Verlag.
61. **Ehrlich, H., et al.**, *Modern Views on Desilicification: Biosilica and Abiotic Silica Dissolution in Natural and Artificial Environments.* Chemical Reviews, 2010. **110**(8): p. 4656-4689.
62. **Maldonado, M., et al.**, *Decline in Mesozoic reef-building sponges explained by silicon limitation.* Nature, 1999. **401**(6755): p. 785-788.
63. **Birchall, J.D.**, *The essentiality of silicon in biology.* Chemical Society Reviews, 1995. **24**(5): p. 351-357.
64. **Schroder, H.C., et al.**, *Biofabrication of biosilica-glass by living organisms.* Natural Product Reports, 2008. **25**(3): p. 455-474.
65. **Marron, A.O., et al.**, *A family of diatom-like silicon transporters in the siliceous loricate choanoflagellates.* Proceedings of the Royal Society B: Biological Sciences, 2013. **280**(1756).
66. **Werner, D**., *The biology of diatoms*. Vol. 13. 1977: Univ of California Press.
67. **Parkinson, J. and R. Gordon**, *Beyond micromachining: the potential of diatoms.* Trends in biotechnology, 1999. **17**(5): p. 190-196.
68. **Vrieling, E.G., et al.**, *Diatom silicon biomineralization as an inspirational source of new approaches to silica production.* Journal of Biotechnology, 1999. **70**(1): p. 39-51.

69. **Kotzsch, A., et al.**, *Silicanin-1 is a conserved diatom membrane protein involved in silica biomineralization.* BMC Biology, 2017. **15**: p. 65.
70. **Tanaka, A., et al.**, *Ultrastructure and membrane traffic during cell division in the marine pennate diatom Phaeodactylum tricornutum.* Protist, 2015. **166**(5): p. 506-521.
71. **Foo, C.W.P., J. Huang, and D.L. Kaplan**, *Lessons from seashells: silica mineralization via protein templating.* Trends in Biotechnology, 2004. **22**(11): p. 577-585.
72. **Poll, W.H.v.d., E.G. Vrieling, and W.W.C. Gieskes**, *Location and expression of frustulins in the pennate diatoms Cylindrotheca Fusiformis, Navicula pelliculosa, and Navicula Salinarium (Bacillariophyceae)* Journal of Phycology, 1999. **35**(5): p. 1044-1053.
73. **Kröger, N., et al.**, *Characterization of a 200-kDa Diatom Protein that is Specifically Associated with a Silica-Based Substructure of the Cell Wall.* European Journal of Biochemistry, 1997. **250**(1): p. 99-105.
74. **Kröger, N. and R. Wetherbee**, *Pleuralins are involved in theca differentiation in the diatom Cylindrotheca fusiformis.* Protist, 2000. **151**(3): p. 263-273.
75. **Kröger, N., R. Deutzmann, and M. Sumper**, *Polycationic Peptides from Diatom Biosilica That Direct Silica Nanosphere Formation.* Science, 1999. **286**(5442): p. 1129.
76. **Kröger, N., R. Deutzmann, and M. Sumper**, *Silica-precipitating Peptides from Diatoms: The chemical structure of silaffin-1a from cylindrotheca fusiformis* Journal of Biological Chemistry, 2001. **276**(28): p. 26066-26070.
77. **Kröger, N., et al.**, *Species-specific polyamines from diatoms control silica morphology.* Proceedings of the National Academy of Sciences of the United States of America, 2000. **97**(26): p. 14133-14138.
78. **Kröger, N., et al.**, *Self-Assembly of Highly Phosphorylated Silaffins and Their Function in Biosilica Morphogenesis.* Science, 2002. **298**(5593): p. 584.
79. **Poulsen, N., M. Sumper, and N. Kröger**, *Biosilica formation in diatoms: Characterization of native silaffin-2 and its role in silica morphogenesis.* Proceedings of the National Academy of Sciences, 2003. **100**(21): p. 12075-12080.
80. **Dickerson, M.B., K.H. Sandhage, and R.R. Naik**, *Protein- and Peptide-Directed Syntheses of Inorganic Materials.* Chemical Reviews, 2008. **108**(11): p. 4935-4978.
81. **Sumper, M., S. Lorenz, and E. Brunner**, *Biomimetic Control of Size in the Polyamine-Directed Formation of Silica Nanospheres.* Angewandte Chemie International Edition, 2003. **42**(42): p. 5192-5195.
82. **Sumper, M. and N. Kröger**, *Silica formation in diatoms: the function of long-chain polyamines and silaffins.* Journal of Materials Chemistry, 2004. **14**(14): p. 2059-2065.
83. **Vrieling, E.G., W. Gieskes, and T.P. Beelen**, *Silicon deposition in diatoms: control by the pH inside the silicon deposition vesicle.* Journal of Phycology, 1999. **35**(3): p. 548-559.
84. **Lechner, C.C. and C.F.W. Becker**, *A sequence-function analysis of the silica precipitating silaffin R5 peptide.* Journal of Peptide Science, 2014. **20**(2): p. 152-158.
85. **Kröger, N. and M. Sumper**, *The biochemistry of silica formation in diatoms.* Biomineralization, 2000: p. 151-170.
86. **Knecht, M.R. and D.W. Wright**, *Functional analysis of the biomimetic silica precipitating activity of the R5 peptide from Cylindrotheca fusiformis.* Chemical Communications, 2003(24): p. 3038-3039.
87. **Rodríguez, F., et al.**, *Study of the chemical and physical influences upon in vitro peptide-mediated silica formation.* Biomacromolecules, 2004. **5**(2): p. 261-265.
88. **Lechner, C.C. and F.C. Becker**, *Silaffins in Silica Biomineralization and Biomimetic Silica Precipitation.* Marine Drugs, 2015. **13**(8).
89. **Kröger, N., et al.**, *Bioenabled Synthesis of Rutile (TiO2) at Ambient Temperature and Neutral pH.* Angewandte Chemie International Edition, 2006. **45**(43): p. 7239-7243.
90. **Naik, R.R., et al.**, *Controlled formation of biosilica structures in vitro.* Chemical Communications, 2003(2): p. 238-239.

91. **Tacke, R.**, *Milestones in the Biochemistry of Silicon: From Basic Research to Biotechnological Applications.* Angewandte Chemie International Edition, 1999. **38**(20): p. 3015-3018.
92. **Luckarift, H.R., et al.**, *Enzyme immobilization in a biomimetic silica support.* Nat Biotech, 2004. **22**(2): p. 211-213.
93. **Naik, R.R., et al.**, *Entrapment of enzymes and nanoparticles using biomimetically synthesized silica.* Chemical Communications, 2004(15): p. 1684-1685.
94. **Luckarift, H.R., G.R. Johnson, and J.C. Spain**, *Silica-immobilized enzyme reactors; application to cholinesterase-inhibition studies.* Journal of Chromatography B, 2006. **843**(2): p. 310-316.
95. **Miller, S.A., E.D. Hong, and D. Wright**, *Rapid and efficient enzyme encapsulation in a dendrimer silica nanocomposite.* Macromolecular bioscience, 2006. **6**(10): p. 839-845.
96. **Sun, Q., et al.**, *Green and efficient conversion of CO2 to methanol by biomimetic coimmobilization of three dehydrogenases in protamine-templated titania.* Industrial & Engineering Chemistry Research, 2009. **48**(9): p. 4210-4215.
97. **Jin, R.-H. and J.-J. Yuan**, *Shaped Silicas Transcribed from Aggregates of Four-Armed Star Polyethyleneimine with a Benzene Core.* Chemistry of Materials, 2006. **18**(15): p. 3390-3396.
98. **Sano, K.-I., T. Minamisawa, and K. Shiba**, *Autonomous silica encapsulation and sustained release of anticancer protein.* Langmuir, 2010. **26**(4): p. 2231-2234.
99. **Coradin, T. and J. Livage**, *Synthesis, characterization and diffusion properties of biomimetic silica-coated gelatine beads.* Materials Science and Engineering: C, 2005. **25**(2): p. 201-205.
100. **Patwardhan, S.V. and C.C. Perry**, *Synthesis of enzyme and quantum dot in silica by combining continuous flow and bioinspired routes.* Silicon, 2010. **2**(1): p. 33-39.
101. **Patwardhan, S.V.**, *Biomimetic and bioinspired silica: recent developments and applications.* Chemical Communications, 2011. **47**(27): p. 7567-7582.
102. **Boury, B. and R.J. Corriu**, *Auto-organisation of hybrid organic–inorganic materials prepared by sol–gel chemistry.* Chemical Communications, 2002(8): p. 795-802.
103. **Bitar, A., et al.**, *Silica-based nanoparticles for biomedical applications.* Drug Discovery Today, 2012. **17**(19): p. 1147-1154.
104. **Betancor, L. and H.R. Luckarift**, *Bioinspired enzyme encapsulation for biocatalysis.* Trends in biotechnology, 2008. **26**(10): p. 566-572.
105. **Liong, M., et al.**, *Mesostructured multifunctional nanoparticles for imaging and drug delivery.* Journal of Materials Chemistry, 2009. **19**(35): p. 6251-6257.
106. **Slowing, I.I., et al.**, *Mesoporous Silica Nanoparticles for Drug Delivery and Biosensing Applications.* Advanced Functional Materials, 2007. **17**(8): p. 1225-1236.
107. **Lai, C.-Y., et al.**, *A Mesoporous Silica Nanosphere-Based Carrier System with Chemically Removable CdS Nanoparticle Caps for Stimuli-Responsive Controlled Release of Neurotransmitters and Drug Molecules.* Journal of the American Chemical Society, 2003. **125**(15): p. 4451-4459.
108. **Lechner, C.C. and C.F.W. Becker**, *Exploring the effect of native and artificial peptide modifications on silaffin induced silica precipitation.* Chemical Science, 2012. **3**(12): p. 3500-3504.
109. **Mody, K.T., et al.**, *Mesoporous silica nanoparticles as antigen carriers and adjuvants for vaccine delivery.* Nanoscale, 2013. **5**(12): p. 5167-5179.
110. **Guo, H.-C., et al.**, *Immunization of mice by Hollow Mesoporous Silica Nanoparticles as carriers of Porcine Circovirus Type 2 ORF2 Protein.* Virology Journal, 2012. **9**(1): p. 108.
111. **Wang, T., et al.**, *Enhanced mucosal and systemic immune responses obtained by porous silica nanoparticles used as an oral vaccine adjuvant: Effect of silica architecture on immunological properties.* International journal of pharmaceutics, 2012. **436**(1): p. 351-358.
112. **Carvalho, L.V., et al.**, *Immunological parameters related to the adjuvant effect of the ordered mesoporous silica SBA-15.* Vaccine, 2010. **28**(50): p. 7829-7836.
113. **Mercuri, L.P., et al.**, *Ordered Mesoporous Silica SBA-15: A New Effective Adjuvant to Induce Antibody Response.* Small, 2006. **2**(2): p. 254-256.

114. **Huang, Y.-C., et al.**, *Accelerated Fmoc solid-phase synthesis of peptides with aggregation-disrupting backbones.* Organic & Biomolecular Chemistry, 2015. **13**(5): p. 1500-1506.
115. **Genin, M., et al.**, *M1 and M2 macrophages derived from THP-1 cells differentially modulate the response of cancer cells to etoposide.* BMC Cancer, 2015. **15**: p. 577.
116. **Kim, K.-M., et al.**, *Surface treatment of silica nanoparticles for stable and charge-controlled colloidal silica.* International Journal of Nanomedicine, 2014. **9**(Suppl 2): p. 29-40.
117. **Puu, G., et al.**, *Distribution and stability of membrane proteins in lipid membranes on solid supports.* Biosensors and Bioelectronics, 2000. **15**(1): p. 31-41.
118. *Sulforhodamine 101*. [cited 2017; Available from: https://www.sigmaaldrich.com/catalog/product/sigma/s7635?lang=de&region=AT.
119. **Dror, Y., et al.**, *The effect of the serum corona on interactions between a single nano-object and a living cell.* Scientific Reports, 2017. **7**: p. 45758.
120. **Dutta, D., et al.**, *Adsorbed Proteins Influence the Biological Activity and Molecular Targeting of Nanomaterials.* Toxicological Sciences, 2007. **100**(1): p. 303-315.
121. **Guarnieri, D., et al.**, *Effect of serum proteins on polystyrene nanoparticle uptake and intracellular trafficking in endothelial cells.* Journal of Nanoparticle Research, 2011. **13**(9): p. 4295.
122. **Kamalov, M., et al.**, *N-terminal residues of silaffin peptides impact morphology of biomimetic silica particles.* Materials Letters.
123. **Ciccione, J., et al.**, *Unambiguous and Controlled One-Pot Synthesis of Multifunctional Silica Nanoparticles.* Chemistry of Materials, 2016. **28**(3): p. 885-889.
124. Canton, G., et al., *Modified Stöber synthesis of highly luminescent dye-doped silica nanoparticles*. Vol. 13. 2011. 4349-4356.
125. **Lechner, C.C. and C.F.W. Becker**, *Immobilising proteins on silica with site-specifically attached modified silaffin peptides.* Biomaterials Science, 2015. **3**(2): p. 288-297.
126. *TMOS Safety Data Sheet (Sigma Aldrich)*. [cited 2017; Available from: http://www.sigmaaldrich.com/MSDS/MSDS/DisplayMSDSPage.do?country=AT&language=de&productNumber=218472&brand=ALDRICH&PageToGoToURL=http%3A%2F%2Fwww.sigmaaldrich.com%2Fcatalog%2Fproduct%2Faldrich%2F218472%3Flang%3Dde.
127. *TEOS Safety Data Sheet (Sigma Aldrich)*. [cited 2017; Available from: https://www.sigmaaldrich.com/MSDS/MSDS/DisplayMSDSPage.do?country=AT&language=de&productNumber=131903&brand=ALDRICH&PageToGoToURL=https%3A%2F%2Fwww.sigmaaldrich.com%2Fcatalog%2Fproduct%2Faldrich%2F131903%3Flang%3Dde.
128. **Mornet, S., et al.**, *The formation of supported lipid bilayers on silica nanoparticles revealed by cryoelectron microscopy.* Nano letters, 2005. **5**(2): p. 281-285.
129. **Korbel, G.A., G. Lalic, and M.D. Shair**, *Reaction Microarrays: A Method for Rapidly Determining the Enantiomeric Excess of Thousands of Samples.* Journal of the American Chemical Society, 2001. **123**(2): p. 361-362.
130. **Deodhar, G.V., M.L. Adams, and B.G. Trewyn**, *Controlled release and intracellular protein delivery from mesoporous silica nanoparticles.* Biotechnology Journal, 2017. **12**(1): p. 1600408-n/a.
131. **Slowing, I., B.G. Trewyn, and V.S.Y. Lin**, *Effect of Surface Functionalization of MCM-41-Type Mesoporous Silica Nanoparticles on the Endocytosis by Human Cancer Cells.* Journal of the American Chemical Society, 2006. **128**(46): p. 14792-14793.

6 Supplementary Information

ad section 3.1.6:

*Table S 1: Percentages of compound **9** bound to silica particles containing peptide **3**, **4** or **7** after incubation in a 0.025 mg/ml initial conjugate solution for 1.5 hours at RT at particle concentrations of 1 mg/ml, followed by centrifugation (3 min, RT, 14 000 rpm). Supernatants obtained after centrifugation are referred to as "initial supernatants"*

Peptide	Concentration of initial conjugate solution [mg/ml]	Amount of compound 9 in initial conjugate solution [mg]	Absorbance of initial supernatant	Concentration of initial supernatant [mg/ml]	Amount of compound 9 in initial supernatant [mg]	Percentage of compound 9 bound to the particles [%]
3	0.025	0.005	0.053	0.01040	0.00208	**58.4**
4	0.025	0.005	0.052	0.01037	0.00207	**58.6**
7	0.025	0.005	0,055	0.01058	0.00212	**57.6**

*Table S 2: After centrifugation (Table S 1), the precipitates were washed 5 times with 100 µl H_2O (section 2.2.6, 3 min, RT, 14 000 rpm). This table shows the percentages of compound **9** washed off silica particles (from Table S 1) containing peptide **3**, **4** or **7** after the first wash*

Peptide	Amount of compound 9 bound to the particles [mg]	Absorbance of first wash	Concentration of compound 9 in first wash [mg/ml]	Amount of compound 9 in first wash [mg]	Percentage of compound 9 washed off after first wash [%]
3	0.00292	0.005	0.0070	0.00070	**24.0**
4	0.00293	0.007	0.0072	0.00072	**24.6**
7	0.00288	0.009	0.0073	0.00073	**25.3**

*Table S 3: Percentages of compound **9** bound to silica particles containing peptide **3**, **4** or **7** after incubation in a 0.05 mg/ml initial conjugate solution for 1.5 hours at RT at particle concentrations of 1 mg/ml, followed by centrifugation (3 min, RT, 14 000 rpm). Supernatants obtained after centrifugation are referred to as "initial supernatants"*

Peptide	Concentration of initial conjugate solution [mg/ml]	Amount of compound 9 in initial conjugate solution [mg]	Absorbance of initial supernatant	Concentration of initial supernatant [mg/ml]	Amount of compound 9 in initial supernatant [mg]	Percentage of compound 9 bound to the particles [%]
3	0.05	0.01	0.208	0.02148	0.004300	**57.0**
4	0.05	0.01	0.173	0.01899	0.003800	**62.0**
7	0.05	0.01	0.174	0.01906	0.003812	**61.9**

*Table S 4: After centrifugation (Table S 3), the precipitates were washed 5 times with 100 µl H_2O (3 min, RT, 14 000 rpm, section 2.2.6) This table shows the percentages of compound **9** washed off silica particles (from Table S 3) containing peptide **3**, **4** or **7** after the first wash*

Peptide	Amount of compound 9 bound to the particles [mg]	Absorbance of first wash	Concentration of compound 9 in first wash [mg/ml]	Amount of compound 9 in first wash [mg]	Percentage of compound 9 washed off after first wash [%]
3	0.005700	0.026	0.0085	0.00085	**14.9**
4	0.006200	0.053	0.0104	0.00104	**16.8**
7	0.006188	0.026	0.0085	0.00085	**13.7**

*Table S 5: Percentages of compound **9** bound to silica particles containing peptide **3**, **4** or **7** after incubation in a 0.073 mg/ml (experiment performed 3 times) initial conjugate solution for 1.5 hours at RT at particle concentrations of 1 mg/ml, followed by centrifugation (3 min, RT, 14 000 rpm). Supernatants obtained after centrifugation are referred to as "initial supernatants"*

Peptide	Concentration of initial conjugate solution [mg/ml]	Amount of compound 9 in initial conjugate solution [mg]	Absorbance of initial supernatant	Concentration of initial supernatant [mg/ml]	Amount of compound 9 in initial supernatant [mg]	Percentage of compound 9 bound to the particles [%]
3	0.073	0.0146	0.596±0.028	0.049±0.002	0.0098±0.0004	**32.7±3.9**
4	0.073	0.0146	0.571±0.024	0.047±0.002	0.0095±0.0003	**35.2±3.4**
7	0.073	0.0146	0.538±0.022	0.045±0.002	0.0090±0.0003	**38.3±3.2**

*Table S 6: After centrifugation (see Table S 5), the precipitates were washed 5 times with 100 µl H_2O (3 min, RT, 14 000 rpm, section 2.2.6) This table shows the percentages of compound **9** washed off silica particles (from Table S 5) containing peptide **3**, **4** or **7** after the first wash*

Peptide	Amount of compound 9 bound to the particles [mg]	Absorbance of first wash	Concentration of compound 9 in first wash [mg/ml]	Amount of compound 9 in first wash [mg]	Percentage of compound 9 washed off after first wash [%]
3	0.00478±0.00061	0.107±0.007	0.0142±0.0005	0.0014±0.00005	**29.2±3.8**
4	0.00513±0.00055	0.094±0.009	0.0134±0.0006	0.0013±0.00006	**25.3±3.2**
7	0.00560±0.00053	0.076±0.019	0.0121±0.0014	0.0012±0.00014	**21.4±5.3**

*Table S 7: Percentages of compound **9** bound to silica particles containing peptide **3**, **4** or **7** after incubation in a 0.1 mg/ml (experiment performed 3 times) initial conjugate solution for 1.5 hours at RT at particle concentrations of 1 mg/ml, followed by centrifugation (3 min, RT, 14 000 rpm). Supernatants obtained after centrifugation are referred to as "initial supernatants"*

Peptide	Concentration of initial conjugate solution [mg/ml]	Amount of compound 9 in initial conjugate solution [mg]	Absorbance of initial supernatant	Concentration of initial supernatant [mg/ml]	Amount of compound 9 in initial supernatant [mg]	Percentage of compound 9 bound to the particles [%]
3	0.1	0.02	0.842±0.041	0.067±0.003	0.0133±0.0006	**33.3±3.2**
4	0.1	0.02	0.821±0.038	0.065±0.003	0.0130±0.0005	**34.8±3.1**
7	0.1	0.02	0.705±0.069	0.057±0.005	0.0114±0.0010	**43.1±5.1**

*Table S 8: After centrifugation (see Table S 7), the precipitates were washed 5 times with 100 µl H_2O (3 min, RT, 14 000 rpm, section 2.2.6) This table shows the percentages of compound **9** washed off silica particles (from Table S 7) containing peptide **3**, **4** or **7** after the first wash*

Peptide	Amount of compound 9 bound to the particles [mg]	Absorbance of first wash	Concentration of compound 9 in first wash [mg/ml]	Amount of compound 9 in first wash [mg]	Percentage of compound 9 washed off after first wash [%]
3	0.00666±0.00064	0.168±0.032	0.0187±0.0023	0.0019±0.0002	**28.0±6.7**
4	0.00696±0.00063	0.184±0.019	0.0198±0.0014	0.0020±0.0001	**28.4±5.5**
7	0.00862±0.00101	0.158±0.048	0.0179±0.0034	0.0018±0.0003	**20.8±5.1**